Trictide, a Tricellulin-Derived Peptide to Modulate Cell Barriers and to Understand the Tricellular Organization of Tight Junctions

Inaugural-Dissertation

to obtain the academic degree

Doctor rerum naturalium (Dr. rer. nat.)

Submitted to the Department of

Biology, Chemistry and Pharmacy

of Freie Universität Berlin

by Başak Arslan

from Istanbul

2018

The dissertation was written from 29 January 2015 till 9 October 2018 under supervision of PD Dr. Ingolf E. Blasig at the Leibniz-Institut für Molekulare Pharmakologie (FMP).

1st Reviewer: PD Dr. Ingolf E. Blasig Molecular cell physiology Leibniz-Institut für Molekulare Pharmakologie (FMP)

2nd Reviewer: Prof. Dr. Ursula Koch Institute of Biology

Freie Universität Berlin

Date of defence: 28.01.2019

ACKNOWLEDGEMENTS

Firstly, I would like to thank my supervisor PD Dr. Ingolf E. Blasig for his supervision and support along my PhD studies, without him, this work will not be possible. I would also like to thank Prof. Dr. Ursula Koch for reviewing my thesis. As much as Ingolf, I am grateful to Dr. Reiner Haseloff for his constant support both intellectually and technically, Dr. Rosel Blasig and Dr. Lars Winkler for helping me with complicated and stressful animal experiments. I also thank my lovely collegues Dr. Sophie Dithmer, Dr. Olga Breitkreuz-Korff who made this journey bearable and fun and Dr. Christian Staat whom I learned a lot from.

I especially would like to thank Dr. Jimmi Cording who teached me almost everything I know about my project and Berlin. Without him I could not be that excited about science and pursue my science career in this cool city. Aside from Jimmi, I feel lucky to be part of 'tricellulin team' and to work with wonderful people and at this regard I am thankful to Ramona Birke and Anneliese Krüger for being the best team members at the hardest days.

I am more than thankful to Dr. Burkhart Wiesner, Jenny Eichhorst and Dr. Martin Lehmann who have always supported me to improve my project and provided everything I need to finalize this degree. I am also thankful to Dr. Susanne Krug for her input in trictide publication.

Most importantly I should express my gratitude to Dr. Philipp Berndt for just being there, being my friend, supporting me emotionally and scientifically because I cannot imagine a Ph.D. period without him. I also need to thank Erica Tornabene for coming to Berlin and making my first summer colorful and Carolin Müller; we spent some great time together, both in the lab and outside in the city.

I am grateful to know my dearest friends Aslıhan Karabacak, Gizem Inak and Yeşim Yurtdaş who are my family in Berlin and Eray Sahin who helped me everytime I need.

Lastly, I am thankful for my actual family Ekrem-Aynur Arslan, Dilan Bozdağ and Dr. Bilge Batu Oto who always trusted me and lent me hand regardless of distance.

SUMMARY

Tricellulin (Tric) is a tight junction protein at tricellular contacts; however its exact structure, function and regulation are unclear. Tric contributes to the paracellular tightening by intercellular *trans*-interactions between its extracellular loops 2 (ECL2). Consequently, trictide, a peptide derived from the Tric ECL2 was designed as a potential drug enhancer to specifically overcome tissue barriers. This work is aimed to investigate the functional and molecular modulations of tricellular contacts caused by trictide and to understand essential elements and protein interactions of tricellular tight junctions (tTJ) for barrier formation.

Trictide increased the passage of ions, small and larger molecules up to 10 kDa in a concentration dependent manner over duration from 16 h to 47 h after application to human colon epithelial cells. Under normal conditions, lipolysis-stimulated lipoprotein receptor (LSR) and Tric localized at tTJs while occludin (Occl), claudin-5 (Cldn5) and claudin-1 (Cldn1) localized at bicellular TJs (bTJ). After trictide treatment, Tric and LSR moved from tTJs to bTJs, and the bTJ proteins Cldn1 and Occl were internalized. Trictide also decreased the transcellular resistance of brain endothelial cells after 14 h and caused enrichment of Cldn5 around the tri-cellular area. Trictide down-regulated Occl, Tric, Cldn1, Cldn5 in epithelial cells and LSR, Occl, Cldn1 in mouse brain endothelial cells. Trictide-initiated opening of the tricellular sealing tube revealed a Tric-free area at the tricellular region as demonstrated by super resolution microscopy. In different cells, *cis*-interactions of Tric–Tric (tTJs), Tric–Cldn1, Tric–marvelD3, and Occl–Occl (bTJs) were strongly reduced by trictide treatment. In normal brain capillaries of different species, Tric was localized both at bTJs and tTJs while LSR was found exclusively at tTJs. *In vivo*, trictide did not increase the uptake of small molecules by mouse kidney and liver but tended to enhance brain uptake. Circular dichroism spectroscopy and molecular modelling suggested that trictide consists of 50% β-sheet structure resulting in an elongated conformation. Contrarily, scrambled trictide has a globular shape. Molecular docking models of trictide support the assumption that outward-directed aromatic amino acids are involved in a binding to tricellulin.

In conclusion, trictide is a novel and promising tool for overcoming cellular barriers at bTJs and tTJs with the potential to improve permeation of small molecules. Moreover, after targeting the cellular junctions, a connection has been disclosed between the disturbances of mutual interactions and the resulting redistribution of TJ proteins and functional alterations of the barrier.

ZUSAMMENFASSUNG

Tricellulin (Tric) ist ein in trizellulären Kontakten lokalisiertes tight junction (TJ)-Protein; seine genaue Struktur, Funktion und Regulation sind jedoch nicht bekannt. Tric trägt zur parazellulären Dichtheit durch die Ausbildung interzellulärer *trans*-Interaktionen zwischen seinen zweiten extrazellulären Schleifen (ECL2) bei. Daher wurde mit Trictid ein aus dem ECL2 von Tric abgeleitetes Peptid entwickelt, das als potentieller Wirkungsverstärker die spezifische Überwindung von Gewebsbarrieren ermöglichen soll. In der vorliegenden Arbeit werden Trictid-induzierte funktionelle und molekulare Veränderungen trizellulärer Kontakte untersucht um zum Verständnis essentieller Elemente und Proteininteraktionen von trizellulären tight junc-tions (tTJ) für die Ausbildung von Barrieren beizutragen.

In Abhängigkeit von seiner Konzentration erhöhte Trictid die Passage von Ionen und Molekülen mit mM < 10 kDa innerhalb von 16 h bis 47 h nach Zugabe zu Kulturen humaner Darmepithelzellen. Unter Normalbedingungen lokalisierten der Lipolyse-stimulierte Lipoproteinrezeptor (LSR) und Tric in den trizellulären tTJs, während Occludin (Occl), Claudin-5 (Cldn5) und Claudin-1 (Cldn1) in den bizellulären TJs (bTJs) gefunden wurden. Nach Trictid-Behandlung erfolgte die Relokalisation von Tric und LSR zu den bTJ, und Cldn1 und Occl wurden internalisiert. Darüber hinaus verringerte sich der transzelluläre Widerstand von Gehirnendothelzellen 14 h nach Trictide-Zugabe, und eine Anreicherung von Cldn5 im trizellulären Bereich wurde beobachtet. Trictid-Applikation führte zur Herabregulation von Occl, Tric, Cldn1, Cldn5 in Epithelzellen und von LSR, Occl und Cldn1 in murinen Gehirnendothelzellen. Untersuchungen mit superauflösender Mikroskopie zeigen, dass die Trictid-induzierte Proteinrelokalisation die Ausbildung eines Tric-freien Bereichs in der trizellulären Region bewirkte. Die *cis*-Interaktionen Tric-Tric (tTJs), Tric–Cldn1, Tric–marvelD3 und Occl–Occl (bTJs) wurden durch Trictid-Behandlung stark reduziert.

In normalen Gehirnkapillaren verschiedener Spezies lokalisierte Tric in den bTJs und tTJ, während LSR ausschließlich in den tTJ gefunden wurde. *In vivo* wurde die Aufnahme kleiner Moleküle durch Niere und Leber der Maus nicht durch Trictid beeinflußt, jedoch eine tendenziell erhöhte Aufnahme in das Gehirn beobachtet. Circulardichroismus-Spektroskopie und molekulares Modelling lassen darauf schließen, dass Trictid zu 50% eine β-Faltblattstruktur annimmt und in einer gestreckten Konformation vorliegt. Molekulares Docking von Trictid legt nahe, dass auswärts gerichtete Aminosäuren für eine Bindung an Tric von Bedeutung sind.

Die durchgeführten Untersuchungen lassen den Schluß zu, dass Trictid ein neuartiges und vielversprechendes Werkzeug für die Überwindung zellulärer Barrieren von bTJ und tTJ darstellt und das Potential besitzt, als Permeationsverstärker für kleine Moleküle zu dienen. Darüber hinaus wurde durch die zielgerichtete Einflußnahme auf die zellulären Junctions ein Zusammenhang zwischen der Störung der gegenseitigen Interaktionen und der daraus resultierenden Umverteilung der TJ-Proteine und den funktionalen Veränderungen der Barriere aufgedeckt.

TABLE OF CONTENTS

TABLE OF CONTENTS

LIST OF FIGURES

LIST OF TABLES

LIST OF SUPPLEMENTARY MATERIAL

LIST OF ABBREVIATIONS

Actb	β-actin
ANOVA	Analysis of variance
APS	Ammonium persulfate
BBB	Blood-brain barrier
bEND.3	Mouse brain endothelial cell line
BRB	Blood-retina barrier
BSA	Bovine serum albumin
bTJ	Bicellular tight junction
Caco-2	Human epithelial colorectal adenocarcinoma cells
CC	Coiled coil
CD	Circular dichroism
CFP	Cyan fluorescent protein
Cldn	Claudin
CNS	Central nervous system
Ct	Cycle threshold
DAPI	4′,6-diamidino-2-phenylindole
DMEM	*Dulbecco's Modified Eagle's Medium*
DMSO	Dimethyl sulfoxide
dNTP	Deoxyribonucleotide triphosphate
DPBS	*Dulbecco's phosphate buffered saline*
ECIS	Electric cell-substrate impedance sensing
ECL	Extracellular loop
EDTA	Ethylenediaminetetraacetic acid
FCS	Fetal calf serum
FD	FITC dextran
FITC	Fluorescein isothiocyanate
FRET	Fluorescence resonance energy transfer
fw	Forward primer
GAPDH	Glyceraldehyde 3-phosphate dehydrogenase
GFP	Green fluorescent protein
gSTED	Gated stimulated emission depletion super-resolution microscopy
h	Human
h	Hour
HBSS	*Hank's balanced salt solution*
HEK	Human embryonic kidney cells
His	Histidine
HT 29/B6	Human colon epithelial adenocarcinoma cell line
ip	Intraperitoneal
iv	Intravenous
kDa	Kilodalton
LSM	Laser scanning microscopy
LSR	Lipolysis stimulated lipoprotein receptor
LY	Lucifer yellow
m	Mouse
MAGUK	Membrane-associated guanylate kinase

MBP	Maltose binding protein
MBP	Maltose binding protein
MD3	MarvelD3
MDCK-II	Madin-Darby canine kidney cells
MEKK	Mitogen-activated protein kinase kinase
min	Minute
MTT	Methylthiazolyldiphenyl-tetrazoliumbromide
Na-fluorescein	Fluorescein sodium salt
ns	Non-significant
Occl	Occludin
PAGE	Polyacrylamide gel electrophoresis
PB	Phosphate buffer
PEG	Polyethylene glycol
PEI	Polyethylenimine
PFA	Paraformaldehyde
PLL	Poly(L-lysine)
qRT-PCR	Quantitative real time polymerase chain reaction
rev	Reverse primer
RTC	Rat tail collagen
SDS	Sodium dodecyl sulfate
SEM	Standard error of the mean
shRNA	Short hairpin ribonucleic acid
siRNA	Small interfering ribonucleic acid
TAMP	Tight junction associated MARVEL domain containing proteins
TAMRA	5-Carboxytetramethylrhodamine
TEMED	Tetramethylethylenediamine
TER	Transcellular electrical resistance
TFE	Tetrafluoroethylene
TJ	Tight junction
TM	Transmembrane
Tric	Tricellulin
Tric C-term	Recombinant C-terminus of Tric protein
Tris-HCI	Tris hydrochloride
TRQ	Turquoise fluorescent protein
tTJ	Tricellular tight junction
WT	wild-type
YFP	Yellow fluorescent protein
ZO-1	*zonula occludens* protein 1
λ_{ab}	Wavelength of the absorption
λ_{em}	Wavelength of the emission
λ_{ex}	Wavelength of the excitation

1. INTRODUCTION

It is essential to have separate compartments with different molecular compositions for the development and maintenance of multicellular organisms. These compartments are defined by various cellular sheets which function as barriers that maintain the distinct internal environments of each compartment within the organs. For instance, renal tubules and blood vessels are lined with epithelial and endothelial cellular sheets, respectively (Tsukita et al., 2001). Tissue-specific intercellular junctions where individual cells are linked to each other are a critical part of tissue barriers for maintaining the structural integrity. The intercellular space between adjacent cells is sealed to prevent diffusion of solutes through the intercellular space within these sheets. Tissue barriers constitute a line of defense against microorganisms, toxins, and allergens (Chaplin, 2010). The junctional complex of simple epithelial cells is located at the most-apical part of the lateral plasma membrane and consists of three components: tight junctions, adherens junctions, and desmosomes in vertebrates (Farquhar and Palade, 1963). Various human diseases are related to epithelial or endothelial barrier dysfunctions caused by dismodulation of barrier properties like stroke (Luissint et al., 2012; Marchiando et al., 2010) and brain tumors (Tiwary et al., 2018). This causes loss of stromal homeostasis and alters fluid-electrolyte balance between compartments. Disrupted barriers also permit bacterial invasions and allow metastatic cells to break in and out of blood vessels (Mullin et al., 2005).

1.1. ORGANIZATION AND FUNCTION OF EPITHELIUM AND ENDOTHELIUM

Epithelial tissues cover the inner and outer surfaces of the body and act as cellular boundaries. Epithelium is one of the four basic tissue types covering muscle, nerve and connective tissues. Epithelial cells has role in barrier formation, transcellular transport, secretion and selective absorption between the compartments. Epithelia provide protection against mechanical damage, entry of microorganisms, and dehydration. Epithelia have no blood vessels, so it is dependent on the underlying connective tissue for nutrition by diffusion of substances via the basement membrane. Epithelial cells are polarized, apically

exposed to the lumen and basolaterally they are in contact with laterally adjacent epithelial cells and the basement membrane (Fig. 1.1A). The cells of the epithelium are usually in close proximity to each other and are rich in cell-cell contacts (Denker and Nigam, 1998; Rodriguez-Boulan and Macara, 2014).

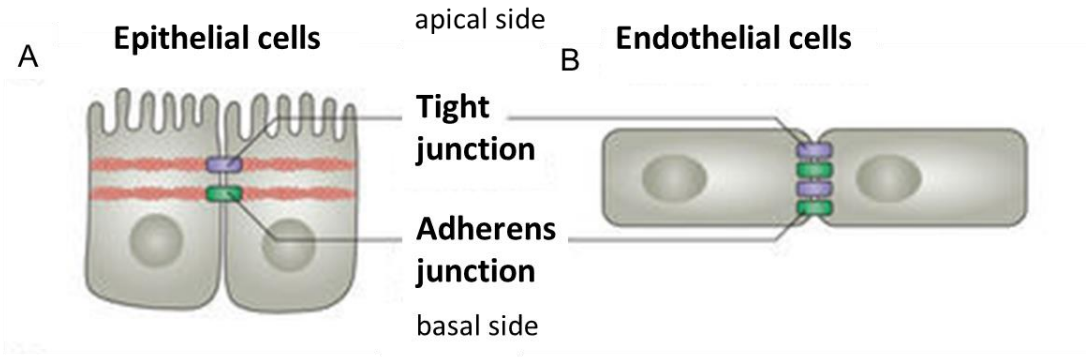

Fig. 1.1 The junctional complex in epithelial cells and endothelial cells. (A) Tight junction (purple) is positioned at the apical part of epithelial cells. Adherens junctions (green) is located below the tight junctions. The orange-belt in the middle is a part of the intracellular actin cytoskeleton that constitute polarized epithelium. **(B)** In endothelium both tight junctions (purple) and adherens junctions (green) are present but intermingled through the junctions. (Modified from Zihni et al., 2016)

Single layered endothelial cells cover blood and lymphatic capillaries and also cover the myocardium. Endothelial cells adhere to one another through junctional structures formed by transmembrane adhesive proteins that are responsible for homophilic cell-to-cell adhesion (Fig 1.1B). In turn, the transmembrane proteins are linked to specific intracellular partners that mediate anchorage to the actin cytoskeleton and, as a consequence, stabilize junctions. Endothelial junctions control permeability to plasma solute, leukocyte extravasation, and infiltration into inflamed areas. Junctional proteins can also transfer intracellular signals, which modulate endothelial cell growth and apoptosis (Bazzoni, 2004).

Endothelial and epithelial cell junctions share common components. Both cell types have two major types of junctions that are responsible for cell-to-cell adhesion: adherens junctions (AJ) and tight junctions (TJ) (Fig. 1.1). Additionally, epithelial cells form desmosomes (which are absent in the endothelium) and gap junctions that facilitate cell-to-cell communication (Fig 1.2). Gap junctions are formed by connexions that are expressed in the endothelium and function as channels for the intercellular passage of ions and small-molecular-weight molecules (Bazzoni, 2004; Zihni et al., 2016) .

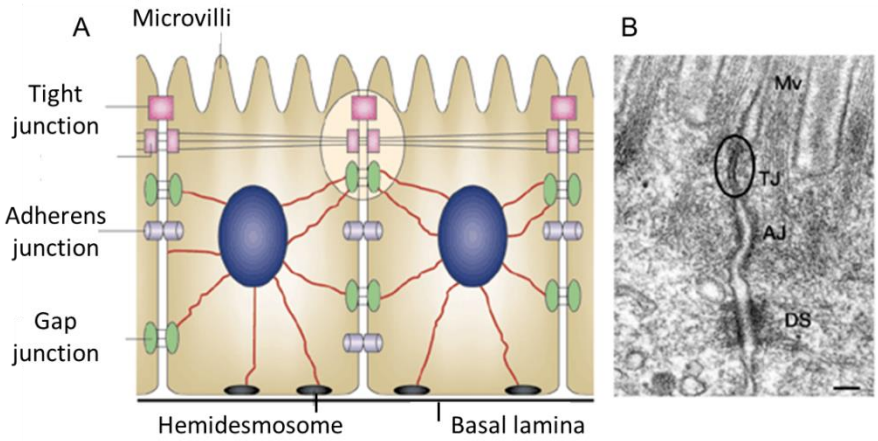

Fig. 1.2 The localization of tight junctions relative to other junctional components of epithelial cells. Schematic illustration of intestinal epithelial cells. The junctional complex containing TJs is circled. TJs are located at the most apical position of lateral membrane. **(B)** Electron micrograph of the junctional complex in mouse intestinal epithelial cells. The tight junction is circled. (Mv, microvilli; TJ, tight junction; AJ, adherens junction; DS, desmosome.) Scale bar, 200 nm. (Modified from Tsukita et al., 2001)

In epithelial cells, junctions are better organized, with TJ and AJ following a well-defined spatial distribution along the intercellular cleft. TJ (or zonula occludens) are concentrated at the apical side of the rim, while AJ (or zonula adherens) are located below the TJ. In contrast, the junctional architecture in endothelial cells is less defined and AJ are intermingled with TJ along the cleft (Fig 1.1) (Bazzoni, 2004; Tsukita et al., 2001; Zihni et al., 2016).

1.2. TIGHT JUNCTIONS

The tight junctions (TJ) were discovered by freeze-fracture electron microscopy, decades before its molecular identification (Staehelin et al., 1969; Staehelin, 1973; Stevenson et al., 1986). TJ strands were observed as a set of continuous or discontinues lines surrounding the apical part of adjacent epithelial cells. The TJ strands can be seen on both sides of the fracture plane. On the P-face, the protoplasmic side of the fracture, the TJ strands are clearly visible. On the E-face, the exoplasmic side, empty grooves complementary to those strands are detectable (Fig. 1.3A) (Shoichiro Tsukita et al., 2001). TJs appear as a series of "kissing points" on ultrathin section electron micrographs (Fig. 1.3B) between the outer

leaflets of the plasma membranes of neighboring cells (Fig. 1.3C). In simple epithelium, AJs and desmosomes mechanically connect adjoining cells, whereas TJs are responsible for intercellular sealing. The intercellular space between opposing membranes in AJs and desmosomes is 15–20 nm apart while this space is completely removed at the "kissing points" (Gumbiner, 1993; Schneeberger and Lynch, 2004).

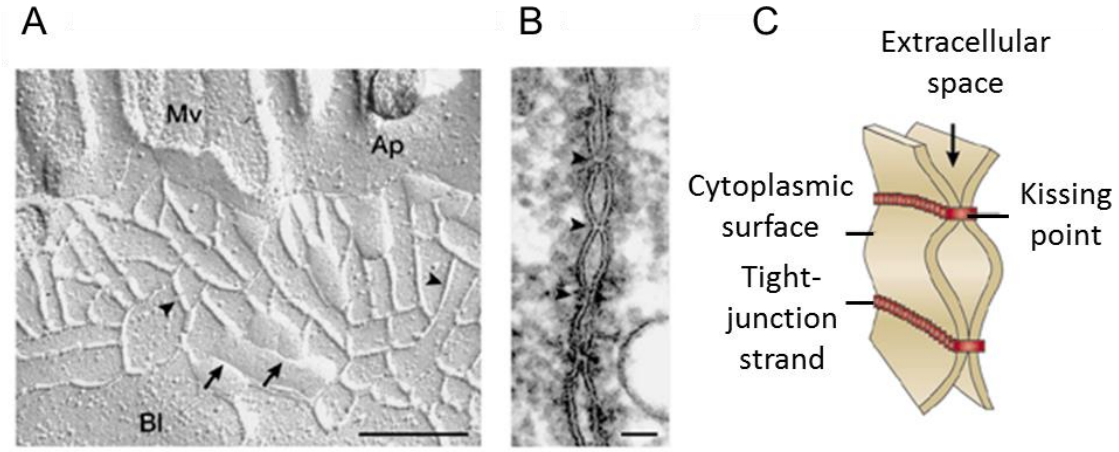

Fig. 1.3. The structure of tight junctions. (A) An image of intestinal epithelial cell taken by freeze-fracture replica electron microscopy. Tight junctions can be observed as continuous, intramembranous strands o(arrowheads) on the P-face with complementary empty grooves on the E-face (arrows). (Mv, microvilli; Ap, apical membrane; Bl, basolateral membrane.) Scale bar, 200 nm. **(B)** The kissing points: tight junctions (arrowheads) seal intercellular space between two cells. **(C)** Three dimensional structural scheme of tight junctions. Tight junction strands from membrane of two opposing cells interact to form the kissing points that tighten intercellular space. (Modified from Tsukita et al., 2001)

There are two permeation pathways through cell barriers: the transcellular pathway passes through the cell, crossing the apical and basolateral cell membranes, while the paracellular pathway passes between the cells through the TJ. TJs function as a barrier for paracellular diffusion of water, ions, metabolites and macromolecules. They also function as a fence, separating apical from basolateral parts of the cell membrane. However, TJs are not simply impermeable barriers. They show ion as well as size selectivity, and differ in tightness depending on the cell type. Generally, the proximal segments in epithelia-forming tubules such as intestine, nephron and sweat gland are more permeable; in comparison with TJs at distal segments, which are categorized as slightly permeable. The tightest TJs are found in skin and urinary bladder. Thus the sealing or permeability function of the TJ is strongly determined by its molecular composition (Fromter and Diamond, 1972). TJ meshwork of strands is formed by transmembrane proteins that play a role in the paracellular barriers. TJs are also associated with cytosolic scaffolding proteins that form the platform between the junctional membrane and cytoskeleton (Guillemot et al.,2008; Zahraoui et al., 2000).

Mainly, TJ transmembrane proteins consist of claudins (Cldns) with 27 members in mammals (Morita, et al., 1999) and TJ-associated MARVEL (MAL and related proteins for vesicle trafficking and membrane link) proteins (TAMPs) (Blasig et al., 2011; Sánchez-Pulido et al., 2002). TAMP family proteins are occludin (Occl) (Furuse et al., 1993), tricellulin (Tric) (Ikenouchi et al., 2005) and marvelD3 (MD3) (Steed et al., 2009). Cytosolic scaffolding proteins, such as *zonula occludens* protein (ZO)-1 to -3 belong to the membrane-associated guanylate kinase (MAGUK) family (Stevenson et al., 1986).

1.2.1. Bicellular and tricellular tight junctions

In endothelial or epithelial cell sheets, TJs are located between two cells (bicellular TJs) or where three cells (tricellular TJs) meet. These points are called either bicellular or tricellular contacts. At tricellular contacts, apically localized bicellular TJ (bTJ) strands meet and turn into basolateral direction to connect three cells. These triple pair structures firmly attach and extend to form a structure called central sealing tube (Staehelin, 1973) (Fig. 1.4A). Other bTJ strands connect to this central sealing tube laterally in order to strengthen the TJ strand network (Wade and Karnovsky, 1974).

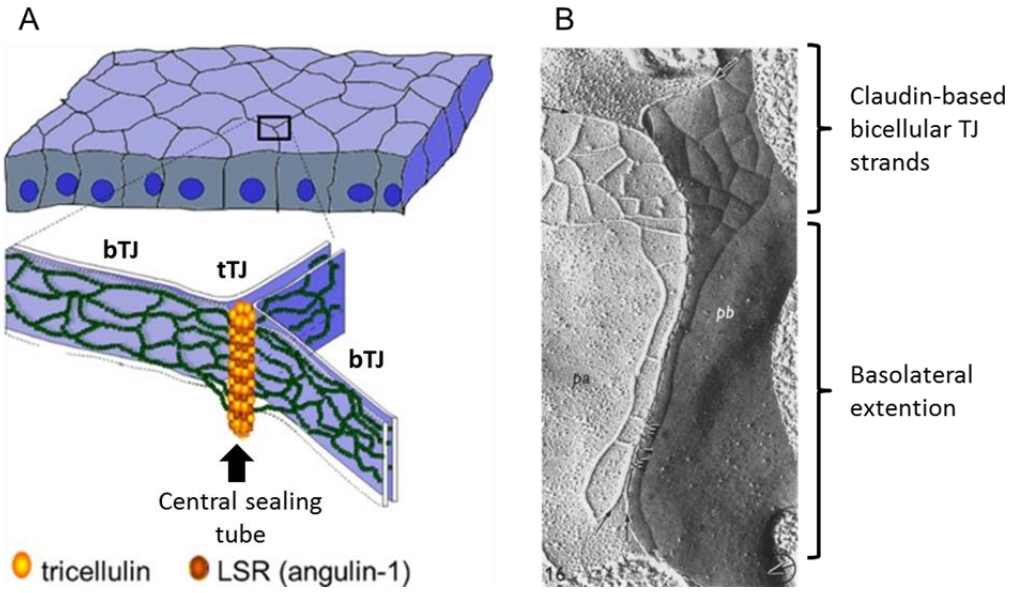

Fig. 1.4 Structure of tricellular and bicellular tight junctions. (A) A schematic illustration of tricellular and bicellular tight junctions. The central sealing tube in the middle is formed by tricellular tight junction proteins; tricellulin and lipolysis-stimulated lipoprotein receptor (LSR) and elongates through basal direction. (bTJ, bicellular tight junctions; tTJ, tricellular tight junctions). (Modified from Krug et al., 2017). **(B)** Freeze-fracture replica electron microscopic image of tricellular tight junctions of neighbouring epithelial cells (from mouse renal cortical collecting duct). Tricellullar TJ strands turn to extend basolaterally. Claudin-based tight junctions can be observed at the bicellular area. (Modified from Staehelin et al., 1973)

Staehelin and his colleagues initially proposed the tricellular cell-cell TJ model in 1973. Today the model is still valid and evolving with additional discoveries. Tric and LSR (Lipolysis-stimulated lipoprotein receptor or Angulin-1) are the main actors of central sealing at tricellular contacts (Krug et al., 2009; Masuda et al., 2011). The composition of TJ proteins varies between bicellular and tricellular junctions. Bicellular TJs regulate passage of small ions, water and constitute a barrier against other molecules while macromolecules can pass through tricellular TJs (tTJ). The length of the central sealing tube is about 1 µm, depending on the type of cell. Its radius is estimated as 5 nm, which allows transfer of macromolecules up to 10 kDa (Krug et al., 2009; Staehelin, 1973; Wade and Karnovsky, 1974).

1.3. TIGHT JUNCTION PROTEINS

1.3.1. Claudins

Cldn1 and Cldn2 were the earliest discovered members of the Cldn family as integral membrane proteins at TJs (Furuse et al., 1998). Cldns are a large family of TJ proteins with 26 members currently identified in human. Their molecular masses are between 21-34 kDa (Günzel and Yu, 2013; Mineta et al., 2011). Cldns belong to the tetraspan proteins, thus possessing four transmembrane domains: an intracellular short N-terminal, an intracellular longer C-terminal region, a small intracellular loop and two extracellular two loops (ECL), of which the first loop is larger than the second. The first crystal structures of Cldns provided more insight about spatial organization and ion homeostasis across TJs (Suzuki et al., 2014). Cldn family includes a signature sequence (GLW) within ECL1 and COOH-terminal PDZ-binding motif, through which most of the Cldns interact with tight-junction associated scaffolding or adaptor proteins (Günzel and Yu, 2013).

According to phylogenetic analysis, Cldns with higher sequence similarity were grouped as classical Cldns: 1-10, 14, 15, 17 and 19. Cldn 11, 16, 18, 21, 25 were accepted as non-classic Cldn. (Krause et al., 2008; Mineta et al., 2011, Günzel and Fromm, 2012). Cldns are also classified based on their physiological role in paracellular transport, complete sealing (Cldn1, 3-6, 8, 9, 11, 14, 18, 19) and formation of channels that are permeable for anions (Cldn10a and 17), cations (Cldn2, 10b and 15) or water (Cldn2) (Günzel and Fromm, 2012). There is still not much information about the exact function of the rest of the Cldn family (12, 13, 20, 22-27).

Homophilic and heterophilic interactions can take place between Cldns (Furuse et al., 1999). If the interaction occurs between two Cldns within the plasma membrane of the same cell, a *cis*-interaction prompts Cldn oligomerization (Piontek et al., 2008). The interaction via the paracellular space between two cells is called *trans*-interaction (Fig. 1.5). Residues in the ECL1 are involved in the formation of paracellular ion pores and the determination of their charge selectivity (Alexandre et al., 2007). ECL2 of Cldn5 contributes to *trans*-interaction between Cldn oligomers from two opposing plasma membranes and generates polymerization of TJ strands within the paracellular space (Piontek et al., 2008). This formation explains the specific role of Cldn5, which is to

tighten the BBB for molecules <800 Da (Nitta et al., 2003). The combination of Cldns expressed in tissues determines the barrier properties of the respective tissue (Kiuchi-Saishin et al., 2002).

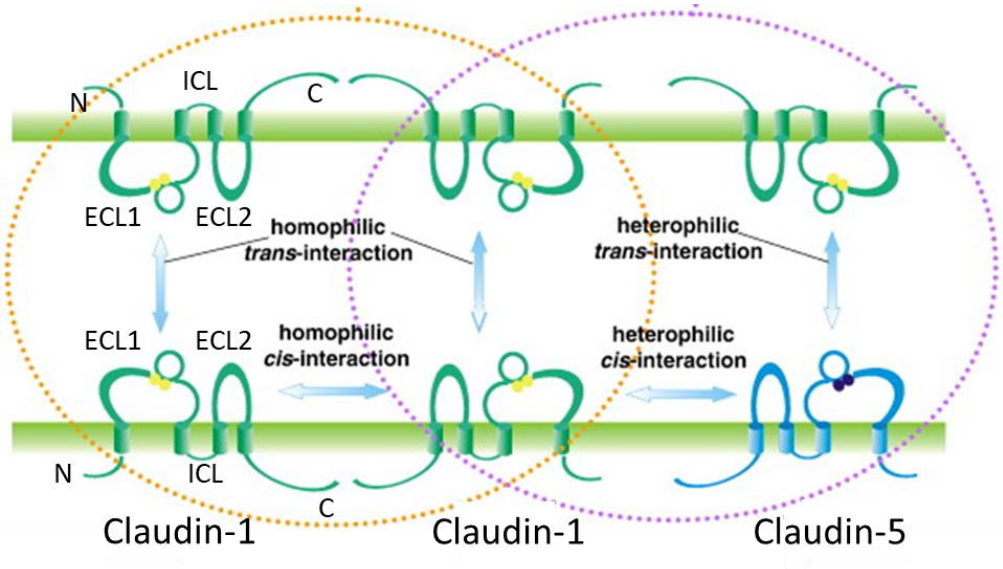

Fig. 1.5 Schematic illustration of claudin structure and their way of interaction. Claudins are tetraspan membrane proteins with two extracellular loops (ECL), cytosolic N- or C-terminal tails and a short intra cellular loop (ICL). Claudins can make *cis*- and *trans*- interactions through cytosolic N- or C-terminal tails and through extracellular loops, respectively. Furthermore these interactions can occur between identical proteins (homophilic, yellow dotted circle) or between two different proteins (purple dotted circle). (Modified from Krause et al., 2008)

For instance, the knock-out model of Cldn1 demonstrated that lack of Cldn1 causes massive transepidermal dehydration. So Cldn1 is an essential component of epidermal barrier (Furuse et al., 2002). Cldn5 also has a barrier-forming function as it was confirmed by Cldn5 deficient mice and stable transfection of cell lines (Amasheh et al., 2005; Nitta et al., 2003). Cldn2 was shown to reduce transepithelial resistance (Furuse et al., 2001) by forming paracellular channels for small cations (Amasheh et al., 2002). It is typically found in leaky, proximal segments of tubular epithelia such as proximal tubule (Kiuchi-Saishin et al., 2002) and small intestine (Markov et al., 2010). There are contradictory statements about Cldn4: its overexpression leads to a strong decrease in cation permeability, while the permeability for anions remains unchanged (Van Itallie et al., 2001). In addition, the presence of Cldn4 increases the TJ complexity (Colegio et al., 2002). On the other hand, Hou and his colleagues claim that Cldn4 has a sodium channel function (Hou et al, 2010). Cldn10 exists in several splice variants and depending on the expression background, it

functions as pore-forming Cldn with anion-selective (Cldn10a) (Van Itallie et al., 2006) or cation-selective (Cldn10b) (Günzel et al., 2009) properties (Olinger et al., 2018). Claudin domain containing (CLDND) 1 (Cldn25) is a non-classical Cldn (Mineta et al., 2011). It was recently found that Cldn25 mRNA levels decreased transiently 24 h after cerebellar hemorrhage. Moreover, Cldn25 knockdown increased the permeability of human bronchial epithelial cells (HBECs) by small molecules (Ohnishi et al., 2017).This large functional spectrum of Cldns is also reflected in specific expression patterns in the various endothelia and epithelia.

1.3.2. Tight junction associated MARVEL proteins

The TAMP family shares a conserved tetra-spanning MARVEL domain, which is mostly responsible for membrane apposition and is concentrated in cholesterol-rich microdomains (Sánchez-Pulido et al., 2002). Members of the TAMP family are Occl (Furuse et al., 1993), Tric (Ikenouchi et al., 2005) and MD3 (Steed et al., 2009) (Fig. 1.6A). The structure of the TAMP family consists of four transmembrane domains, cytosolic N- and C-terminus, an intracellular and two extracellular loops similar to Cldns (Raleigh et al., 2010).

TAMPs have heterophilic (Occl-MD3, Tric-MD3) and homophilic (Occl, Tric, MD3) *cis* interactions and homophilic *trans* interactions (Occl) (Cording et al., 2013; Raleigh et al., 2010). TAMPs form TJ strands in the presence of another tight junction protein like a Cldn. For instance, Cldn1 and Cldn5 improved enrichment of Occl and Tric at cell–cell contacts. The membrane mobility of Occl and Tric was reduced when they were co-expressed with Cldn1 (Cording et al., 2013). TAMP knockdowns cause greater reductions in transepithelial electrical resistance (TER) compared to when TAMPs are knocked down as combinations. This suggests that TAMPs make both overlapping and unique contributions to TJ assembly and barrier function (Raleigh et al., 2010).

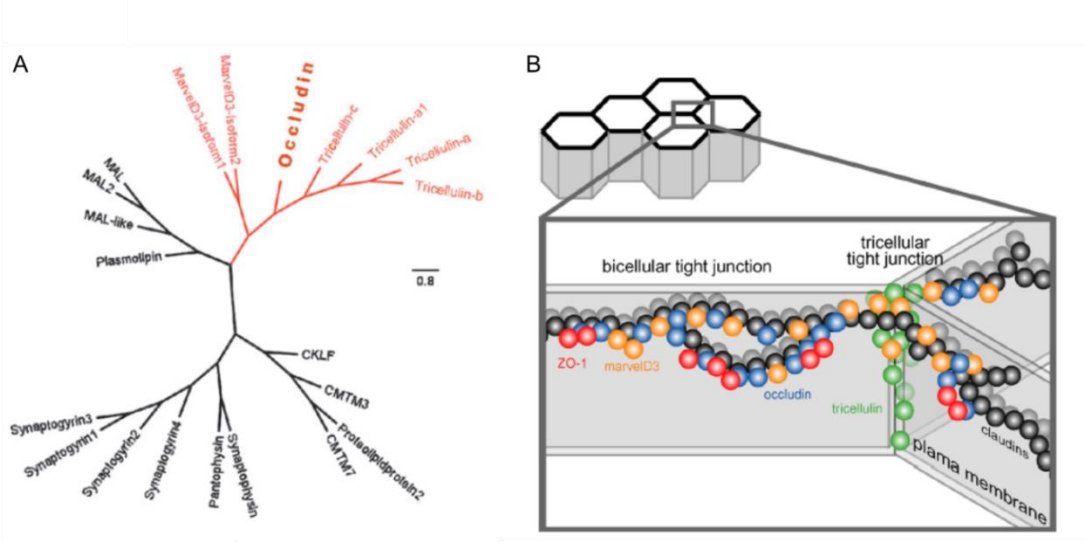

Fig. 1.6 Classification of tight junction associated MARVEL domain containing proteins (TAMPs) and the organization of TAMPs together with other junctional proteins. (A) Human TAMPs are marked as red within the phylogenetic tree of the MARVEL domain containing protein superfamily. **(B)** The scheme illustrates a tricellular tight junction area with tricellulin (green balls) localizing at three cell meeting points and elongating at basal direction. Claudins form the backbones of bicellular tight junctions and they are represented as black balls within continuous strands here. Occludin (blue balls) is primarily found in bicellular junctions. MarvelD3 (orange balls) can be observed at both bicellular and tricellular tight junctions. Both occludin and claudins can interact with *zonula occludens* protein 1 (ZO-1). (Modified from Raleigh et al., 2010).

1.3.3. Occludin

The first identified integral TJ membrane protein was Occl (65 kDa) (Furuse et al., 1993). Occl has four transmembrane domains, two extracellular loops and three intracellular domains consisting of a short intracellular loop, a short N-terminal and a long C-terminal tail (Fig. 1.7A). There is also a conserved MARVEL domain (Raleigh et al., 2010) that facilitates self-association and directs Occl to locate in basolateral membrane (Yaffe et al., 2012). The extracellular regions may interact with other TJ proteins of the opposing cells in so-called *trans* interaction (Cording et al., 2013). The first extracellular loop is rich in tyrosine and glycine and plays a role in the cell-cell junction. The second extracellular loop has a role in integrating Occl in the TJ complex and in formation of the paracellular barrier (Citi and Cordenosi, 1998; Medina et al., 2000). The second extracellular loop has two conserved cysteine residues that form an intramolecular disulfide bond that play a role in the redox-dependent *trans*- and *cis*-interactions of Occl (Fig. 1.7A) (Bellmann et al., 2014).

The C-terminus has an ELL domain consisting of an antiparallel coiled-coiled hairpin structure (also called coiled-coil-domain). This conserved domain is originally found in the RNA polymerase II elongation factor ELL. This domain may interact with other proteins belonging to the MAGUK family (Li et al., 2005). This includes the proteins ZO-1, ZO-2 and ZO-3 (Tsukita and Furuse, 1998), as well as F-actin of the cytoskeleton (Wittchen et al., 1999). The C-terminal tail of Occl and TRIC-a demonstrate considerable homology (Ikenouchi et al., 2005).

To what extent Occl is essential for the TJ, is controversial. On the one hand, knockout mice show no impairment of barrier function. On the other hand an essential barrier function of Occl is demonstrated within the TJ strands (Schulzke et al., 2005). Moreover postnatal growth retardations, like histological abnormalities in several tissues and male sterility, are found in knockout mice (Saitou et al., 2000). In order to explain this weak phenotype, a compensatory mechanism is proposed to maintain barrier integrity. For instance, knockdown of Occl altered the localization of Tric from tTJs to bTJs. The presence of Occl should exclude Tric from bTJs and support Tric's tricellular localization (Ikenouchi et al., 2008). This interplay between Occl and Tric supports the argument that members of TAMP family have distinct but also overlapping functions enabling them to compensate for each other (Raleigh et al., 2010). Last of all, Occl is accepted as a general TJ marker because it is expressed in every epithelial and endothelial barrier (Blasig et al., 2011).

1.3.4. MarvelD3

MD3 was discovered as the third member of TAMP family (Steed et al., 2009). The human MD3 has two isoforms: MD3 isoform-1 contains 401 amino acids (44.9 kDa); isoform-2 comprises 410 amino acids (45.9 kDa). Two isoforms differ in the sequence of the MARVEL domain and size of cytosolic C-terminal tail but are identical in N-terminal tail. The C-terminal tail of MD3 does not have coiled coil domain unlike Occ and Tric. Since the C-terminal tail is the binding site of Occl and Tric to ZO-1, it is assumed that MD3 does not interact with ZO-1 (Raleigh et al., 2010; Steed et al., 2009). It is expressed in epithelial-rich tissues like colon, colonic epithelium, kidney (isoform-2) and liver (isoform-

1) differentially (Raleigh et al., 2010). It localizes mostly at bicellular apical regions of cells co-localizing with Occl and ZO-1 (Raleigh et al., 2010; Steed et al., 2009).

Depletion of MD3 does not have any effect on formation of functional paracellular barrier. It does not cause mislocalization of other TJ proteins like Occl. Interestingly, TER is increased after depletion of MD3 (Steed et al., 2009). It was demonstrated that MD3 is transported to TJs immediately after synthesis and in accordance with TER development (Raleigh et al., 2010). Taken together, MD3 is not essential for junctional association but still a determinant of paracellular permeability.

In 2014, it was reported that MD3 is a dynamic junctional regulator of the MEKK1–c-Jun NH2-terminal kinase (JNK) pathway (Steed et al., 2014). This pathway is responsible for cell proliferation and migration. Expression levels of MD3 oppositely linked with JNK activity, because MD3 recruits MEKK1 to junctions, causing for down-regulation of JNK phosphorylation and inhibition of JNK-regulated transcriptional mechanisms. This interplay between MD3 internalization and JNK activation is important for cell survival and prevention of tumor formation (Steed et al., 2014).

1.3.5. Tricellulin

Tric (MarvelD2) is the first TJ protein discovered as a component of tTJs (Ikenouchi et al., 2005). The genes encoding for both human Occl and Tric are located in human chromosome 5. To date, four human isoforms of Tric have been described: TRIC-a is the longest form with 558 amino acids (64 kDa) and is the most common point of reference when Tric is mentioned. TRIC-a has four transmembrane regions: two extracellular loops and three intracellular regions consisting of a short loop, a short N-terminal and a long C-terminal region (Fig, 1.7A). It is composed of seven exons and has a C-terminal CC-domain that is 32% identical to that of Occl (in total 51% similar) (Fig. 1.7B) (Riazuddin et al., 2006). Tric N-terminal domain is suggested to be involved in guiding Tric to tricellular contacts while the C-terminus is responsible from the basolateral translocation of Tric (Westphal et al., 2010). The first extracellular loop is similar to Occl, rich in glycine and tyrosine (49.5%), so it can be assumed that it is also necessary for the formation of cell-cell

contacts. Mutations within TRIC-a lead to non-syndromic deafness (DFNB49) (Riazuddin et al., 2006).

The isoform Tric-a1 (62 kDa TRIC-a1) is very similar to TRIC-a but lacks the third of the seven exons. Tric-b (TRIC-b) is a shorter isoform (458 amino acids, 51 kDa) that is highly different in the C-terminus of TRIC-a (Fig. 1.7B). The crystal structure of C-terminal coiled-coil part has been recently reported as a potential component in dimeric arrangement (Schuetz et al., 2017).

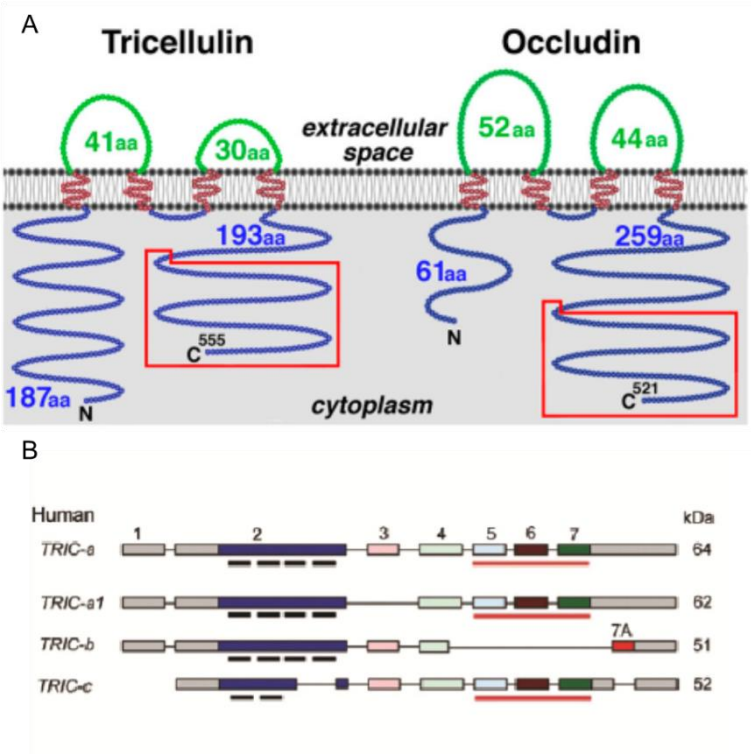

Fig. 1.7 Scheme of predicted structure of tricellulin and occludin and isoforms of human tricellulin. (A) Both tricellulin and occludin are tetraspan membrane proteins with two extracellular loops, cytosolic N- and C-terminal tail and a short intracellular loop. Tricellulin has a longer N-terminal tail while occludin has longer extracellular loop. Their C-terminal tail is 32% identical to each other (Ikenouchi et al., 2005). **(B)** The isoforms of human Tric. The numbers indicate the order of exons. The black bars of exon two mark the predicted transmembrane domains, the red line marks the occludin coiled-coil domain, grey areas symbolize untranslated segments (Riazuddin et al., 2006).

It was well known that bTJ proteins like Cldns (Furuse et al., 2002; Nitta et al., 2003) or Occl (Schulzke et al., 2005) are tightening the cell barriers. However tricellular contacts were considered as weak points within the barrier. With the discovery of Tric, it is now

understood that Tric is the tightening component of epithelial cell barrier at tricellular junctions (Ikenouchi et al., 2005). When Tric is expressed in an endogenously low Tric expressing cell line, paracellular electrical resistance is increased and permeability to ions and larger solutes is decreased (Krug et al., 2009). Tric knockdown experiments exhibited that, in the absence of Tric, epithelial barrier tightness is not maintained in parallel with cell confluency and the continuity of TJ network is considerably disturbed (Ikenouchi et al., 2005). On the other hand, overexpression of Tric is decreasing permeability for macromolecules (4-10 kDa) but not affecting the ion permeability (Krug et al., 2009). This paradox suggested the tTJ central tube as a pathway for macromolecules based on its calculated radius that can enable this passage (Krug et al., 2009; Staehelin, 1973). After strong overexpression, tricellulin was detected at both tri- and bicellular contacts equally (Krug et al., 2009). The systemic deletion of Tric in mice ($Tric^{-/-}$) causes progressive hearing loss linked to the degeneration of cochlear hair cells (Kamitani et al., 2015).

It has already been stated that Tric has strong interactions with other TAMP members and Cldns in addition to its compensatory functions. It was observed that under reducing conditions, Occl weakens at bTJ and Tric shows co-localization with ZO-1 and partly with Occl Two important information proceed. First Tric should compensate for Occl's function even though Occl and Tric do not interact directly (Cording et al., 2013; Raleigh et al., 2010). Second, Tric trimerization at tricellular contacts should be disrupted so that it can be shifted to bTJs (Cording et al., 2015). The Cys residues in ECL2 of Tric are important for *trans*-interactions and paracellular sealing because *trans*-association is interrupted in the absence of those residues as well as under reducing conditions. This relates the ECL2 region of Tric with extracellular binding of three Tric proteins at tTJs. The trimerization and tightening effect of Tric between three cells is superimposed on tricellular *cis*-interaction along one plasma membrane (Cording et al., 2015).

Tric is strongly expressed in epithelial-derived tissues like kidney, small intestine, stomach and lung (Ikenouchi et al., 2005). It is expressed at medium levels in liver. Tric expression is lower in organs having less epithelial tissue: spleen, lymph nodes, testis, brain (Ikenouchi et al., 2005; Raleigh et al., 2010). Tric localization is also reported in brain endothelial regions (cerebrum, cerebellum, retina, choroid plexus) and brain microvessels (Iwamoto et al., 2014; Mariano et al., 2013). Likewise it has been stated that Tric

expression in peripheral nervous system (sciatic nerve) is more abundant then in the central nervous system (Kikuchi et al., 2010).

There is limited information about the regulatory mechanism over TJ formation and maintenance. Tric might be phosphorylated (Ikenouchi et al., 2005). Even though c-Jun N-terminal kinase is associated with Tric phosphorylation, it has not been clearly identified (Kojima et al., 2010). Recently a mechanism pointing out the relation between Tric down-regulation and ulcerative colitis (UC) was reported. It is found that in UC interleukin 13 receptor α2, a proinflammatory cytokine, downregulates Tric and increases luminal uptake of antigens resulting from barrier defects (Kojima et al., 2010). Moreover, it was also shown that posttranslational modifications like ubiquitination plays a role in down-regulation of Tric at protein level after forming a complex with Tric (Jennek et al., 2017).

1.4. TIGHT JUNCTION SCAFFOLDING PROTEINS

The membrane-associated guanylate kinase (MAGUK) family proteins of TJs include the ZO proteins that have three N-terminal PDZ domains, one Src homology 3 (SH3) domain and a guanylate kinase (GUK) domain (Itoh et al., 1999). PDZ domain is a protein interaction module that plays role in attaching receptor proteins in the membrane to cytoskeletal components and regulates signal transduction complexes (Lee and Zheng, 2010). ZO-1 (Stevenson et al., 1986), ZO-2 (Gumbiner et al., 1991) and ZO-3 (Balda et al., 1993) are members of ZO proteins. The ZO proteins are scaffold proteins, which on the one hand bind directly to transmembrane proteins of the TJs and on the other hand are connected with signalling and structural proteins for the regulation of TJ structure and function (Fanning and Anderson, 2013). ZO-1 is the first junctional protein identified at TJs (Stevenson et al., 1986) and ZO-1 deficient mice are embryonic lethal (Katsuno et al., 2008). ZO-1 comprises N-terminal protein binding domain (PDZ1) for the main transmembrane barrier proteins Cldns (Furuse et al., 1998), Occl (Fanning et al., 1998; Furuse et al., 1994) and Tric through its conserved C-terminal CC-domain (Ikenouchi et al., 2005; Riazuddin et al., 2006) and links TJ proteins directly to the actin cytoskeleton. Knockdown of ZO-1 in epithelial cells caused delay in barrier formation (McNeil et al., 2006; Umeda et al., 2004). Moreover it has been reported that Tric does not localize at tTJ

in ZO-1 and-2 double negative cells (Ikenouchi et al., 2007). However once TJs are formed in the ZO-1 lacking cells, TER and passage of large molecules were stated at normal levels (Umeda et al., 2004). ZO proteins play an important role at the formation and function of adherens junctions (Ikenouchi et al., 2007) and gap junctions (Giepmans and Moolenaar, 1998) in addition to TJs. ZO-1 is accepted as general marker for cell junctions.

1.5. THE ANGULIN-PROTEIN FAMILY

The angulin-proteins are single-pass transmembrane proteins, which localize at tTJs. The family consists of LSR (angulin-1), immunoglobulin (Ig)-like domain-containing receptor (ILDR)1 (angulin-2) and ILDR2 (angulin-3) proteins (Higashi et al., 2013; Masuda et al., 2011). They are expressed in several epithelial tissues at different degrees (Higashi et al., 2013). At least one splice isoform of angulin proteins localize at tTJs and scarcely at bTJs (Higashi et al., 2013; Reaves et al., 2017). Immunoreplica of electron microscopy have revealed LSR at the central sealing elements of tTJs. LSR is an important protein for barrier function because knockdown of LSR in epithelial cells causes decrease in TER and increase in macromolecular passage (Masuda et al., 2011). The expression of angulin-2 protein reverses the effect of LSR knockdown cells on TER and permeability of macromolecules (Higashi et al., 2013). Moreover, knockout of angulin-2 protein causes deafness with progressive cochlear hair cells degeneration (Higashi et al., 2015).

LSR knockdown cells also exhibited bicellular membrane localization of Tric instead of tTJs. Contrarily LSR keeps its tricellular position at Tric knockdown cells (Masuda et al., 2011). When angulin binding deficient mice is generated, it was observed that Tric is not present at tTJs while angulin-2 can still localize at tTJs (Nayak et al., 2013). This suggests that angulins are the foundation of tTJs at tricellular contacts and recruit Tric to tTJs. The interaction between conserved cytoplasmic C-terminal tails of Tric and angulins is necessary for recruitment of Tric to tTJs (Higashi et al., 2013; Masuda et al., 2011).

It is reported that LSR is a BBB enriched protein, expressed in parallel with BBB development and specifically expressed at tTJs of CNS blood vessels. Thus, LSR knockout mice cannot complete sealing of BBB and dies on embryonic day 15.5. Similarly,

neurological disorder models that lack functional BBB showed down-regulation of LSR. However LSR knockout mice have no impact on ultrastructure of TJ and the knockout also does not affect expression and localization of other junctional proteins like Occl, Cldn5 and ZO-1 (Sohet et al., 2015).

Recently, a cancer protective role of LSR has been suggested. Hence LSR deficient epithelial cancer cells show increased cell proliferation *in vitro* and larger cysts in 3D cultures (Czulkies et al., 2016). Furthermore, knockdown of LSR causes increased cell migration, proliferation and invasion in endometrial cancer cell lines (Shimada et al., 2016).

1.6. TRICELLULAR TIGHT JUNCTIONS IN BLOOD-BRAIN BARRIER

The blood-brain barrier (BBB) is formed by endothelial cells lining brain microvessels. It constitutes a barrier between circulating blood and central nervous system (brain and spinal cord) (Fig. 1.8). The permeability through BBB is strictly controlled by several mechanisms that include BBB specific proteins (transporters) responsible from transcellular pathway and TJ proteins limiting the passage between adjacent endothelial cells (Abbott, 2013; Greene and Campbell, 2016). This way BBB maintains the ionic composition of the interstitial fluid bathing the neurons and also shields the gentle neuronal tissue from blood borne agents like pathogens and immune cells. Through BBB, there is low rate of vesicular transport and channels that provide rapid exchange of molecules are not present (Greene and Campbell, 2016).

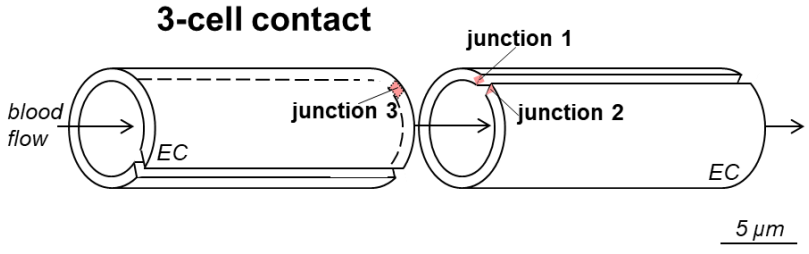

Fig. 1.8 Schematic illustration of brain microvascular endothelial cells and position of tricellular tight junctions (tTJ). Single layered endothelial cells cover the blood capillaries and form a barrier between blood circulation and brain. Since endothelial cells are more flat compared to epithelial cells, the structure of the tTJs are also different. That is why, an exemplary tTJ of a brain capillary is illustrated above. EC, Blood capillary formed by single endothelial cells (provided from I. E. Blasig).

Cldn5 is the dominant tight-junction protein of the BBB because it is highly expressed in capillary endothelial cells and seals the paracellular spaces (Nitta et al., 2003; Ohtsuki et al., 2007). For the first time, Tric is found to be expressed in tTJs but also in bTJs of brain microvascular endothelial cells (Mariano et al., 2013). Furthermore, both Tric and LSR were specifically concentrated at TJs of brain and retina endothelial cells that contribute to formation of BBB and brain-retinal barrier (BRB) (Iwamoto et al., 2014). Importance of LSR - a tricellular tight junction protein - for sealing of BBB during embryonic development has already been described in previous chapter (Sohet et al., 2015). Even though tTJ in endothelial cells is not well-characterized yet, recent studies emphasize presence of tTJs in brain endothelial cells and evidenced their role in the BBB formation and tightness.

1.7. THE IMPORTANCE OF TRICELLULAR TIGHT JUNCTIONS IN PATHOLOGICAL EVENTS

It was already explained that mutation of Tric causes non-syndromic deafness in humans (Riazuddin et al., 2006). Angulin-family proteins and their functional importance have also been discovered rather recently (chapter 1.5). LSR (angulin-1) was identified first as a lipoprotein receptor (Yen et al., 1999) and liver-specific knockdown resulted with hypertriglyceridemia in mice (Narvekar et al., 2009). In addition, human angulin-3 is linked with type 2 diabetes (Dokmanovic-Chouinard et al., 2008), which might have developed due to hypertriglyceridemia.

Numerous bacteria attack tricellular junctions to infect epithelial cells. For instance, *S. flexneri* organizes extending pseudopodia at tricellular junctions in a Tric-dependent way (Fukumatsu et al., 2012). On the other hand, group A *Streptococcus* bacteria is reported to target tricellular junctions specifically by interaction with Tric to overcome the epithelial barrier (Sumitomo et al., 2016). In pancreatic cancer cell lines, Tric is distributed from membrane to nucleus with decreasing differentiation order. Tric expression in nucleus is assumed to stimulate cell proliferation and finally related to lymph node metastasis (Takasawa et al., 2016).

1.8. DRUG DELIVERY BY MODULATION OF TIGHT JUNCTIONS

Most drugs cannot pass tissue barriers properly because of their size or hydrophilicity. Hence, there are two ways of passage through cell sheets for drugs: transcellular and paracellular routes. Several strategies have been developed to enhance drug passage through tissue barriers via these routes. First strategy is to introduce prodrugs that are inactive compounds by changing the transcellular permeability or increasing lipophilicity. Passage can also be achieved by drugs coupled with specific ligand of transporters (Brandsch et al., 2008). Those inactive compounds are activated by enzymatic reactions. Recently liposomes (El Maghraby et al., 2008), filled with nanoparticles (Dai, Jiang, and Lu, 2018; Kreuter and Gelperina, 2008) are also used for passage via BBB. The paracellular strategies are mainly based on ultrasound (Burgess and Hynynen, 2014) and mannitol (Kobrinsky et al., 1999). Other paracellular routes with small molecules are sodium caprate (Lindmark et al., 1998), peptides (Nusrat et al.,2005) and small interfering ribonucleic acid (siRNA)(Campbell et al., 2009) as promising ways of transiently modulating the TJs. Thus, TJ proteins responsible from the paracellular tightening can be modulated by TJ protein specific peptides.

1.9. TIGHT JUNCTION PEPTIDOMIMETICS

Peptides are derived from parts of TJ proteins specifically to target barriers and enhance passage of small and large molecules. To date, Occl and Cldn derived peptides are more common due to the fact that they are the most studied TJ proteins. The most related and important Occl and Cldn derived peptides and their effects are summarized in Table 1 and Table 2. Peptides are designed based on target tissue and its Cldn composition. Parts of target TJ protein that is maintaining the paracellular tightness are explicitly selected. So far all peptidomimetic methods are focused on opening bTJ areas. But recently tricellular TJ proteins are discussed as a target molecule to enable passage of macromolecules (Cording et al., 2017; Krug et al., 2017).

Table 1. Occludin peptidomimetics

Derived from	Target	Effect		Literature
		In vitro	***In vivo***	
$ECL1_{81-125}$ $ECL2_{184-227}$ (chicken)	A6 cells-*Xenopus laevis* kidney	- ↑ permeability, ↓ TER <5 µM. - no changes in cell morphology - ↓ Occl in TJs and totally in cells. - ZO-1, ZO-2, cingulin, E-cadherin not affected.		Wong and Gumbiner, 1997
$ECL1_{100-108 \text{ or } 109}$ (chicken)	A6 cells-*Xenopus laevis* kidney	- ↓ in TER -ZO-1 localization is not changed		Lacaz-Vieira et al., 1999
$ECL2_{209-230}$ (rat)	Blood-testis barrier (BTB)	Sertoli cells (EC) - Disturbs assembly of Sertoli cells - Interferes with Occl-Occl interactions - ↓ in TER	Intratesticular injection - Antispermatogenic effect - Disruption of BTB - Reversible infertility	Chung et al., 2001
$ECL1_{90-135}$ (A) $ECL2_{196-243}$ (B) (human)	Caco-2 cells	- ↑ permeability by A after 2 h but not B. - Lipoamino acid addition to N-term, protects the peptide from degradation and aggregation → rapid apical effect		Tavelin et al., 2003
Cyclic Occl	HUVEC	- Disorganized junctional Occl - Increase neutrophil chemotaxis time and dose independently		Oshima et al., 2003
$ECL1_{101-121}$ $ECL2_{210-228}$ (human)	Polarized human intestinal epithelial cell line (T84)	- Two peptides exhibited different conformation - ECL2: selectively interacted with Occl, Cldn1 and JAM-A - ECL2: Disabled recovery of TJ strands -ECL1: Filed to associate with protein components		Nusrat et al., 2005
$ECL1_{90-103}$ (human)	Human airway epithelial (WD HAE) cells	- Rapid ↓ TER dose-dependently, permeable for ≤2000 kDa - Redistribution of Occl and ZO-1 6h after peptide administration - Cldn1 and-4 unchanged		Everett et al., 2006
$ECL2_{209-230}$ (rat)	Blood-testis barrier (BTB)		Intraperitoneal injection - Transient and reversible disruption of BTB - Partial germ cell loss from testis - Specific to only BTB because peptide was inserted into mutant FSH	Wong et al., 2007

↓, decrease; ↑, increase; ECL, extracellular loop; TER, transcellular electrical resistance; TJ, tight junctions; HUVEC, human umbilical vein endothelial cells; Occl, occludin; ZO-1, *zonula occludens* protein-1; ZO-2, *zonula occludens* protein-2; FSH, follicle stimulating hormone; EC, epithelial cells; Caco-2, human colon carcinoma epithelial; Cldn1, claudin-1; JAM-A, junctional adhesion molecule-A.

Table 2. Claudin peptidomimetics

Derived from	Target	Effect		Literature
		In vitro	***In vivo***	
Claudin-1 $ECL1_{53-80}$	Human intestinal epithelial cells T84	- Reversibly interferes with TJ structure and function - Interacted with Cldn1 and Occl	Oral administration - ↑ permeability across gastric epithelium, little effect on small intestinal epithelium	Mrsny et al., 2008
Claudin-1 $ECL1_{53-81}$ (rat)	Rat perineurial barrier	- Paracellular opening of different epithelial barriers -Redistributes Cldn1 and Occl - Peptide internalized by clathrin pathway -TJ morphology is altered in a more parallel way	Perineurial injection in rats - ↑ permeability ≤66 kDa - ↓ Cldn1 mRNA, protein expression - Opening of blood-nerve barrier, drug delivery facilitation	Sauer et al., 2014; Staat et al., 2015; Zwanziger et al., 2012
Claudin-5 $ECL1_{53-81}$ (murine)	Blood-brain barrier	Brain endothelial and Cldn5 transfected EC) - ↑ permeability ≤40 kDa - Cldn5 down-regulated and redistributed from cell contacts to cytosol - Drug delivery enhanced	iv injections in mouse tail - ↑ Brain uptake of small molecules	Dithmer et al., 2017
cCPE	Intestinal epithelium with Cldn3 or Cldn4	- ↑ permeability ≤ 66 kDa, ↓ TER, ↓ of Occl, ZO-1 (Caco-2)	Rat jejunum epithelium - ↑ permeability ≤ 20 kDa	Katahira et al., 1997; Kondoh et al., 2006; Winkler et al., 2009; Veshnyakova et al., 2012

↓, decrease; ↑, increase; ECL, extracellular loop; TJ, tight junctions; Occl, occludin; EC, epithelial cells; Cldn1, claudin-1, Cldn5, claudin-5; Cldn3, claudin-3; Cldn4, claudin-4; iv, intravenous; cCPE, c-terminal region of *Clostridium perfringens* enterotoxin; ZO-1, *zonula occludens* protein-1; Caco-2, human colon carcinoma epithelial;

1.10. STATE OF RESEARCH

Tric is a unique TJ protein due to its tricellular localization and important role in maintaining paracellular tightness. To date, most studies have focused on Tric's barrier forming function and interaction with other TJ proteins. However, it is necessary to have expression profile of Tric in all organs and specific tissues. For instance, we lack clear information about the localization of Tric in brain capillaries, the knowledge which would facilitate the

investigation of endothelial cell barriers. Tric is located at the central of TJ network and it interacts with both bicellular and tricellular TJ proteins because it extends through the basolateral part. Certainly advancing technology and microscopy techniques will help to reveal the interaction and localization of TJ proteins establishing complicated TJ organization.

It is known that TJ proteins compensate for each other when any one of them is knocked down or modulated. Nevertheless, it is not possible to make detailed explanations without the information about the signalling pathway that regulates transcription of Tric. The complete crystal structure of Tric is unavailable. Likewise there is not much information about the link between pathologies and altered Tric expression, structure and function. Most importantly, Tric can be targeted in the course of developing a peptide-based barrier opening approach like Cldn and Occl peptidomimetics. This would be a more specific therapeutic strategy due to Tric's distinct location.

2. AIM

There is limited knowledge about structure, function and regulation of tricellular contacts. This study focused therefore on understanding the tricellular organization of TJ proteins which is involved in tissue barriers. To modulate tricellular structure and paracellular tightness, a tricellulin ECL2 derived peptide called “trictide” was designed. Tric ECL2 region plays a role in interactions of Tric between adhering cells and contributes to paracellular tightness. The aim was to specify a peptidomimetic approach to tricellular junctions by modulating tricellulin and to develop trictide as a potential drug enhancer to overcome tissue barriers. Thus, functional and molecular alterations caused by trictide were investigated.

Time- and concentration dependency of trictide on paracellular passage towards different markers will be examined to demonstrate function of trictide as barrier opener. To recognize the molecular basis of functional changes in barriers, the alterations in localization of Tric and several Tric interacting TJ proteins will be inspected after trictide. In addition, changes in the localization, disruption of *cis*-interactions between TJ proteins within the plasma membrane, up- or down-regulation of protein and mRNA expressions will be studied. After cellular studies, trictide administration in mice are planned to prove the impact of trictide *in vivo*. Tracer uptake of major organs, mRNA expressions of TJ proteins in brain and kidney and also stability of the peptide in blood plasma will be investigated. In order to understand the molecular function of trictide, the tertiary structure and secondary structural elements should be elucidated. The structure of non-functioning control peptide (scrambled trictide) will also be analyzed to visualize structural differences relevant to the effectiveness of the trictide. Finally, tricellular TJ morphology in brain capillaries will be examined. In order to fully comprehend the functional consequences of trictide treatment, localization and amount of TJ proteins within brain capillaries will be inspected.

Overall, the functional and molecular modifications caused by trictide will enable to realize necessary components and protein interactions of tricellular TJs for a functional barrier. Moreover, trictide will be tested as a novel peptidomimetic by targeting the tricellular TJs and opening the tissue barriers that can be considered as a drug enhancer in future studies.

3. MATERIALS AND METHODS

3.1. MATERIALS

The tables below summarize the chemicals and consumables used in this study, with the supplier listed as well. Unless stated otherwise, all basic chemicals were purchased from Thermo Fisher Scientific Inc., USA.

Table 3. Chemicals

Substance	Supplier
2-Methylbutane	Carl Roth, Karlsruhe, Germany
Acetic acid	VWR Chemicals, Darmstadt, Germany
Acetone	VWR Chemicals, Darmstadt, Germany
Acetonitril	J. T. Baker, Deventer, The Netherlands
Acrylamid/Bisacrylamid mixture 40%	Carl Roth, Karlsruhe, Germany
Agarose	Serva Electrophoresis GmbH, Heidelberg, Germany
Albumin Fraction	Carl Roth, Karlsruhe, Germany
Ammoniumperoxidsulfate (APS)	Bio-Rad Laboratories GmbH, Munich, Germany
Ampicillin	Carl Roth, Karlsruhe, Germany
Collagen (rat tail)	Roche, Mannheim, Germany
Dimethyl Sulphoxide(DMSO)	Sigma-Aldrich, Steinheim, Germany
dNTP (Deoxynucleotide) mix(10 mM)	Fermentas Life Science, St. Leon-Rot, Germany
Dulbecco's modified eagle medium	Life Technologies, Darmstadt, Germany
Dulbecco's phosphate buffered saline	Life Technologies, Darmstadt, Germany
Ethanol	VWR Chemicals, Darmstadt, Germany
Ethylenediaminetetraacetic acid	Carl Roth, Karlsruhe, Germany
Ethylenglykol	Carl Roth, Karlsruhe, Germany
Fetal calf serum albumin	Life Technologies, Darmstadt, Germany
Geneticin (G418)	Carl Roth, Karlsruhe, Germany
Glycerol	Carl Roth, Karlsruhe, Germany
Hank's balanced salt solution	Life Technologies, Darmstadt, Germany
Hoechst 33342	Life Technologies, Darmstadt, Germany
Isopropanol	Chemicals, Darmstadt, Germany
Kanamycin	Carl Roth, Karlsruhe, Germany
L-cysteine	Carl Roth, Karlsruhe, Germany
MEM Non-Essential Amino Acids Solution (100X)	Life Technologies, Darmstadt, Germany
Methanol	VWR Chemicals, Darmstadt, Germany
Milk powder	Carl Roth, Karlsruhe, Germany
Opti-minimal-essential-medium	Life Technologies, Darmstadt, Germany
Paraformaldehyde (PFA)	Sigma-Aldrich, Steinheim, Germany
Penicillin/streptomycin	Carl Roth, Karlsruhe, Germany
Polyethylenimine (PEI)	Polyscience, Eppelheim, Germany
Poly-L-lysine (PLL)	Sigma-Aldrich, Steinheim, Germany
Ponceau	Sigma-Aldrich, Steinheim, Germany
Rotiphorese Gel 30	Carl Roth, Karlsruhe, Germany
Sodium- Dodecyl sulfate	Sigma-Aldrich, Munich, Germany
Tetramethylethylenediamine	Carl Roth, Karlsruhe, Germany
Trichloroacetic acid	Carl Roth, Karlsruhe, Germany
Tricin	Carl Roth, Karlsruhe, Germany
Tris Base	Carl Roth, Karlsruhe, Germany
Triton X-100	Carl Roth, Karlsruhe, Germany
Trypsin/Ethylenediaminetetraacetic acid-solution	Life Technologies, Darmstadt, Germany
Tween 20	Carl Roth, Karlsruhe, Germany

Table 4. Devices

Device	Supplier
Agarose gel chamber Agagel Mini	Biometra GmbH, Göttingen, Germany
Analytical scale, AT21 Comparator	Metler Toledo, Gießen, Germany
Blotting system Mini Trans-Blot® Cell	Bio-Rad Laboratories GmbH, Munich, Germany
Centrifuge 5415C	Eppendorf, Hamburg, Germany
Centrifuge 5810R	Eppendorf, Hamburg, Germany
Clean bench S-1200	BDK Luft- und Raumtechnik, Sonnenbühl-Genkingen, Germany
Confocal spinning disk microscope Nikon_CSU	Nikon GmbH, Düsseldorf, Germany
Cryocontainer, CryoTherm Bio-Safe	Cryotherm GmbH Kirchen/Sieg, Germany
Cryostat, CM 3000 Leica	Leica Microsystems, Wetzlar, Germany
Direct Detect Spectrometer	Merck Chemicals GmbH, Darmstadt, Germany
Dounce tissue grinder set	Sigma-Aldrich Chemie GmbH, Steinheim, Germany
Electric cell-substrate impedance sensing (ECIS) instrument ECIS 1600R + 16 well array station	Applied Biophysics Inc, Troy, NY, USA
Electrophoresis power supply (SDS-PAGE), Powerpac 1000	Bio-Rad Laboratories GmbH, Munich, Germany
Electrophoresis power supply (agarose gel) Consort E835	Sigma-Aldrich Chemie GmbH, Steinheim, Germany
Flow cytometer, FACSAria	Becton Dickinson, Heidelberg, Germany
Fluorescence microscope, Zeiss Axiovert 135 TV	Carl Zeiss Jena GmbH, Jena, Germany
Fluorescence Scanner, FLA-5000	Fujifilm, Tokio, Japan
Glass plates (SDS-PAGE) Hoefer, vertical slab gels	Hoefer, Pharmacia Biotech Inc. San Francisco, CA, USA
Hand electrode, EVOM Voltohmmeter WPI	WPI, Sarasota, USA
Heating block, Thermomixer 5436	Eppendorf, Hamburg, Germany
Hemocytometer	Carl Roth GmbH, Karlsruhe, Germany
Incubator for cell culture CB210	Binder GmbH, Tuftlingen, Germany
Laminar Flow Hood, S-1200	BDK Luft- und Raumtechnik, Sonnenbühl-Genkingen, Germany
Laser scanning microscope LSM 780 &710	Carl Zeiss Jena GmbH, Jena, Germany
Laser scanning microscope 510 META-NLO	Carl Zeiss Jena GmbH, Jena, Germany
Leica SP8 TCS STED microscope	Leica Microsystems, Wetzlar, Germany
Light microscope, IMT-2	Olympus Europa GmbH, Hamburg, Germany
Magnetic stirrer, IKAMA ® RCT	IKA®-Labortechnik, Staufen, Germany
Monochromator-based microplate detection system, Safire	Tecan Group Ltd, Männedorf, Switzerland
PCR-thermocycler, DNA Engine	Bio-Rad Laboratories GmbH, Munich, Germany
pH-meter, CG 840	Schott AG, Mainz, Germany
Real Time PCR system StepOne TM Real-Time PCR system, 48/96 well	Life Technologies GmbH, Darmstadt, Germany
General type scale MC1 LC 2200S	Sartorious AG, Göttingen, Germany
SDS-PAGE gel chamber, Mini-PROTEAN® Tetra Vertical Electrophoresis Cell	Bio-Rad Laboratories GmbH, Munich, Germany
Shaker, TH 15	Edmund Bühler GmbH, Hechingen, Germany
Spectral photometer NanoDrop, 2000c	Thermo Fisher Scientific GmbH, Bremen, Germany
Spectropolarimeter, J-720	Jasco, Tokyo, Japan
Transilluminator, ChemiDoc™ MP System #1708280	Bio-Rad Laboratories GmbH, Munich, Germany
Vortex device, VF-2	IKA -Labortechnik, Staufen, Germany
Waterbath, 1002 GFL	GFL, Burgwedel, Germany
Sonorex super ultrasonic bath	Bandelin, Berlin, Germany

Table 5. Consumables	**Supplier**
1µ-Slide 8 Well Glass Bottom	Ibidi, Martinsried, Germany
Amicon Ultra-15 Centrifugal Filter Device (30K, 100K)	Merck Millipore, Billerica, MA, USA
BD Falcon (polystyrene Round-Bottom)	BD, Dickinson, Franklin Lakes, NJ, USA
Cell culture flask, CellBIND *Surface*	Corning, NewYork, USA
Cell culture flask, Cellstar	Greiner Bio-One Frickenhausen, Germany
Cover glasses 24x50 mm	Roth, Karlsruhe, Germany
Coverslips (diameter 12 and 30 mm)	Menzel GmbH, 15 Braunschweig, Germany
Cryogenic vial 1.2 mL	Corning, NewYork, USA
Dako Pen, Delimiting pen	Agilent, Santa Clara, CA, USA
Direct Detect Assay-free Cards	Merck Chemicals GmbH, Darmstadt, Germany
ECIS chip 8W10E+	Ibidi GmbH, Planegg / Martinsried, Germany
Electroporation cuvette	Peqlab, Biotechnologie GmbH, Erlangen Germany
Filter, Millicell (CM)	Merck Millipore, Darmstadt, Germany
Filter, Millicell (PCF)	Merck Millipore, Darmstadt, Germany
MicroAmp Fast Optical 96-Well Reaction Plate	Life Technologies GmbH, Darmstadt, Germany
MicroAmp Optical Adhesive Film	Life Technologies GmbH, Darmstadt, Germany
Mini-PROTEAN TGX 4–20% Protein Gel	Bio-Rad Laboratories GmbH, Munich, Germany
Nitrocellulosemebrane, Hyband-ECL, 0,45 µm	GE Healthcare, Little Chalfont, UK
Omican 100 insulin syringes	B. Braun Vet Care GmbH, Tuttlingen, Germany
Pall Nanosep centrifugal device with Omega membrane 10 kDa	Sigma-Aldrich Chemie GmbH, Steinheim, Germany
Quarz cuvette, 100-QS	Hellma Analytics, Müllheim, Germany
Super frost ultra plus object slide	Menzel GmbH, 15 Braunschweig, Germany
Tissue culture plate, 48 wells	Corning, NewYork, USA
Tissue culture plate, 6-, 24- , 96 wells	TPP, Trasadingen, Germany
ZipTip, C18 columns	Merck Millipore, Darmstadt, Germany

Table 6. Commercial solutions/enzymes and kits

Solution	**Supplier**
1 kb DNA Ladder (GeneRuler TM)	Fermentas Life Science, St. Leon-Rot, Germany
6x DNA loading dye	Fermentas Life Science, St. Leon-Rot, Germany
AccuPol DNA Polymerase	VWR International GmbH, Darmstadt, Germany
Amylose resin	New England Biolabs, Ipswich, MA, USA
DNA clean and concentrator-5 kit	Zymo Research, Irvine, CA, USA
dNTPs (10 mM)	Fermentas Life Science, St. Leon-Rot, Germany
E.Z.N.A. Plasmid Mini Kit I	VWR International GmbH, Darmstadt, Germany
Fast Digest HindIII and Not I	Fermentas Life Science, St. Leon-Rot, Germany
GeneMATRIX Universal RNA Purification Kit	EURx Ltd. Gdansk, Poland
Immu-Mount	Thermo Fisher Scientific Inc., Waltham, MA, USA
Lumi-Light Western Blotting Substrate	Roche Diagnostics GmbH, Mannheim, Germany
Luminaris Color HiGreen qPCR Master Mix, high ROX qPCR Master Mix	ThermoFisher Scientific, Waltham, MA, USA
Maxima First Strand cDNA Synthesis Kit for RT-qPCR	Thermo Fisher Scientific Inc., Waltham, MA, USA
PageRuler Plus Prestained Protein Ladder	Thermo Fisher Scientific Inc., Waltham, MA, USA
ProLong Gold Antifade Mountant	Thermo Fisher Scientific Inc., Waltham, MA, USA
SuperSignal West Femto Maximum Sensitivity	ThermoFisher Scientific, Waltham, MA, USA
SYBR Safe DNA gel staining solution (10000x concentrated in DMSO)	Invitrogen GmbH, Darmstadt, Germany
T4-DNA-ligase	Promega, Madison, WI, USA
Talon Superflow Metal Affinity	Clontech Laboratories, Mountain View, CA, USA
Taq DNA Polymerase + Buffer	Roboklon GmbH, Berlin, Germany
Tissue-Tek	VWR International GmbH, Darmstadt, Germany
ZR Plasmid Miniprep TM -Classic	Zymo Research Corp, Irvine, CA, USA

Table 7. Antibodies

Primary antibodies	**Species**	**Concentration**	**Supplier**
Anti-Tricellulin # 48-8400	rabbit	0.25 mg/ml; IF 1:150, STED 1:100 IHC 1:75, WB:1:1000	Invitrogen, Thermo Fisher Scientific, Schwerte, Germany
Anti- Claudin-1 #51-9000	rabbit	0.5 mg/ml; IF 1:150, STED 1:100, WB 1:1000	Invitrogen, Thermo Fisher Scientific, Schwerte, Germany
Anti-Occludin #33-1500	mouse	0.5 mg/ml; IF: 1:150, IHC: 1:100, STED 1:100, WB 1:1000	Invitrogen, Thermo Fisher Scientific, Schwerte, Germany
Anti- Claudin-5 #34-1600	rabbit	0.25 mg/ml WB: 1:1000 STED, IF: 1: 100	Invitrogen, Thermo Fisher Scientific, Schwerte, Germany
Anti- Claudin-5 #1548773A	mouse	0.5 mg/ml, IF, IHC 1:100	Invitrogen, Thermo Fisher Scientific, Schwerte, Germany
Anti- GAPDH #G8795	mouse	1 mg/ml WB 1:1000	Sigma-Aldrich, Munich, Germany
Anti MarvelD3 # AV44715	rabbit	1 mg/ml WB: 1:500	Sigma-Aldrich, Munich, Germany
Anti- ZO-1 #339100	mouse	0.5 mg/ml STED: 1:100	Invitrogen, Thermo Fisher Scientific, Schwerte, Germany
Anti- ZO-1 #LSC124822	rat	0.5 mg/ml STED 1:100	BIOZOL Diagnostica Vertrieb GmbH, Eching, Germany
Anti-LSR #ABIN949343	mouse	50 µg/ml IF: 1:150 IHC: 1:50 WB: 1:500	Abnova, Taipei City, Taiwan
Anti-6X-His #MA1-21315	mouse	1 mg/ml WB 1:1000	Invitrogen™, Thermo Fisher Scientific, Schwerte, Germany
Secondary antibodies	**Species**	**Concentration**	**Supplier**
Anti-Rabbit Atto 488 #18771	goat	1 mg/ml IF 1:250	Sigma-Aldrich Chemie GmbH, Steinheim, Germany
Anti-Mouse_IgG-Cy3(555) #A10520	goat	1 mg/ml IF 1:250	Invitrogen, Thermo Fisher Scientific, Schwerte, Germany
Anti-Rabbit HRP #1708241	goat	0.8 mg/ml WB: 1:1000	Bio-Rad Laboratories Inc., Hercules, CA, USA
Anti-Mouse HRP #1706516	goat	0.8 mg/ml WB: 1:1000	Bio-Rad Laboratories Inc., Hercules, CA, USA
Alexa fluor 594 anti-rabbit IgG Ref # A11072	goat	2 mg/ml STED 1:300	Life Technologies, Eugene, Oregon, USA
Alexa fluor 594 anti-rat IgG Ref# A11007	goat	2 mg/ml STED 1:300	Life Technologies, Eugene, Oregon, USA
Alexa fluor 594 F(ab')anti-mouse IgG Ref#A11020	goat	2 mg/ml STED 1:1000	Life Technologies, Eugene, Oregon, USA
Abberior STAR 635P anti mouse IgG #2-0002-007-5	goat	1 mg/ml STED 1:300	Abberior GmbH, Göttingen, Germany
Abberior STAR 635P anti rabbit IgG #2-0012-007-2	goat	1 mg/ml STED 1:300	Abberior GmbH, Göttingen, Germany

IF, immunofluorescence; WB, western blot; IHC, immunohistochemistry; STED, stimulated emission depletion.

Table 8. Plasmids

Plasmid	Characteristics	Reference
pEYFP-C1-Tric	5.3 Kb; Ampr/Neor, SV 40 ori, pUC ori, PCMV IE; EYFP(reporter) N-terminal, tric	O. Huber, Charite-Berlin, 2009, Germany
pECFP-C1-Tric	5.3 Kb; Ampr/Neor, SV 40 ori, pUC ori, PCMV IE; ECFP(reporter) N-terminal, tric	O. Huber, Charite-Berlin, 2009, Germany
pEYFP-C1-Occl	5.3 Kb; Kanr/Neor, SV 40 ori, pUC ori, PCMV IE; EYFP(reporter) N-terminal, occludin	C. Bellmann, FMP-Berlin, 2010, Germany
pECFP-C1-Occl	5.3 Kb; Kanr/Neor, SV 40 ori, pUC ori, PCMV IE; ECFP(reporter) N-terminal, occludin	C. Bellmann, FMP-Berlin, 2010, Germany
pEYFP-C1-MD3	5.3 Kb; Kanr/Neor, SV 40 ori, pUC ori, PCMV IE; EYFP(reporter)N-terminal, marvelD3	J. Cording, FMP-Berlin, 2011, Germany
pECFP-C1-MD3	5.3 Kb; Kanr/Neor, SV 40 ori, pUC ori, PCMV IE; EYFP(reporter)N-terminal, marvelD3	M. Balda, UCL-London, UK
pETRQ-C1-Cld1	5.3 Kb; Kanr/Neor, SV 40 ori, pUC ori, PCMV IE; EYFP(reporter) N-terminal, Cld1	N. Gehne, FMP-Berlin, 2013, Germany
pEYFP-N1-Cld1	5.3 Kb; Ampr/Neor, SV 40 ori, pUC ori, PCMV IE; EYFP(reporter) C-terminal, Cld1	S. Müller, FMP-Berlin, 2006, Germany
pMAL-C2X	6.7 kb; Ampr; pMB1 ori; M13 ori; Ptac; lacIq; lacZα; Maltose-binding protein (MBP) N-terminal	New England Biolabs (NEB), Ipswich, USA

Table 9. Primers used for qRT-PCR

Primer	**Sequence (5'→3')**	
	fw	*rev*
hActb	GGACTTCGAGCAAGAGATGG	AGCACTGTGTTGGCGTACAG
hTric	AGGCAGCTCGGAGACATAGA	TCACAGGGTATTTTGCCACA
hOcln	TCCAATGGCAAAGTGAATGA	GCAGGTGCTCTTTTTGAAGG
hMarveld3	GGACCCGGAGAGAGACCAG	CTCCGAAGGGGGTTCACT
hLSR	GTGACCCTGCCCTGTACCTA	TCAACGTAGGGGTTGTAGCC
hZO1	GAACGAGGCATCATCCCTAA	CCAGCTTCTCGAAGAACCAC
hCldn1	CGATGCTTTCTGTGGCTAAAC	GAGGGCATCACTGAACAGATAG
hCldn5	GAGGCGTGCTCTACCTGTTT	GTACTTCACGGGGAAGCTGA
mActb	TTTGAGACCTTCAACACCCC	ATAGCTCTTCTCCAGGGAGG
mTric	GAGAATCCTGGGTGTGGTGG	TTTCGATGACAACGACGGGT
mOcln	ACTCCTCCAATGGCAAAGTG	CCCCACCTGTCGTGTAGTCT
mMarveld3	TGGAGAAGTCCCGTCAAAGC	AGCCACTATAAGCCCCTCCA
mLSR	GACCTGACCTTCGAGCAGAC	AGGAAGAAGAGGAGGCTTGC
mCldn1	GATGTGGATGGCTGTCATTG	CGTGGTGTTGGGTAAGAGGT
mCldn5	CTGGACCACAACATCGTGAC	GCCGGTCCAGGTAACAAAGA
mCldn12	AACTGGCCAAGTGTCTGGTC	AGACCCCCTGAGCTAGCAAT
mCldn25	CTACATGGCGGCCTCCATAG	CGATGCCGCTATTGTGGTTG
mZO1	CCCACCCCCATCTCAGAGTA	GGGACAGCTTTAGGCATGGT

Table 10. Primers used for mutagenesis PCR of hTric ECL2

Primer	**Sequence (5'→3')**	
	fw	*rev*
Y322I	GGCCTCTGCATCTATCCGTTATTTAATA CACCA	AAATAACGGATAGATGCAGAGGCCACC TCG
Y322A	GGCCTCTGCGCGTATCCGTTATTTAATA CACCA	AAATAACGGATACGCGCAGAGGCCACC TCG
F326A	CCGTTAGCGAATACACCAGTG	TGTATTCGCTAACGGATAGTAGCA
F334I	GCAGTGATATGCCGGGTAGAAGGA	CCGGCATATCACTGCATTCACTGG

Table 11. Primers used for amplification of recombinant proteins

Primer	**Sequence (5'→3')**	
	fw	*rev*
hTric C-term$_{(362-558)}$	GCATTAGCTTAAAGTTATGGAGGCATGA G	GCTTATAGCGGCCGCTTAAGAATA ACC TTG

Primers used for MBP-hTric ECL2

Primer	**Sequence (5'→3')**	
	fw	*rev*
hTric ECL2$_{(313-336)}$	AATGATACCAACCGAGGTGGCCTCTGCT AC	CCGGCAGAACACTGCATTCACTGGTGT ATT

Different biological samples were listed in Table 12. In addition, C57BL/6 mice obtained from the MDC animal facility (Berlin, Germany) were used for the purposes of this dissertation.

Table 12. Eukaryotic cells and bacteria

Cell type/bacteria	Description	Source
bEND.3	Mouse brain endothelial cell line	Zwanziger et al., 2012b
Caco-2	Human epithelial colorectal adenocarcinoma cells	Bayer Pharma AG, Berlin, Germany
HEK-293	Human embryonic kidney cells	ATCC, Manassas, VA, USA
HT29/B6	Human epithelial colon adenocarcinoma cells	S. Krug, Charite–Berlin, Germany
MDCK-II	Madin-Darby canine kidney cells	ATCC, Manassas, VA, USA
Escherichia coli	BL21	Life Technologies, Darmstadt, Germany

Table 13. Fluorescent size markers for permeation experiments

Size marker for permeation	Supplier	Fluorescence properties
FD10, 10 kDa	Sigma-Aldrich Chemie GmbH, Steinheim, Germany	λ_{ex} = 485 nm, λ_{em} = 520 nm
FD40, 40 kDa	Sigma-Aldrich Chemie GmbH, Steinheim, Germany	λ_{ex} = 485 nm, λ_{em} = 520 nm
Lucifer Yellow, 0.4 kDa	Sigma-Aldrich Chemie GmbH, Steinheim, Germany	λ_{ex} = 425 nm, λ_{em} = 520 nm
Sodium fluorescein	Sigma-Aldrich Chemie GmbH, Steinheim, Germany	λ_{ex} = 460 nm, λ_{em} = 515 nm

FD, fluorescein isothiocyanate–dextran; λ_{ab}, wavelength of the absorption; λ_{ex}, excitation wavelength; λ_{em}, emission wavelength.

Table 14. Other colored markers

Type of marker	Supplier	Fluorescence properties
Ethidium bromide solution, 1%	Carl Roth, Karlsruhe, Germany	λ_{ab} = 210 or 285 nm
Hoechst 33342	Thermo Fisher Scientific, Schwerte, Germany	λ_{ex} = 350 nm, λ_{em} = 461 nm
Methylthiazolyldiphenyl-tetrazoliumbromide (MTT)	Sigma-Aldrich Chemie GmbH, Steinheim, Germany	λ_{ab} = 570 nm
Fluorescein sodium	Sigma-Aldrich Chemie GmbH, Steinheim, Germany	λ_{ex} = 460 nm, λ_{em} = 515 nm
Neutral red solution, 0.5 % in acetic acid pH 5.2	Sigma-Aldrich Chemie GmbH, Steinheim, Germany	λ_{ab} = 540 nm
TAMRA	Thermo Fisher Scientific, Schwerte, Germany	λ_{ex} = 543 nm, λ_{em} = 560 nm
Tricellulin-YFP fusion protein		λ_{ex} = 514 nm, λ_{em} = 516-537 nm
Occludin-CFP fusion protein		λ_{ex} = 442 nm, λ_{em} = 480-520 nm
Claudin-1-TRQ fusion protein		λ_{ex} = 458 nm, λ_{em} =462-494 nm

TAMRA, (5-(and-6)-Carboxytetramethylrhodamine); YFP, yellow fluorescent protein; CFP, cyan fluorescent protein, TRQ, turquoise fluorescent protein; λ_{ab}, wavelength of the absorption; λ_{ex}, excitation wavelength; λ_{em}, emission wavelength.

Table 15. Software

Program	Manufacturer / Source
BIOVIA Discovery-Studio, version 4.5	Accelrys, San Diego, USA
BLAST	NCBI, Rockville Pike, USA
Huygens Professional	Scientific Volume Imaging, Hilversum, The Netherlands
ImageJ, version 1.49k	W. Rasband, National Institutes of Health, Maryland, USA
I-TASSER	Roy et al., 2010; Zhang, 2008
Leica Application Suite X (LAS X)	Leica Mikrosysteme Vertrieb GmbH, Wetzlar, Germany
Mendeley	Elsevier, New York City, NY, USA
MS Office 2010	Professionel Microsoft, Unterschleißheim, Germany
PEP-FOLD	Shen et al., 2014; Thevenet et al., 2012
Prism 5, version 5.04	GraphPad, San Diego, USA
Spectra Manager, version 1.54.03	Jasco, Tokyo, Japan
StepOne Software version 2.2.1	Applied Biosystems, Foster City, USA
Zeiss LSM Image Browser, version 4.2.0.121	Carl Zeiss, Jena, Germany
ZEN 2010B SP1	Carl Zeiss, Jena, Germany

3.2. METHODS

3.2.1. Peptide design and synthesis

Peptides were synthesized automatically by peptide chemistry facility (FMP-Berlin, Germany) using 9H-fluoren-9-ylmethoxycarbonyl (Fmoc) chemistry. Identity and quality of peptides were verified by high-performance liquid chromatography and mass spectrometry, showing a purity of ≥95% (220 nm) and the expected masses. Trictide (Table 16) comprises extracellular loop 2 (ECL2) of human tricellulin-a ($Tric_{313–336}$); Cys321 and Cys335 were replaced by Ser to avoid unspecific oligomerization. As a control, a scrambled variant (scrambled peptide, Table 16) was used. Peptides were amidated at the C-terminus. Trictide was labelled N-terminally with 5,6-carboxytetramethylrhodamine (TAMRA) (Table 16).

Table 16. Peptide sequences

Peptide	Description	Sequence
Trictide	ECL2 of human tricellulin, 313–336	NDTNRGGLSYYPLFNTPVNAVFSR-NH2
Scrambled trictide	Control peptide	DNLNRGGASYTPFYLNVPNFVTSR-NH2
TAMRA-trictide		TAMRA-NDTNRGGLSYYPLFNTPVNAVFSR-NH2

3.2.2. Cell Culture

3.2.2.1. Routine cell culture work

The cells (Table 12) were incubated at 37 °C and 5% or 10% CO_2 in cell-specific medium and cell-culture flasks (Table 17). After washing (2x, *Dulbecco's phosphate-buffered saline,* without Ca^{2+} and Mg^{2+}, DPBS-/-) and dissociation with trypsin/ethylenediaminetetraacetic acid (EDTA) solution at 37 °C, they were resuspended in the new medium and centrifuged (150xg, 4 min). The pellet was taken up in new medium, resuspended and transferred on cell culture flasks (Table 17) or tissue culture plates (Table 5).

Table 17. Culturing conditions of eukaryotic cells

Cell type	Medium compositions	CO_2	Culture flask	Cell dissociation
bEnd.3	DMEM, 4.5 g/l glucose, 10% FCS, 100 U/ml penicillin, 100 µg/ml streptomycin	10%	Cellstar#	0.25%Trypsin/0.02% EDTA
Caco-2	DMEM, 1 g/l glucose, 20% FCS, 100 U/ml penicillin, 100 µg/ml streptomycin, 1x NEAA	5%	CellBIND# *Surface*	0.25%Trypsin/0.02% EDTA
HT29/B6	RPMI 1640 Medium with stable L-glutamine, 10% FCS, 100 U/ml penicillin, 100 µg/ml streptomycin	5%	Cellstar#	0.25%Trypsin/0.02% EDTA
MDCK-II HEK-293	DMEM, 1 g/l glucose, 20% FCS, 100 U/ml penicillin, 100 µg/ml streptomycin*	10%	Cellstar#	0.25%/0.05% Trypsin /0.02% EDTA

* after transfection cultured with geneticin (final 0.5 µg/ml); DMEM, *Dulbecco's modified eagle*-medium; EDTA, ethylenediaminetetraacetic acid; FCS, fetal calf serum albumin; NEAA, non-essential amino acids; RPMI, *Roswell Park Memorial Institute*-Medium, %, (v/v); #, further information about products can be find in Table 5.

3.2.2.2. Cryopreservation and thawing of cells

Almost confluent cells (around 85% conflueny) were washed (2x, DPBS-/-), dissociated with trypsin/EDTA (Table 17) and centrifuged at 150xg, 4 min. The cell pellet was resuspended in freezing medium (90% fetal calf serum (FCS), 10% DMSO) and aliquoted in cryotubes. The tubes were first cooled down to -20 °C at a cooling rate of 1 °C/min and finally stored in liquid nitrogen at -196 °C.

For reactivation, the cryoculture was thawed in a 37 °C water bath and immediately resuspended in cell-specific medium (Table 17). This suspension was centrifuged (150xg, 4 min) to eliminate DMSO in freezing medium. After centrifugation, the cell pellet was resuspended in new medium and transferred to a cell culture flask.

3.2.2.3. Cell counting

An aliquot of the cell suspension was diluted 1:2 with cell-specific medium. From that, 20 µl were applied to a Neubauer counting chamber. After counting the 4 counting areas, the cell count/ml was calculated by taking the mean of cell number (total cell number/number of counted areas) and multiplied by 10^4 and the dilution factor 2.

3.2.2.4. Transfection and obtaining stable transfected cell lines

Tissue culture plates (6 wells) were used for the preparation of stably transfected cell lines. Wells were coated with poly-L-lysine (PLL, 20 µg/ml in DPBS-/-) (1 h, 1.5 ml), washed (2x, DPBS-/-) and HEK-293/MDCK-II cells seeded there (2.2.2.1). Medium was removed and transfection procedure was initiated at a confluency of 90%. The plasmid DNA (2 µg) as well as polyethyleneimine (PEI) (10 µl) were mixed separately with 250 µl Opti-minimal essential medium per well and incubated for 5 min. Then the DNA and PEI were mixed (1:1) and left for 20 min of additional incubation before finally being added to the culture plates (3 ml transfection medium/10 cm^2). The next day the selection antibiotic, geneticin (final 0.5 µg/ml), was added. After 48 h the transfection success was verified by microscopic analysis of the fluorescently tagged proteins.

3.2.2.5. Cell cultivation on coverslips and filters

For MDCK-II, HEK-293 and Caco-2 cells, the coverslips (1.1 cm^2, 9.6 cm^2) were coated with PLL (20 µg/ml in DPBS-/-) while for bEnd.3 cells the coverslips were coated with rat tail collagen (0.67 mg/ml in 0.2% acetic acid). For each coverslip 0.3 ml/cm^2 of coating material is applied and incubated at 22 °C for 1.5 h. The coverslips were washed (DPBS-/-) prior to cell seeding of the cells. The cells were seeded on coverslips under the conditions described in 3.2.2.1.

For Caco-2 cells, the filters were coated with 150 µl rat tail collagen (0.67 mg/ml in 0.2% acetic acid, 1:2 in DPBS-/-) per filter (type: CM, pore size 0.4 µm, Table 5) and dried overnight on a 37 °C hot plate. The washing (DPBS-/-) step was followed by equilibration of the filters with cell-specific medium (apical 400 µl, basal 600 µl, Table 17) for 2 h in the incubator. Then $18 \cdot 10^4$ cells were seeded per filter (culture area: 4.2 cm^2).

HT-29/B6 cells were grown on permeable supports (type: PCF, 3 µm pore-size, Table 5) and left for monolayer differentiation for seven days.

3.2.2.6. Application of peptide on cells

The peptides (Table 16) were weighed by analytical balance (AT21 Comparator, Metler Toledo) and dissolved in cell-specific medium (Table 17) at 37 °C. Before the peptide treatment, the medium was taken off and replaced by peptide-containing medium.

TAMRA-labelled peptides are first dissolved in DMSO (1% of total volume) and then in cell-specific medium.

3.2.3. Functional assays

The tightness of the cell monolayer was determined by transcellular electrical resistance (TER) and paracellular permeation measurements. While TER reflects permeability to ions, permeation measurements enabled us to draw conclusions about the permeability of a cell barrier for molecules of different sizes (Table 13). The combination of both methods allows correlation of change, in the paracellular tightness and in the permeability for certain molecular sizes.

3.2.3.1. Measuring transepithelial electrical resistance

The TER of the Caco-2 filter cultures (Table 17) was measured every 24 h with chopstick electrodes (on a 37 °C hot plate, three measurements per filter, each value by 120°). Before treatment, filter cultures reached TER values of 205.2±10.6 Ω•cm^2 (empty control subtracted, representative values of an experiment, n=21). For the calculation of TER, the average electrical resistance of the empty filter (Ω_L) was extracted from the mean electrical resistance of the cell-grown filter (Ω_Z) and multiplied by the growth area of the filters (cm^2).

$$TER = \left(R_{Cell\ layer} - R_{Empty\ filter}\right) \cdot A \qquad (\Omega \cdot cm^2)$$

$R_{Cell\ layer}$ Resistance of the cell layer between apical and basolateral compartment of cell containing filter

$R_{Empty\ filter}$ Resistance of the cell layer between apical and basolateral compartment of cell-free filter

A Culture area

Filters were grouped leading to similar initial TER values and then were treated with scramble peptide or trictide.

3.2.3.2. Permeation assays

All steps were carried out with 37 °C pre-warmed solutions. Fluorescein isothiocyanate (FITC)–dextran 10 (FD10, 10 kDa), FITC-dextran 4 (FD4, 4 kDa), lucifer yellow (LY, 457 Da) and FITC-dextran 40 (FD40, 40 kDa) were used as permeation markers (Table 13). The permeation coefficient (P_C) was calculated according to formula below.

$$[P_C]=\frac{dQ}{dt} \cdot \frac{1}{A \cdot C_i \cdot 60} \qquad (cm/s)$$

d*Q*/d*t*	Amount of the diffused permeation marker	(µg/min)
A	Growth area of filters	(cm^2)
C_i	Initial concentration of size marker (apical)	(µg/ml)
60	Conversion factor *min* to *s*	

For experiments with Caco-2 cells, three filters were used per each condition. The filters were placed on a 37 °C hot plate and washed 2x with Hank's balanced salt solution with Ca^{2+} and Mg^{2+} (HBSS+/+) (apical 400 µl, basolateral 600 µl). Then the 400 µl permeation solution (8 µM FD10, 0.4 mM FD4, 100 µM LY or 2.5 µM FD40 in HBSS +/+) was applied apically and 600 µl HBSS+/+ was applied basolaterally. During 30 min of incubation on 37 °C hot plate, every one filter from each condition was discarded every 10 min. 3 aliquots of 150 µl were removed from basolateral section of each filter and placed on a tissue culture plate (96 wells). The fluorescence intensities of fluorescence markers (Table 13) were measured with the fluorescence plate reader (Safire, Tecan).

The permeability measurements of the HT-29/B6 cells were taken in multi-well plates in HEPES-Ringer containing unlabeled dextran 4 kDa (FD4; 0.4 mM) at 37 °C. After apical addition of FITC-labeled and dialyzed 4 kDa dextran, basolateral samples were analyzed for their FD4 concentration at 0, 20, 40, and 60, 120 min.

3.2.3.3. Cell viability

Cell culture plates (48 wells) were coated with PLL (20 µg/ml in DPBS-/-, 0.3 ml/well, 5 h) and washed (DPBS-/-). Cells were seeded and grown until they became sufficiently confluent to be tested with substances. Subsequently, the cells were washed (DPBS-/-) and each well was treated with 200 µl of 2.3.5-triphenyltetrazolium chloride (MTT) solution (0.5 mg/ml in Dulbecco's modified Eagle's medium (DMEM), 1 g/L glucose, without phenol red) (Weyermann et al., 2005) or neutral red solution (0.005% in DMEM 1 g/l glucose, without phenol red). After 3 h in the 37 °C incubator, cells were washed with 200 µl/well extraction solution (MTT: 5% Triton X-100, 2% 2N hydrochloric acid, 93% isopropanol; neutral red: 1% acetic acid, 50% ethanol). After 15 min on the vibrator, the absorbance of the homogenates was measured (MTT, 570 nm; neutral red, 540 nm) with a fluorescence plate reader (Safire, Tecan).

3.2.3.4. Electric cell-substrate impedance sensing

Initially, the electric cell-substrate impedance sensing (ECIS) arrays (ECIS chip 8W10E+) were cleaned by 10 mM L-cysteine (200 µl/well) and incubated for 10 min. This treatment constitutes a hydrophilic layer and prepared the surface for protein adsorption. Furthermore it reduces the variation between ECIS wells and improves reproducibility. After washing (3x with cell-specific culture medium), cell-specific culture medium was added to the arrays (200 µl/well) and a high current (3 mA), high frequency (64 kHz) pulse was applied to clean the electrodes (electrical stabilization). The bEND.3 ($5 \cdot 10^4$/well) and Caco-2 ($15 \cdot 10^4$/well) cells were seeded into disposable 8-well electrode arrays of the ECIS and placed in an incubator at 37 °C and 10% CO_2 while the electrical resistance was recorded. When stable TER values were reached [for bEnd.3 cells 1504±206 $\Omega \cdot cm^2$ (n=8, peptide-free medium controls) and for Caco-2 cells 1351±34 $\Omega \cdot cm^2$ (n=10, peptide-free medium controls) compared to the cell-free control with $311 \pm 4\ \Omega \times cm^2$], cells were treated with trictide (50-150 µM), scrambled trictide (150 µM) or peptide-free medium only. The transcellular electrical resistance (TER) was recorded over time (70-100 h) with 1 h intervals, at multiple frequencies (between 100 and 80000 Hz) but 4000 Hz was used to evaluate the TER.

3.2.4. Histological methods

3.2.4.1. Obtaining cryosections

C57BL/6N mice between 8 and 20 weeks of age were sacrificed, their brains removed and immediately frozen in 2-methylbutane on dry ice for 5 min. Unless the brains were intended for immediate use, they were stored at -80 °C. Before cryosectioning, brains were embedded in Tissue-Tek (Table 6) on a metal disc and adapted to -18 °C. 8 µm sections were cut using a microtome blade (MX35 Ultra, ThermoFisher Scientific) at -18 °C. The cut sections were transferred to super frost ultra plus object slides (Table 5) and let stand at room temperature to eliminate excess water. The slides were stored at -80 °C.

The human cortical cryosections were already provided by AMS Biotechnology (Abingdon, United Kingdom) as embedded in Tissue-Tek. They were prepared the same way as mouse brains.

3.2.4.2. Immunohistochemistry of cryosections

Mounted cryosections were taken from -80 °C, fixed with methanol at -20 °C for 10 min. After washing step (1x 0.5% BSA in DPBS-/-) for 5 min and 1x sterile water for 3 min) on a shaker at room temperature, brain sections were circled with water-repelling pen (Dako Pen). 100 µl of primary antibodies (Table 7) were diluted in 0.5% BSA in DPBS-/-, added either together or separately, and left for overnight incubation at 4 °C. The slides were washed again (3x 0.5% BSA in DPBS-/- for 5-10 min and 1x DPBS-/- for 3 min) on a shaker. The secondary antibodies (Table 7) were diluted in DPBS-/-, 100 µl of antibody solution was added on top of brain sections and left at room temperature for 1 h in a dark place. The slides were washed (3x DPBS-/- for 5-10 min) on a shaker and then treated with Hoechst 33342 (16.23 µM in DPBS-/-) for 10 min in the dark. Finally the slides were washed (1x sterile water for 3 min), mounted with Immu-Mount (Table 6), and left for 30 min incubation on 37 °C hot plate. The immunostained slides were stored at 4 °C. For STED microscopy, secondary antibodies were exchanged with STED specific antibodies (Table 7). Cells were mounted in Prolong Gold Antifade (Table 6) and left for 24 h at room temperature before STED microscopy session.

3.2.5. Microscopic investigation

Unless stated otherwise, laser scanning microscopy (LSM 780 &710 Plan-Apochromat 63x/1.4 or 100x/1.4 oil lenses) was used together with ZEN 2010B SP1 software to conduct the experiment. The settings were selected according to the fluorescence properties of the secondary antibodies (Table 7) and markers (Table 14).

3.2.5.1. Immunocytochemistry on cover glasses and filters

The coverslips were placed in a 24-well-tissue culture plate and coated with PLL (20 µg/ml in DPBS-/-, 0.3 ml/well, 1 h, for Caco-2 and MDCK-II cells) or rat tail collagen (0.67 mg/ml in 0.2% acetic acid, 50 µl/well, for bEND.3 cells). Cells were seeded and grown until they became fully confluent. Before fixation, cells were washed twice with ice-cold DPBS-/-. The coverslips were placed into a staining tray with ice-cold acetone for 5 min and ice-cold ethanol for 1 min. After washing for 1 min with ice-cold DPBS-/-, samples were treated with blocking buffer (1% bovine serum albumin (BSA), 0.05% tween20 in DPBS-/-) for 15 min in order to prevent unspecific binding. Cells were incubated with a primary antibody (Table 7) diluted in the blocking buffer for 1 h at room temperature and in a humid chamber. The coverslips were washed (4x 2 min with DPBS-/- then 1x 2 min with blocking buffer) and the cells were incubated with a fluorophore coupled secondary antibody (Table 7), diluted in the blocking buffer for 30 min at room temperature and in a dark humid chamber. Finally the coverslips were washed (4x 2 min with DPBS-/- then 1x 2 min with sterile water) and mounted with Immu-Mount and left for 30 min incubation on 37 °C hot plate.

For cells on filters, cells were first washed twice by addition of ice-cold DPBS-/- into apical and basal compartments. The same fixation protocol as explained above was applied by addition of fixing agents into apical compartments of the filters. Filters were then taken out by cutting with a blade and treated with primary and secondary antibodies the same way as the coverslips. Details related to microscopy techniques can be found in chapter 3.2.5.4.

3.2.5.2. Live cell imaging

The cells cultured on 9.6 cm^2 coverslips (3.2.2.5) were washed 3 times with HBSS+/+, microscoped in HBSS+/+ and kept in 37 °C chamber. The staining of the cell nuclei was

carried out with Hoechst 33342 (5 µM in HBSS+/+, ≥10 min). For the live cell imaging with spin disk confocal microscopy (Nikon_CSU, Germany), glass bottom 8-well cuvette was coated with PLL (20 µg/ml in DPBS-/-, 0.3 ml/well, 1 h). YFP-occludin MDCK-II cells were seeded on glass bottom 8-well cuvettes in (1:3, 0.3 ml/well, in no-phenol red cell specific medium) and waited until they became confluent.

Plan-Apochromat 40x air objective was utilized, and the microscope was adjusted to zoom automatically. Cells were kept inside a regulated chamber (37 °C and 5% CO_2), and every 15 min an image was taken from each pre-saved position and condition over the course of 15 h. TAMRA-trictide was dissolved first in DMSO and then in cell-specific medium [final 10 µM peptide concentration and 1% DMSO (v/v)]. Afterwards TAMRA-trictide was added in wells (30 µl/well from 100 µM stock peptide solution) after the first image.

3.2.5.3. Fluorescence resonance energy transfer

The measurement of the fluorescence resonance energy transfer (FRET) is a distance dependent, radiationless transfer of energy from an excited donor fluorophore to a suitable acceptor fluorophore. FRET is only possible if the molecules are less than 10 nm apart (Sekar and Periasamy, 2003). For analysis of *cis*-interactions between TJ proteins along the cell membrane at cell–cell contacts, HEK cells growing on coverslips (9.6 cm^2) were co-transfected with plasmids encoding Cldn1–YFP and Cldn1-TRQ, YFP–Occl and CFP–Occl, YFP–Tric and CFP–Tric, and CFP–MD3. After 48 h, transfectants were treated with peptide-free medium, 50 µM scrambled peptide- and 50 µM trictide-containing medium, respectively. After another 24 h, living cells were transferred into HBSS +/+ and analyzed by ZEISS LSM 510 META NLO microscope using a PlanNeofluar 100x/1.3 oil objective. For FRET at bTJs, acceptor photobleaching principle was applied (Cording et al., 2013; Kenworthy, 2001). Photobleaching of YFP was performed using 30–40 pulses of the 514 nm argon laser line at 100% intensity (Table 14). Before and after acceptor bleaching, CFP intensity (Table 14) images were recorded to calculate changes in donor fluorescence in the area of cell-cell contacts. We always measured areas with similar CFP and YFP fluorescence intensities. The FRET efficiency (E_F) was calculated as below:

$$E_F = \frac{(I_a - I_b) \cdot 100}{I_a}$$

E_F FRET efficiency

I_a CFP fluorescence intensity after photobleaching

I_b CFP fluorescence intensity before photobleaching

MDCK-II cells were used for FRET measurements in three-cell contacts and treated with peptide-free medium, 50 µM scrambled peptide-, 50 µM and 100 µM trictide-containing medium, respectively.

3.2.5.4. Stimulated emission depletion microscopy (STED)

The coverslips were placed in a 24-well-tissue culture plate and coated with PLL (20 µg/ml in DPBS-/-, 0.3 ml/well, 1 h, for Caco-2 and MDCK-II cells) or rat tail collagen (0.67 mg/ml in 0.2% acetic acid, 50 µl/well, for bEND.3 cells). Cells were seeded and grown until they became fully confluent. Before fixation, cells were washed three times with ice-cold DPBS-/-. The coverslips were placed into a staining chamber with 4% paraformaldehyde (PFA) for 15 min at room temperature. After washing three times with ice-cold DPBS-/-, samples were treated with permeabilization buffer (0.1% Triton X-100 in DPBS-/-) for 10 min. Afterwards, the coverslips were rinsed three times with DPBS-/- and left to incubate with blocking buffer (2% BSA in DPBS-/-) for 1 h at room temperature. Cells were incubated with primary antibody dilutions (Table 7) (1% BSA in DPBS-/-) overnight in a humid chamber at 4 °C. The coverslips were washed (3x 5 min with DPBS-/-) and the cells were incubated with a STED-specific fluorophore coupled secondary antibody (Table 7) (diluted in DPBS-/-) for 1 h in a dark humid chamber at room temperature. Finally the coverslips were washed (3x 10 min with DPBS-/- then 2x 10 min with sterile water) and mounted with Prolong Gold Antifade (Thermo Fischer Scientific) and left for 24 h incubation at room temperature before time gated STED (gSTED) microscopy. STED imaging with time-gated detection was performed on a Leica SP8 TCS STED microscope (Leica Microsystems) equipped with a pulsed white light excitation laser (NKT Photonics).

Dual-channel STED imaging was performed by sequentially exciting Atto647N and Alexa 594 at 646 nm and 598 nm, respectively. Both dyes were depleted with a 775 nm STED laser. One optical section as acquired with an HC PL APO CS2 100x/1.40-N.A. oil objective (Leica Microsystems) (a scanning format of 1.024x1.024 pixel, 8 bit sampling and 6 fold zoom) can yield a pixel dimension of 18.9x18.9nm. Time-gated detection was set from 0.3–6 ns for all dyes. Fluorescence signals were detected sequentially by hybrid detectors at the appropriate spectral regions separated from the STED laser. To minimize thermal drift, the microscope was housed in a heatable incubation chamber (LIS Life Imaging Services). The effective lateral resolution of the SP8 TCS STED microscope was previously determined using 40 nm fluorescent beads (Life Technologies; excitation/emission maxima at 505/515 nm or 660/680 nm) to be 45 nm for the 647 nm channel (Grauel et al., 2016). Raw data obtained from gSTED imaging were deconvolved using Hygens Professional (Scientific Volume Imaging, Netherlands) software and analyzed by custom macro (ImageJ).

3.2.6. Protein biochemistry methods

3.2.6.1. Cell lysis of eukaryotic cells

Cells were washed with ice cold DPBS-/- and, after removal of DPBS-/-, they were scraped off with DPBS-/- (600 µl/9.6 cm^2 well). The remaining cells were collected with additional 600 µl of DPBS-/- and transferred into an eppendorf tube. The tube was centrifuged (150xg, 4 min, 4 °C) and DPBS-/- was removed from cell pellet. Extraction buffer (Table 18, 90 µl/per tube) was added on cell pellet. Cells were resuspended 3-5 times with a pipette and left for incubation on ice for 20 min. Following incubation, the tube was centrifuged (13000xrpm, 1 min, 4 °C) and extraction buffer was discarded. The pellet was homogenized with benzonase-mixture (5 µl/tube) (Table 18) again with a pipette and placed in thermomixer at 37 °C for 10 min. After 10 min, the mixture was homogenized well with a pipette (200 µl pipette tip) and mixed with solubilization buffer (16.6 µl/per well) (Table 18). The mixture was incubated with a thermomixer (Table 4) at 97 °C for 3 min. Finally the extraction buffer (11.7 µl/tube) was added, protein concentrations of the samples were measured (chapter 3.2.6.2) and stored at -80 °C.

Table 18. Ingredients of cell lysis buffers

Extraction-buffer	25 mM HEPES, 150 mM NaCI, 1% Triton X-100, 1:10 protease inhibitor (freshly added), pH 7.4
Solubilization-buffer	50 mM Tris, 5 mM EDTA, 1% SDS, pH 8.8
Benzonase-mixture	1.5 M Tris, 25 mM $MgCI_2$, 35 U/ml benzonase, pH 8.8 in ddH_2O.

HEPES, (4-(2-hydroxyethyl)-1-piperazineethanesulfonic acid); EDTA, ethylenediaminetetraacetic acid; SDS, sodium dodecyl sulfate; dd, double distilled.

3.2.6.2. Determination of protein concentration

The protein concentration was measured by Direct Detect Spectrometer system (Merck Chemicals GmbH) that measures amide bonds in protein chains and determines an intrinsic component of every protein without relying on amino acid composition, dye binding or redox potential. For that purpose, 2 µl of the sample was loaded as triplicates on Direct Detect assay-free card (Table 5). A mixture of solubilization-extraction buffer and benzonase solutions (Table 18) was used as blank. The mean of measurements from triplicates was taken as final protein concentration (mg/ml).

3.2.6.3. Sodium dodecyl sulphate polyacrylamide gel electrophoresis

The samples were prepared as 30 µg protein/well in a 25 µl mixture of 1x loading buffer and ddH_2O per well. The separation of cell lysates was carried out by SDS-polyacrylamide gel electrophoresis (SDS-PAGE) in 12% Tris-gycine gels (Table 19) at 100 V and 22 °C. For optional checking of the purity of the purified proteins, the SDS gel was then stained with Coomassie staining solution (0.2 g Coomassie Brilliant Blue G250, 25 ml 95% ethanol, 17 ml 96% perchloric acid per 400 ml distilled water).

Table 19. SDS-PAGE

Running buffer	25 mM Tris-HCl, 192 mM Glycine, 0.1% SDS pH 8.3
Stacking gel buffer	1.5 M Tris-HCl pH 8.8
Separating gel buffer	0.5 M Tris-HCl pH 6.8
	12% Tris-glycine-gel
Stacking gel	3.4 ml ddH_2O, 0.63 ml stacking gel buffer, 0.83 ml 30% Acrylamide/Bisacrylamide, 50 µl 10% SDS, 50 µl 10% APS, 5 µl TEMED
Separating gel	3.3 ml ddH2O, 2.5 ml separating gel buffer, 4 ml 30% acrylamide/bisacrylamide, 100 µl, 10% SDS, 100 µl 10% APS, 4 µl TEMED
5x SDS Loading buffer	225 mM Tris/HCl (pH 6.8), 5% (w/v) SDS; 50% (v/v) glycerol, 0.25 M DTT; 0.05% (w/v) bromophenol blue

Tris-HCl, tris (hydroxymethyl) aminomethane hydrochloride; APS, ammonium peroxodisulfate; SDS, sodium dodecyl sulfate; TEMED, tetramethylethylenediamine; sizes were determined in comparison to PageRuler Plus prestained protein ladder (Thermo Fischer Scientific) (5 µl/well).

3.2.6.4. Western blot

For the specific detection of a protein in a protein mixture, a Western blot analysis was performed. After equilibration of the nitrocellulose membrane and the SDS gel for 10 min in transfer buffer (25 mM Tris-HCl, 190 mM glycine, 20% methanol, pH 8.3), protein transfer was carried out in a wet blot apparatus (Bio-Rad) at 4 °C for 1 h at 100 V. The blot was blocked with 5% milk powder (Table 3) in TBST [50 mM Tris-HCl, 150 mM NaCl, 0.05% Tween-20 (Table 3), pH 7.4] for 1 h at room temperature on a shaker (Table 4)**.** Incubation with the primary antibodies was carried out in a suitable dilution (Table 7) overnight at 4 °C. The peroxidase-coupled secondary antibody (1:1000 in 1% milk powder, Table 5) was incubated after washing the membrane (6x, TBST) for 1 h at 22 °C. After another washing step (6x, TBST), chemiluminescence detection of the proteins took place: the membrane was wetted with 500 µl of developer solution [SuperSignal West Femto Maximum Sensitivity Substrate (Table 6), luminol/enhancer solution and stable peroxide solution were 1:1 mixed] for 5 min, and chemiluminescence in transilluminator (Table 4) detected. The band intensities were analyzed by ImageJ.

3.2.6.5. Peptide detection in blood plasma

TAMRA-trictide (10 µM) was dissolved in 1% DMSO and completed with mouse blood plasma (see chapter 3.2.7.2 for preparation). The blood plasma was incubated up to 48 h at 37 °C. At hour zero, as well as after 2, 4, 8, 12, 13, 24 h, and 48 h, 160 µl aliquots were taken and precipitated with 60 µl of acetonitrile/99% ethanol (1:1) (30 min, 4 °C). After centrifugation (20000xg, 15 min, 4 °C), supernatant was taken and filtered through Nanosep 10K Omega filters (Table 5) by centrifugation (5000xg, 10 min, 17 °C) and analyzed by SDS-PAGE. For the separation of the peptides with SDS-PAGE, 10 µl of the filtrate was resuspended in 5x loading buffer (Table 19), denatured (5 min, 95 °C), cooled on ice and separated in mini-protean TGX gel at 100 V and 22 °C (Table 4). The fluorescence of TAMRA (Table 14) was detected in the gel documentation system and measurement of band intensities quantified by the ImageJ software (Table 15).

Parallel to this experiment, stability of trictide in blood plasma was investigated. Additional samples were prepared with trictide (800 µM) incubated [dissolved firstly in DPBS-/- (10x)] in mouse blood plasma up to 48 h. After the separation of supernatant, samples were filtered through 22 microns pipette tip filters (ZipTip C18 columns, Table 5) and analyzed by mass spectrometry.

3.2.6.6. Expression and purification of maltose-binding protein tagged proteins

Recombinant proteins were fused N-terminally with maltose-binding protein (MBP) for affinity purifications. For Tric ECL2, amino acid residues 312–339 of the human sequence were used. Proteins were expressed in *Escherichia coli* BL21, harvested and resuspended in binding buffer (20 mM Tris/HCl, pH 7.4, 200 mM NaCl, 1 mM ethylenediaminetetraacetic acid). Cells were lysed via sonication (sonorex super ultrasonic bath, 300 W) and centrifuged (39000xg), and the supernatant was incubated (1 h, 4 °C) with amylose resin. MBP-proteins were eluted with binding buffer containing 10 mM maltose.

3.2.6.7. Purificaton of His-tagged proteins

The recombinant N-terminally His-tagged C-terminal tail of human Tric was purified for further co-immunoprecipitation. Bacterial pellets were resuspended in lysis buffer (5 ml/g) (Table 20) and centrifuged (10000xg, 30 min, at room temperature). The supernatant was used for further purification. The columns (20 ml) were loaded with 2 ml Ni-NTA agarose matrix. The supernatant was added to the column and incubated with the column material for one hour at room temperature. The supernatant was run twice over the column. Then, the columns were washed three times with 10 mM imidazole and finally eluted with 4 ml of 200 mM imidazole (4x1 ml each) (Table 20). Elution was stored at -20 °C. Before concentrating the eluate, the protein concentration was measured. The samples were diluted into 10 mM imidazole with PBS -/- and then concentrated to 1 mg/ml protein concentration by centrifugal filter device (Amicon ultra-15, Table 5).

Table 20. Buffer and solutions for protein purification	**Ingredients**
Lysis Buffer	100 mM $NaH_2PO_4 \cdot H_2O$, 10 mM Tris-HCl, 6 M guanidine hydrochloride in 1.8 Ω H_2O, pH 8.0 (adjusted with NaOH)
Washing solution	10 mM imidazole in DPBS-/-
Elution solution	200 mM imidazole in DPBS-/-

DPBS-/-, Dulbecco's phosphate buffered saline without Ca^{2+} and Mg^{2+}

3.2.6.8. Co-immunoprecipitation

In order to analyze the binding between human Tric and recombinant N-terminally His-tagged cytosolic C-terminal tail of human Tric ($hTric_{363-558}$), proteins were co-precipitated. The columns were placed in a 2 ml tube (without closing the tip) and loaded with 500 µl of Talon Superflow Metal Affinity (Table 6). Then, the columns were washed (3x with 300 µl

of 10 mM imidazole in DPBS-/-) before being loaded with 500 µl of the concentrated protein. The columns were completely sealed and left to incubate for 2 h at 8 °C. A protein-free control was included for each protein sample. Afterwards, the supernatant was removed and the columns were washed (3x with 300 µl of 10 mM imidazole). In the next step, the columns (controls and samples) were each loaded with 300 µl cell lysates, sealed and incubated overnight at 8 °C. The next day, the columns were washed (3x with 300 µl of 10 mM imidazole in DPBS-/-) and transferred to a new 1.5 ml closable tube and loaded with 80 µl of 200 mM imidazole for elution. The sealed columns were incubated at room temperature for 45 min. Subsequently, the solutions were centrifuged (13000xg, up to 2 min, at room temperature) and the elution fraction was obtained. The final samples were prepared for SDS-PAGE gel electrophoresis.

3.2.7. *In vivo* investigations in mice

The studies on mice were approved by the Office for Health and Social Affairs of Berlin and carried out according to the valid German animal welfare regulations.

3.2.7.1. Peptide injections and detection of fluorescent dyes

C57BL/6N mice (10–19 weeks old, 18–23 g) were housed in MDC-Berlin animal facility, kept on 12:12 h dark–light, and fed standard diet *ad libitum* according to German animal welfare law in Berlin (G0030/13, LaGeSo).

For dye-uptake studies in organs, 800 µM of trictide dissolved in DPBS+/+ (3.6 µmol/kg) were injected into the tail vein (i.v.). The injection volume was adjusted according to the weight of the animals (for 22 g adult mouse, 100 µl of the fluorescent dye solution). After 4 or 24 h, 2% Na-fluorescein (376 Da, w/v, dissolved in DPBS+/+) was administered (i.v.). After 10 min, mice were anesthetized with i.p. injection of anesthesia mixture (0.18 mg/g ketamine and 0.024 mg/g xylazine in distilled water, 350 µl/mice). Under deep anesthesia, mice chests were opened, hearts were prepared by insertion of a butterfly cannula in left ventricle and perfused transcardially with 25 mL DPBS+/+ containing 6250 IU heparin (flow rate 1.5 ml/min). The harvested brain, kidney and a lobe of liver were frozen in 2-methylbutane on dry ice for 7 min and stored at -80 °C until further use.

For the biochemical detection of the fluorescent dyes, 100 mg of the perfused brain, kidney or liver were homogenized on ice in 250 µl DPBS+/+ (Dounce tissue homogenizer), 250 µl of 60% trichloroacetic acid were added, and the homogenate was left for overnight incubation at 4 °C. After centrifugation (18000xg, 20 min, 4 °C), the fluorescence intensity of the Na-fluorescein within the supernatant was measured in 96-well plates at the appropriate wavelength (Table 14) by a TECAN-reader (Table 4). A set of standard samples was included within the same plate, and a standard curve obtained from those samples was used to calculate the amount of Na-fluorescein uptake related to weight of organs (µmol/kg).

3.2.7.2. Obtaining blood plasma

C57BL/6 mice were sacrificed immediately after cervical dislocation, and cardiac blood was taken from the left ventricle. The blood was incubated with heparin (25 IU/ml) and immediately mixed and centrifuged (750xg, 15 min, at room temperature). The yellow fraction on top of the precipitate was transferred to a test tube and immediately used for investigations of peptide stability as first use preference. Otherwise the fraction was stored at -20 °C for later use.

3.2.8. Molecular biological methods

3.2.8.1. Quantitative real time polymerase chain reaction

Total RNA was isolated from tissue or eukaryotic cells by using the Universal RNA Purification Kit (Table 6), transcribed into cDNA (complementary DNA) using the Maxima First Strand cDNA Synthesis Kit (Table 6) for quantitative real time polymerase chain reaction (qRT-PCR) and stored at -20 °C. The mouse- or human-specific primers (Table 9) were designed by Philipp Berndt and tested for its binding specificity using Blast (Table 15).

qRT-PCR was carried out in the StepOne Real-Time PCR System (Life Technologies GmbH), according to the cycling protocol in Table 19, using the Luminaris Color HiGreen high ROX qPCR Master Mix. The Master Mix contained a Taq polymerase that emits a fluorescent signal upon binding to the double stranded cDNA. During qRT-PCR the detected fluorescence increases proportionally to the DNA accumulation.

20 µl of the reaction mix were pipetted according to Table 21 in each well of a MicroAmp Fast Optical 96-well reaction plate (Table 5). For data analyses and export the StepOne Software v2.2.1 (Table 15) was used. In order to evaluate the data, the cycle threshold (Ct) value was set to 0.4, within the linear phase of the logarithmic amplification plot for all tested primers. Ct value gives the number of cycles completed in order to detect a real signal from the samples. Threshold is determined as a level above background fluorescence. In order to calculate relative expression of the examined genes, Ct values were normalized to β-actin (Actb, as a housekeeping gene): Actb ($\Delta Ct = Ct_{target} - Ct_{Actb}$). To compare the expression between two groups, ΔΔCt (ΔΔCt = ΔCtB - ΔCtA) was calculated. cDNA amplification during the PCR is exponential. A single peak at the calculated temperature indicated specific amplification of cDNA; therefore, unspecific products were identified by melting curves.

Table 21. qRT-PCR protocol

Component	**Concentration**	**Cycling protocol**			
Luminaris Color HiGreen qPCR Master mix (2x)	1x	**Step**	**Temperature (°C)**	**Time**	**Number of cycles**
Primer (fw)	0.3 µM	Uracil-DNA glycosylase pre-treatment	50	2 min	1
Primer (rev)	0.3 µM	Initial denaturation	95	10 min	1
cDNA	≤ 0.5 ng/µl	Denaturation	95	15 s	40
		Annealing/	60	60 s	

qRT-PCR, quantitative real time polymerase chain reaction; fw, forward; rev, reverse; cDNA, complementary DNA.

3.2.8.2. Molecular cloning

A thermocycler (Bio-Rad Laboratories GmbH) was used to clone recombinant N-terminally His-tagged cytosolic C-terminal tail of human Tric (hTric363-558) DNA from N-terminally YFP-tagged human Tric cDNA using primers (Table 11). The composition of PCR mixture and the thermal cycling conditions for a reaction volume of 30 µl are shown in Table 20. The PCR product was purified using the DNA Clean and Concentrator-5 kit (Table 4) according to the supplier's manual. The concentration was photometrically determined using the NanoDrop 2000c (Thermo Fisher Scientific GmbH).

Table 22. PCR protocol

Component	Concentration	Cycling protocol			
10x key buffer	1x	**Step**	**Temperature (°C)**	**Time**	**Number of cycles**
dNTP mix	0.2 mM	Initial denaturation	95	2	1
Template DNA	0.5 ng/µl	Denaturation	95	30 s	35
Primer (fw)	0.5 µM	Annealing	65	45 s	
Primer (rev)	0.5 µM	Elongation	72	1	
Taq DNA Polymerase	1 µl	Final elongation	72	5	1

PCR, polymerase chain reaction; dNTP, deoxynucleotide fw, forward; rev, reverse; cDNA, complementary DNA.

In order to ligate PCR product with the pET-28a (+) expression vector (Addgene, USA), both DNA and target vector were digested with Hind III and Not I fast digest restriction enzymes (Table 6). The restriction was performed in a volume of 40 µl for the PCR product or 30 µl for the plasmid DNA (Table 23) at 37 °C for at least 4 h. After restriction, the PCR product and the plasmid DNA were separated by agarose gel electrophoresis. Agarose gel bands that were observed at the expected size were cut out. The DNA was extracted using the Zymoclean Gel DNA Recovery Kit (Table 6) following the product protocol. The concentration and the degree of purity of the extracted DNA were determined by photometric measurement of the absorption at 260 and 280 nm using the NanoDrop 2000c.

Table 23. Protocol of DNA restriction

Restriction of the PCR product		**Restriction of the plasmid product**	
Component	**Amount**	**Component**	**Amount**
PCR product	30 µl	Plasmid DNA	20 µl
Fast digest buffer (10x)	4 µl	Fast digest buffer (10x)	3 µl
Fast digest enzyme (HindIII)	2 µl	Fast digest enzyme (HindIII)	2 µl
Fast digest enzyme (NotI)	2 µl	Fast digest enzyme (NotI)	2 µl

PCR, polymerase chain reaction.

The ligation of the PCR product and the linearized plasmid DNA was performed in 20 µl of reaction mix (Table 24) for 14 h at 16 °C. The ligase was inactivated by heating at 65 °C for 10 min.

Table 24. Protocol of Ligation

Component	Concentration
Ligase buffer (10x)	1x
Plasmid DNA	5 ng/µl
PCR product	Molar ratio of 5:1 plasmid DNA
T4 DNA ligase	20 units/µl

3.2.8.3. Preparation of electrocompetent bacteria

An *E. coli* BL21 culture in 500 ml LB medium was grown (200xg, 37 °C, without antibiotic) until it reached an OD 600 nm=0.6. After cooling for 30 min on ice and centrifuging (3000xg, 10 min, 4 °C), the pellet was resuspended in 160 ml ice-cold distilled water, divided into four portions and centrifuged again (1500xg, 15 min, 4 °C). Supernatants were discarded and pellet was resuspended with 40 ml of ice-cold distilled water and centrifuged (1500xg, 15 min, 4 °C). The pellet was resuspended in 10% glycerol. After centrifugation for the last time (1500 g, 15 min, 4 °C), it was resuspended in 1 ml of ice-cold 10% glycerol, aliquoted and stored at -80 °C.

3.2.8.4. Transformation of electrocompetent bacteria

An aliquot of 150 µl of electrocompetent bacteria was thawed on ice and transferred into an electroporation cuvette together with 0.5 µl of the plasmid DNA. The bacteria were exposed to 1.8 kV, allowing the cells to take up the plasmid. The transformed bacteria were immediately incubated with 500 µl LB medium at 37 °C for 1 h. Selection of positive clones was provided by kanamycin (100 µg/ml) containing agar plates. The bacteria was plated on agar plates and incubated overnight at 37 °C. The next day we picked positive clones from single colonies. Mini-cultures (5 ml of LB medium with 100 µg/ml Kanamycin) were inoculated and left for overnight incubation (200xg, 37 °C). Those mini-cultures were either used for preparation of glycerol stocks or purification of plasmid DNA by DNA purification kits (Table 6).

3.2.8.5. Site directed mutagenesis

Aromatic residues in tricellulin extracellular loop 2 (Y322, Y323, F326, F334) were mutated into alanine or isoleucine (Chapter 4.3.8). Primers that carry the modified codon were given in Table 10. The PCR master mix with a volume of 80 µl (Table 25) contained an AccuPOL DNA Polymerase (Table 6) with high proofreading capacity for replication of the plasmid DNA. Gradient PCR program (51, 51.3, 52.5, 54.2, 56.5, 59.1, 61.8, 64.5, 67,

69.1, 70.6, 71.5 °C) was applied due to high variation between the melting temperatures of primers. The PCR product was purified using the DNA Clean and Concentrator-5 kit (Table 6) following the product instructions.

Table 25. Gradient PCR protocol

Component	Concentration	Cycling protocol			
AccuPol buffer (10x)	1x	**Step**	**Temperature (°C)**	**Time**	**Number of cycles**
dNTP mix	0.2 mM	Initial denaturation	95	2 min	1
Template DNA	500 ng/rxn	Denaturation	95	1 min	35
Primer (fw)	0.2 µM	Annealing	51-71.5 °C	30 s	
Primer (rev)	0.2 µM	Elongation	72	11 min	
Taq DNA Polymerase	0.025 U/µl	Final elongation	72	5 min	1

PCR, polymerase chain reaction; dNTP, deoxynucleotide; rxn, reaction; fw, forward; rev, reverse; cDNA, complementary DNA.

3.2.9. Biophysical methods

3.2.9.1. Circular dichroism spectroscopy

The circular dichroism (CD) spectroscopy was applied to detect possible structural differences between effective and ineffective peptides. The technique is based on optically active substances absorbing different degrees of circularly polarized light. Therefore, tricellulin peptides (50 µM) were dissolved in phosphate buffer (10 mM, pH 7.2) in order to determine the proportion of secondary structural elements (α-helix, β-sheet, β-loop). The remaining portion was considered disordered. By adding the surfactant SDS (0.5 mM in phosphate buffer) below the critical micelle concentration (9-10 mM, (Niraula et al., 2014), a possible induction of β-sheet structures should be examined (Zhong and Johnson, 1992). Above the critical micelle concentration, SDS led to the induction and stabilization of α-helices (Gopal et al., 2012). Trifluoroethanol (60% TFE in phosphate buffer) has the property of favoring induction of α-helices (Buck, 1998). The measurements were taken with the spectropolarimeter J-720 (Table 4), at 22 °C, from 190-260 nm, in 0.1 cm quartz cuvettes (Table 5). Per measurement, 8 accumulations were made with a resolution of 0.1 nm and a measuring speed of 20 nm/min. For analysis, the data was subtracted from the buffer-based spectrum. Molar residual ellipticity [θ] was calculated considering the amino acid number using the Spectra Manager program (Corrêa and Ramos, 2009): characteristic

of α-helical elements in L-AS peptides are ellipticity minima at 208 and 222 nm, and a maximum at 192 nm. For β-sheet structures, there is a minimum at 217 nm and a maximum at 195 nm. Unordered elements show a minimum <200 nm (Greenfield and Fasman, 1969). The secondary structural components of the peptides were determined with the Spectra Manager using reference spectra (Yang, Wu & Martinez, 1986).

$$[\theta] = \frac{\theta}{10 \cdot C \cdot d} \qquad (\text{deg} \cdot cm^2 \cdot decimol^{-1})$$

$$[\theta]_{MRE} = \frac{\theta}{n} \qquad (\text{deg} \cdot cm^2 \cdot decimol^{-1})$$

θ Ellipticity *(mdeg)*

C Molar concentration $(mol \cdot l^{-1})$

d Layer thickness of the cuvette (cm)

n Number of the amino acids

3.2.9.2. Three-dimensional structure prediction of peptides

3D-structure model of trictide peptides was prepared using the program Pepfold (http://bioserv. rpbs.univ-paris-diderot.fr/PEP-FOLD/) (Shen et al., 2014)Thévenet et al., 2012). Different models varying in their 3D-structure were obtained; models fitting best to experimental data were selected for further analysis. To gain insight into the binding mechanism of trictide, we created docking models of the Pepfold trictide model to the iTasser (Table 15) model of human Tric ECL2. The suggested binding surfaces were based on the hydrophobic potentials of the two structures and were depicted using Discovery Studio Visualizer (Table 15).

3.2.9.3. Mass spectroscopic detection of peptides in the blood plasma

For mass spectrometric detection of TAMRA peptides in blood plasma, samples were prepared according to procedures detailed in chapter 3.2.6.5, concentrated (rotary vacuum concentrator, 45 °C, 5.5 torr/min vacuum), and dissolved in 5% acetonitrile/0.1% TFA in an ultrasonic bath (Table 4). The sample was desalted and re-concentrated using ZipTip C18 columns (Table 5). After washing (3x, 50% acetonitrile, 0.1% TFA) and equilibration (3x, 0.1% TFA, pH 7.0), the columns were loaded with the sample by pipetting 10 times. After washing (3x, 0.1% TFA, pH 7.0), the sample was eluted in 1.5 µl 65% acetonitrile/0.3% TFA directly on an Opti-TOF 384er plate (Thermo fischer scientific). For each sample, 0.5 µl of α-cyano-4-hydroxycinnamic acid (5 mg/ml in 75% acetonitrile/0.3% TFA) was added. Peptides were detected with the mass spectrometer (AB SCIEX TOF / TOF 5800, SCIEX, Germany).

3.2.10. Statistsics

Data analysis and generation of graphs were achieved by employing GraphPad Prism® 5.04 and Microsoft Excel 2010 (Table 15). Results are given as mean±SEM. One-way analysis of variance (ANOVA) followed by Dunn's multiple comparison test were used to determine significant difference between two groups. The two-way ANOVA test followed by Bonferroni's comparison test was used to determine significant differences between more than two groups. Differences were considered significant if $p \leq 0.05$ for $n \geq 4$ (* $p \leq 0.05$, ** $p \leq 0.01$, *** $p \leq 0.001$, ****$p \leq 0.0001$).

4. RESULTS

4.1. TRICELLULIN IS HIGHLY EXPRESSED IN KIDNEY AND COLON

For selection of suitable model systems for tricellulin derived peptidomimetic research, the expression of tricellulin was compared among different organs. Tric mRNA levels were quantified in several organs isolated from WT mice: brain (cortex and whole), eye, kidney (cortex and medulla), heart, lung, liver, testis, spleen, jejunum, duodenum, ileum and colon (Table S1). The lowest Tric expressing organs were spleen, brain cortex, testis and whole brain. Organs expressing Tric at medium levels were heart, ileum, jejunum, lung and duodenum. Colon was the highest Tric expressing organ, followed by kidney medulla, kidney cortex, liver and eye (Fig. 4.1). Due to high expression in the colon, we chose colon carcinoma cell line (Caco-2) as a cell culture model for modulating barrier permeability.

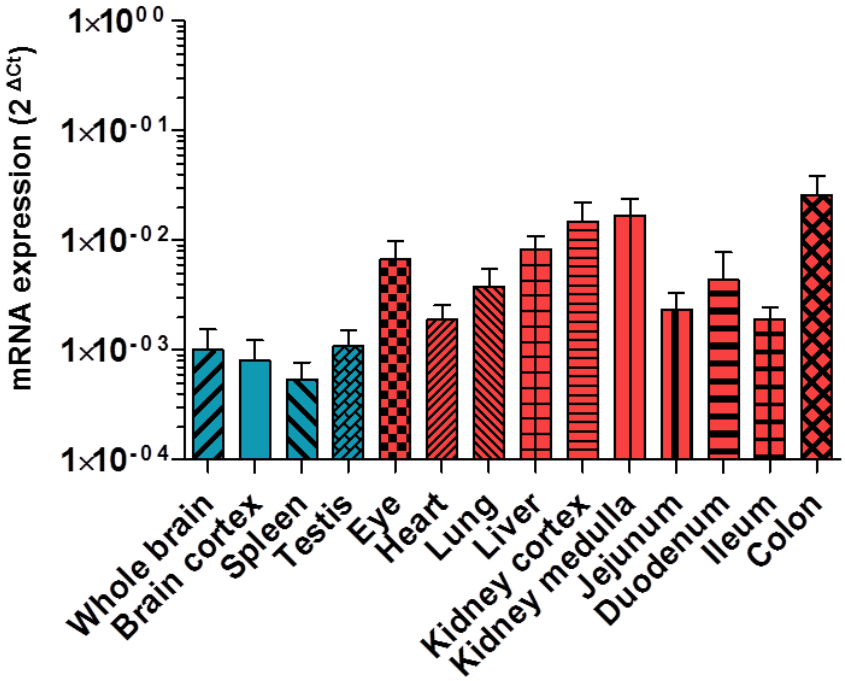

Fig. 4.1 Tricellulin is highly expressed in most of the epithelial tissue dominant organs and less in endothelial tissue dominant organs of mice. Messenger RNA (mRNA) expression of wild-type mice organs was given. Four organs with the lowest tricellulin expression were given as blue bars, and the rest of the organs expressing tricellulin at higher levels were given as red bars. mRNA normalized to β-actin (Actb) ($\Delta Ct = Ct_{junction\ protein} - Ct_{actin}$); Ct, Cycle threshold; mean±SEM, n=8.

4.2. TIGHT JUNCTION PROTEINS WERE DETECTED IN MOUSE AND HUMAN BRAIN SECTIONS

The aim of the following experiment is to observe tricellular cell-cell contacts particularly in mouse brain capillaries to reveal localization of Tric with respect to other TJ proteins. Imaging of Tric in brain tissues is an unsolved problem due to the low expression levels and the unique morphology of tricellular contacts of capillary endothelial cells in general and of brain capillary specifically. Human and mouse brain slices were immunostained to observe localization of Tric (3-cell TJ marker), Cldn5 (2-cell TJ marker), Occl (2-cell TJ marker), ZO-1 (general junction marker) and LSR (3-cell TJ marker). Occl and Cldn5 expression are well-described at the BBB, and their expression was known to be higher than that of other TJ proteins (Mariano et al., 2013; Pan et al., 2017). That is why they were used as co-staining for confirmation of brain capillaries.

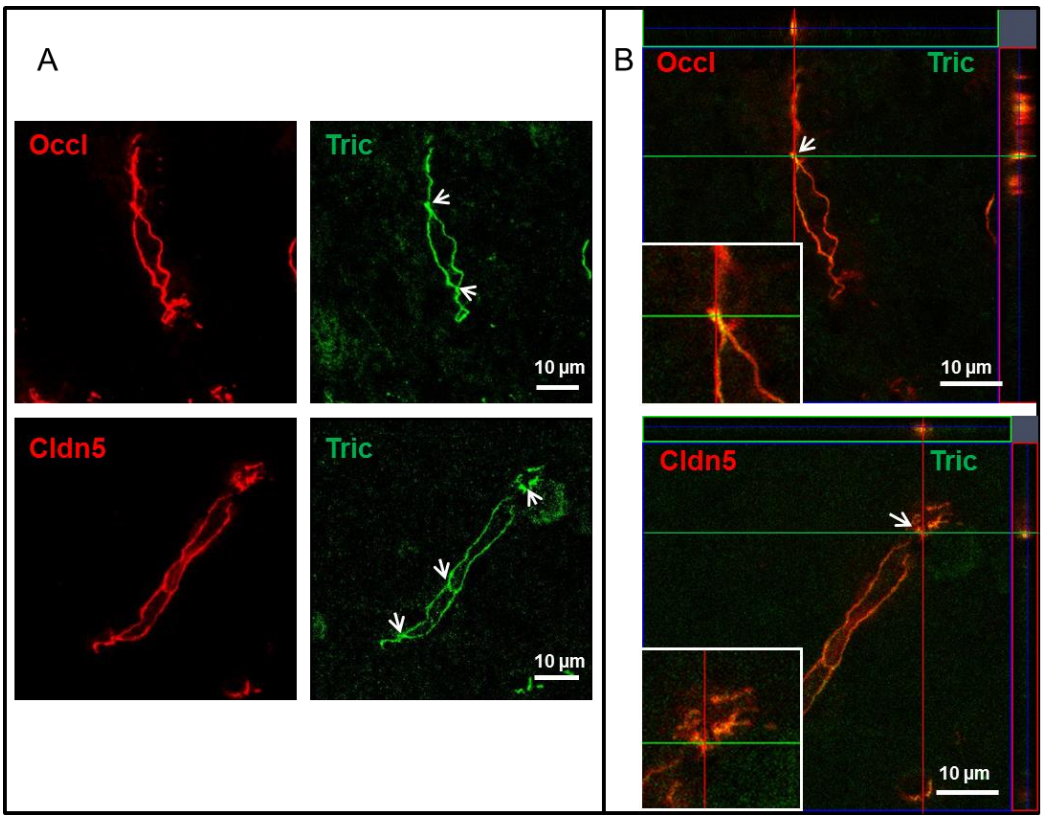

Fig. 4.2 Tricellulin localizes throughout cell-cell contacts and is enriched at tricellular contacts in Z-direction of the mouse brain capillaries. (A) Immunohistochemical images of brain slices (8 µm cryosections) were given. Brain capillaries from region of forebrain cortex were stained with rabbit anti-tricellulin (Tric), mouse anti-occludin (Occl) and mouse anti-claudin5 (Cldn5) antibodies. Tricellular contact points (white arrows). **(B)** 3D reproduction of Z-stacks. Tricellulin signal extends via Z-direction (see intersection points on side windows). Tricellular contacts were emphasized in 2X enlarged images.

Both Occl-Tric and Cldn5-Tric co-stainings gave signal along the bicellular contacts of the capillary. Tric signal (green) was stronger at points where three capillary contacts join together (Fig. 4.2A, white arrows). Three-dimensional reproduction using Z-stack images demonstrated the extension of dot-like Tric signals (yellow) through the Z-direction at tricellular contact of the capillaries (Fig. 4.2B, insets).

The second objective of this chapter was to visualize localization of tricellular TJ markers in human brain microvessels. Tric and LSR both localize at tricellular contacts (Iwamoto et. al., 2014; Sohet et al., 2015) while Occl and ZO-1 proteins localize to bicellular capillary contacts. Tric was expressed and observed at tricellular contacts with dot-like structure (Fig. 4.3A, white arrows). Labelling with LSR-ZO1 antibody combination revealed that LSR was also expressed and localized precisely at tricellular contacts of brain capillaries (Fig 4.3A, green arrows).

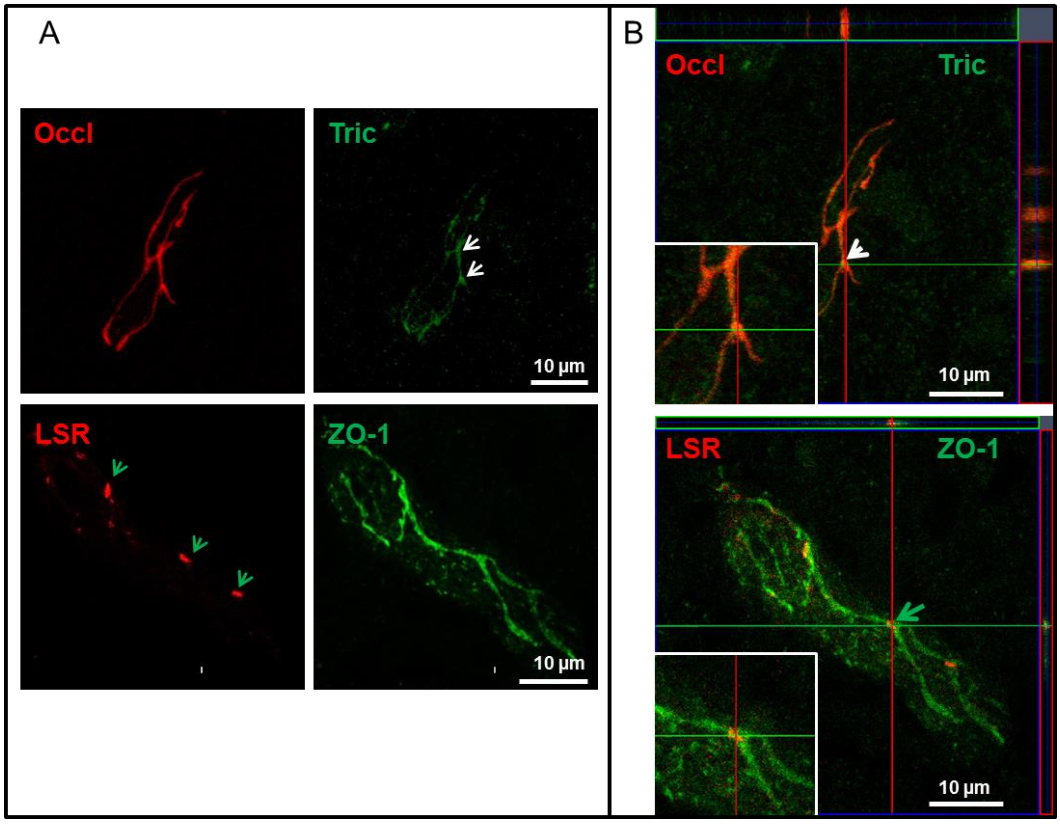

Fig. 4.3 Tricellulin and lipolysis stimulated lipoprotein receptor (LSR) are expressed in human brain capillaries and localize in contacts between tricellular membrane surface patches. Immunohistochemical images of human brain cortex slices (8 µm cryosections) were stained with mouse anti-occludin (Occl), rabbit anti-tricellulin (Tric), rabbit anti-LSR and rat anti-*zonula occludens* protein 1 (ZO-1) antibodies. **(A)** Co-staining of Occl and Tric: tricellular Tric localization (white arrows), co-staining of LSR and ZO-1: tricellular LSR localization (green arrows). **(B)** 3D reproduction of Z-stacks. Tricellulin (white arrow) and LSR (green arrow) signal extended through Z-direction. Tricellular contacts were emphasized in 2X enlarged images.

After the three-dimensional reproduction using Z-stack images, the distinct tricellular localization of LSR (green arrows) and enrichment of Tric (white arrows) extending in Z-direction was observed relative to the bicellular capillary contacts (Fig. 4.3B). Imaging TJ proteins within healthy brain tissues enabled us to compare their localization and expression pattern to tissues of the peptide administered animals.

4.3. TRICELLULIN PEPTIDOMIMETIC TO PERMEABILIZE CELL BARRIER

4.3.1. Recombinant tricellulin extracellular loop two affects barrier integrity

Recombinant MBP fused ECL2 of Tric was used to investigate its effect on the transepithelial electrical resistance (TER) of Caco-2 cells. MBP treated cells (negative control) displayed a non-significant decrease of TER to 78 ± 18%, and furthermore 90 µM MBP-Tric ECL2 treatment decreased to 78 ± 10%. However, 280 µM MBP-Tric ECL2 clearly dropped TER to 53 ± 6% after 24 h (Fig. 4.4A).

In order to identify changes at protein level in parallel to the TER changes, transwell filters were investigated immunocytochemically. MBP-Tric ECL2-free media treated samples showed typical Occl localization at bicellular contacts and Tric localization at tricellullar contacts (Fig. 4.4B, green arrowheads). Confocal microscopy resolution did not enable distinct localization of Occl and Tric at tricellular contacts (see chapter 4.3.5.2). That is the reason for the overlapping (yellow) signal of Occl (red) and Tric (green) at tricellular contacts (Fig. 4.4B, see enlarged images). Occl staining was sharp and continuous in the bicellular area. Samples treated with 280 µM MBP did not change normal localization of both proteins. 90 µM MBP-Tric ECL2 treatment resulted in internalization of vesicles and submembranous attachment of Occl protein along bicellular regions of cells. Tric signals were localizing at bicellular cell membrane (Fig. 4.4B, green arrows) and also at internalized vesicles (yellow arrows). But there were still Tric molecules localizing at tricellular contacts (Fig. 4.4B, green arrowheads). 280 µM MBP-Tric ECL2 increased the degree of internalization for both Occl and Tric. Occl was observed at internalized vesicles together with Tric (Fig. 4.4B, yellow arrows) and its signal was decreased at cell membrane compared to the untreated sample. Tric localization was also observed at bicellular area (green arrows) that was unusual compared to the untreated control (Fig.

4.4B). Due to the clear effect of recombinant Tric ECL2 on paracellular localization tightness reduction, Tric ECL2 region has been selected as an approach for overcoming cellular barriers at bTJs and tTJs, with the potential to improve drug delivery transiently.

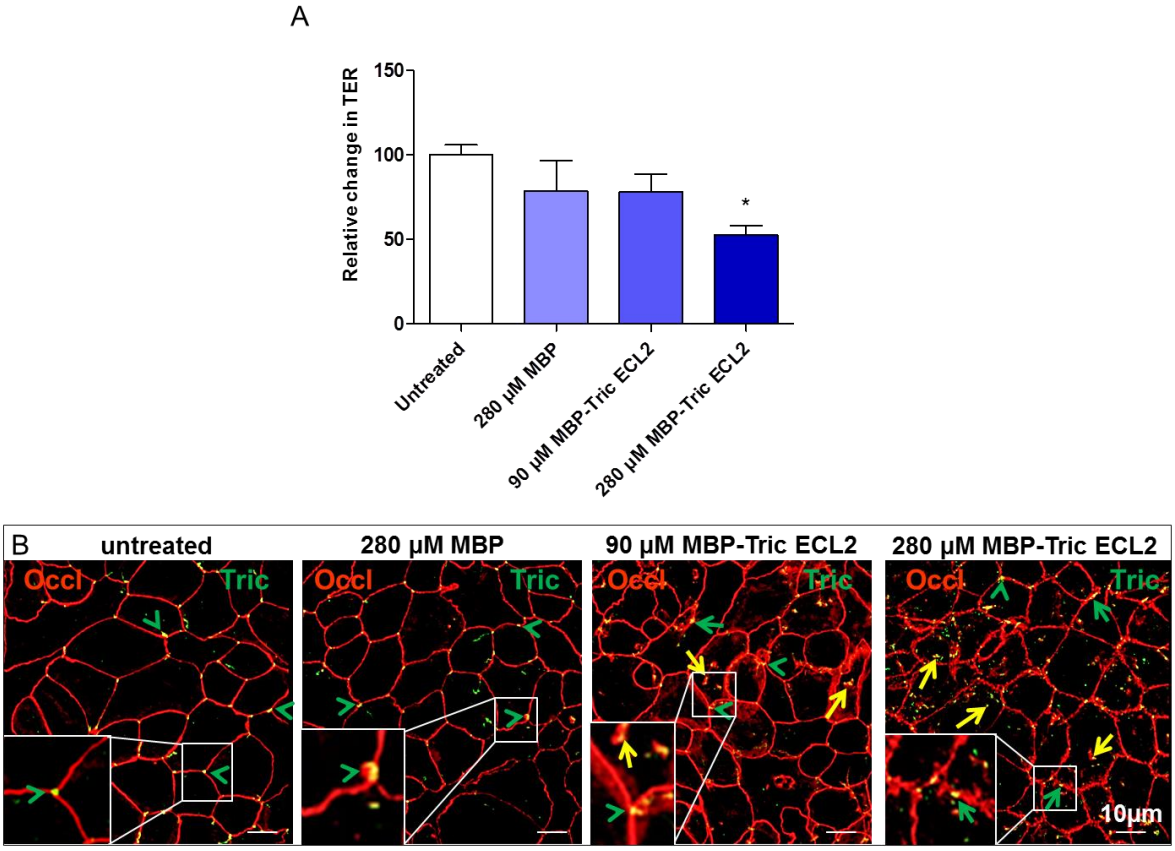

Fig. 4.4 Administration of the recombinant extracellular loop 2 (ECL2) of human tricellulin (Tric) causes redistribution of Tric and occludin (Occl) from the plasma membrane to the cytosol and weakens the paracellular barrier of human colon carcinoma epithelial (Caco-2) cells. (A) Transepithelial electrical resistance (TER) after 24 h of incubation with MBP (maltose binding protein) or MBP–Tric ECL2. One-way ANOVA test was applied prior to Dunnett's comparison *post hoc* test. Mean±SEM, n=3, * P < 0.01 relative to untreated control. **(B)** Immunocytochemistry showed effects of MBP–Tric ECL2 compared with MBP-Tric ECL2-free (untreated) and MBP treatment alone; incubation time: 24 h. Green arrowheads indicate tricellular localization of Tric; yellow arrows indicate intracellular Tric and Occl; green arrows indicate dot-like localization of Tric at the bicellular plasma membrane.

4.3.2. The synthetic peptide trictide affects human epithelial colorectal adenocarcinoma cell line 2

The experiments with MBP-Tric ECL2 showed promise for further development of a Tric ECL-based approach to cell barrier modulation. Trictide, a synthetic peptide, was derived from human Tric ECL2 due to reproducibility and pharmaceutical applications. The effect

of trictide was investigated in a variety of epithelial and endothelial cell lines chosen according to their TJ protein expression profile. Caco-2 cells were used preferentially in this chapter for trictide investigations due to their high Tric and broad transmembranous TJ protein's expression profile (Berndt, 2017).

4.3.2.1. Trictide has a concentration dependent effect on cell barrier tightness and a small concentration-difference between cytotoxicity and barrier opening

A variety of trictide concentrations were tested in filter experiments in order to analyze trictide's concentration dependency on tightness of cell barrier. TER was measured after 16 h of incubation with the peptide. TER values relative to the untreated sample (194±7 $\Omega \cdot cm^2$) are given in Fig. 4.5A.

50 µM trictide showed insignificant increase (11.3%) and absolute TER value of 216±9 $\Omega \cdot cm^2$. 100 µM trictide decreased TER to 90% (174±8 $\Omega \cdot cm^2$). 125 µM trictide exhibited 80% of TER (154±2 $\Omega \cdot cm^2$). Only 150 µM trictide and 200 µM trictide significantly decreased TER to 56% (109±13 $\Omega \cdot cm^2$) and 21% (154±2 $\Omega \cdot cm^2$), respectively. 150 µM scrambled trictide displayed TER of 94% (181±7 $\Omega \cdot cm^2$) (Fig. 4.5A). Consequently, a remarkable trictide action was recorded with concentrations ≥ 150 µM.

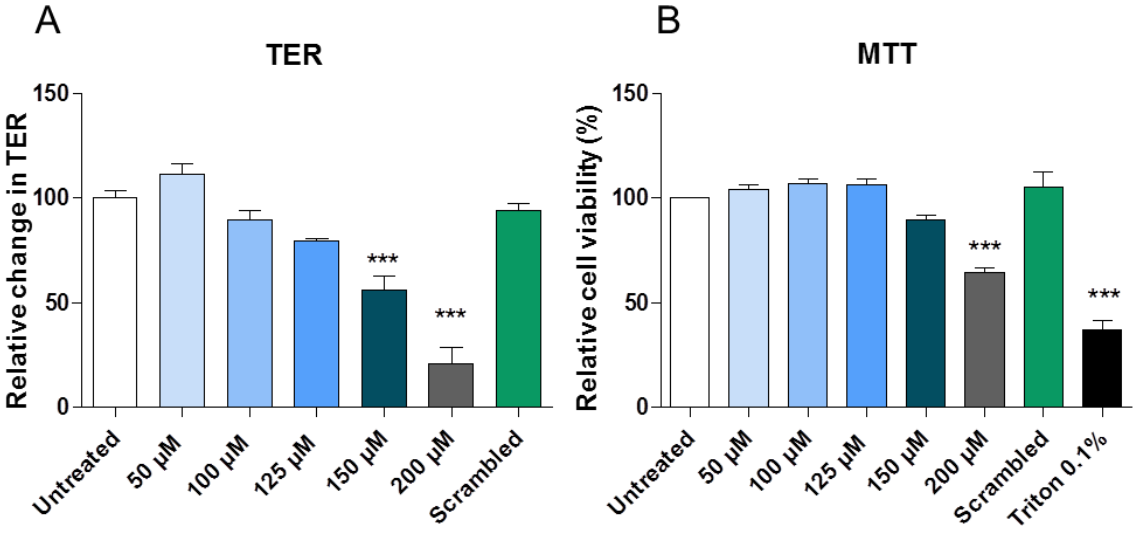

Fig. 4.5 150 µM non-cytotoxic trictide concentration weakens the paracellular barrier of filter-cultured human colon carcinoma epithelial (Caco-2) cells after 16 h of incubation. (A) Transcellular electrical resistance (TER) values of trictide and scrambled trictide are given in comparison to peptide-free control (untreated). n=6. **(B)** Cell viability measurement with MTT [3-(4.5-dimethylthiazol-2-yl)-2.5-diphenyltetrazolium bromide] was applied for cells that were treated with the same concentrations as for TER measurements. As positive control, Triton X-100 was included, n=4. **(A-B)** One-way ANOVA test was applied prior to Dunnett's comparison *post hoc* test. Mean±SEM, *** $P < 0.001$ relative to untreated control.

In order to measure cell viability levels after peptide administration, MTT assay was used. Percentages of cell viability compared to untreated control were: 50 µM (104±2%), 100µM (107±2%), 125 µM (106±3 %), 150 µM (90±2%), 200 µM (64±2%), scrambled trictide (105±7%), and 0.1% triton (37±4%) (Fig. 4.5B). Therefore, ≤150 µM trictide as well as the scrambled peptide were not cytotoxic, and higher concentrations of trictide should be avoided as they might be toxic.

4.3.2.2. The effect of trictide on the impedance of the cell barrier

Changes in cell impedance due to trictide administration were measured by electric cell-substrate impedance sensor (ECIS) over time, which allowed calculation of TER. 150 µM trictide exhibited an increasing resistance up to 163±17% over 16 h, and then the TER drastically decreased to 104±16% after 47 h. 100 µM of trictide caused increase in TER between 16 and 47 h from 110±2 % to 142±4%. Resistance after scrambled trictide remained almost the same at 0 h (86±4%), 16 h (82±7%) and 47 h (83±8%). Thus, trictide appeared to be active after 16 h of incubation; scrambled trictide did not show any effect on the resistance during the same period of time (Fig. 4.6).

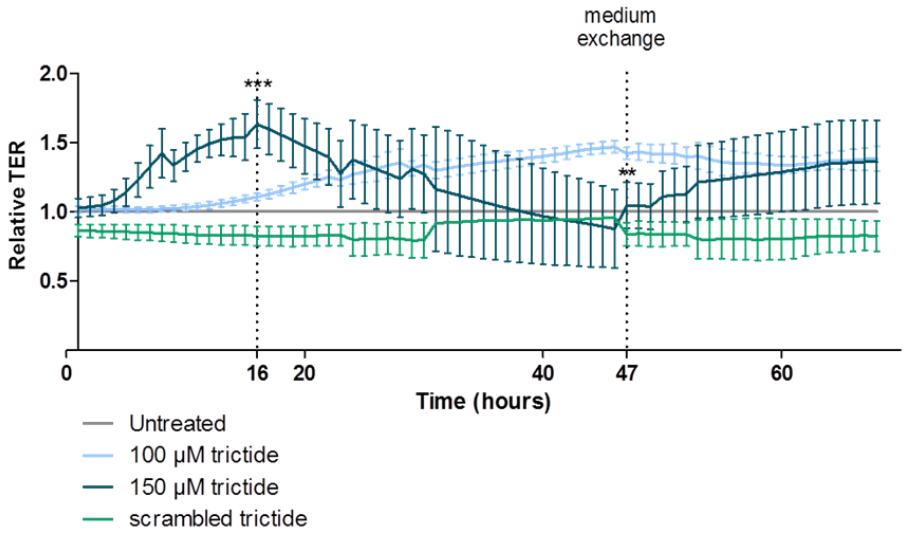

Fig. 4.6 Trictide reversibly influences the barrier of human colon carcinoma epithelial (Caco-2) cells. Effect on transcellular electrical resistance (TER) upon 100 µM and 150 µM trictide and 150 µM scrambled trictide administration compared to peptide-free medium (untreated). Measurements were taken by electric cell-substrate impedance sensor allowing calculation of TER. The graph initiated with peptide administration; at 47 h peptide containing medium was exchanged for peptide-free medium. Total incubation time, 70 h; dotted lines, time points of statistical calculations; two-way ANOVA test was applied prior to Bonferroni's comparison *post hoc* test; mean±SEM; n=4; ** $P \leq 0.01$ (47 h compared to 16 h), *** $P \leq 0.001$ (versus untreated control).

At 47 h, the recovery process was initiated, by exchanging the peptide-containing medium for peptide-free medium. The 150 µM trictide treated sample exhibited an increase of TER up to 136±30% at 69 h. This finding is an indicator of cell barrier recovery followed by removal of peptide. The 100 µM trictide group exhibited slight decline of TER from 142% at 47 h to 138 ± 9% at 70 h. Scrambled trictide did not show any change in TER after the addition of peptide-free medium (Fig. 4.6).

The data displayed unexpected TER increase at 16 h, which would indicate barrier tightening. ECIS measures cellular impedance that reflects transcellular resistance in an alternating current circuit. The dissimilarity between chopstick measurements and ECIS could be due to this technical difference. Repetition of experiment is necessary to confirm this effect.

4.3.2.3. Trictide opens the cellular barrier for molecules up to 10 kDa.

Filter experiments always showed the reduction of transcellular electrical resistance by trictide. Permeation measurements were performed in order to reveal the size of the opening in the barrier. Earlier, the tricellular central sealing tube was calculated as a radius of approximately 5 nm, which allows for the passage of globular macromolecules with a molecular weight of up to 10 kDa (Krug, et. al. 2009; Staehelin, 1973). Paracellular permeability for passage of small molecules and large molecules was measured with fluorescent tracers (LY, 0.45 kDa; FD10, 10kDA, FD40, 40 kDa).

It was observed that 100 µM trictide non-significantly reduced the passage of small molecules to 60±11%. 125 µM trictide showed no change in permeability (106±29%). Passage increased up to 225±26% with 150 µM trictide. 150 µM scrambled trictide did not considerably affect permeability (78±9%). Untreated sample showed basis permeability coefficient for small molecules at $31\pm5\cdot10^{-10}$ cm/s throughout the observation (Fig. 4.7A).

Paracellular permeability measurements for large molecules like FD10 showed for 100 µM trictide 65±15% passage of larger molecules, which is not significant relative to untreated control. 125 µM trictide (92±32%) and 150 µM scrambled trictide 98±22% did not affect passage at all. However, the degree of paracellular permeability for 10 kDa sized molecules increased to 221±54% with 150 µM trictide, which was more than 2 times the permeability of the untreated control. Untreated cells showed control permeability coefficient for the passage of large molecules at $13\pm2\cdot10^{-10}$ cm/s (Fig. 4.7B).

The degree of paracellular permeability for much larger molecules like FD40 was measured as: 100 µM trictide (53±34%), 125 µM trictide (66±21%), 150 µM trictide (108±30%), and 150 µM scrambled trictide (120±49%). None of the concentrations significantly affected permeability towards 40 kDa molecules. The untreated sample exhibited a permeability coefficient of $1.4\pm1\cdot10^{-10}$ cm/s for those much larger molecules (Fig. 4.7C).

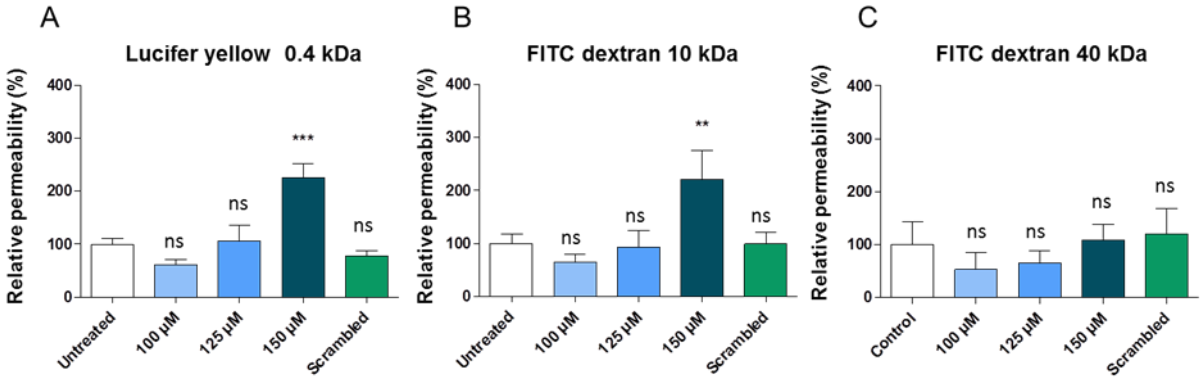

Fig. 4.7 150 µM of trictide opens the paracellular barrier of human colon carcinoma epithelial (Caco-2) cells for small and larger molecules up to 10 kDa. (A) Effect of trictide and scrambled trictide on paracellular permeability coefficient of lucifer yellow (0.4 kDa). **(B)** FITC (fluorescein isothiocyanate) Dextran 10 kDa. **(C)** FITC Dextran 40 kDa. Values were related to substance-free control (untreated) and given as percentage; total incubation time: 16 h; ns, non-significant. One-way ANOVA test was applied prior to Dunnett's comparison *post hoc* test. Mean±SEM, n=5, ** $P < 0.01$, *** $P < 0.001$

Consequently, 150 µM was the only concentration that caused a significant increase in permeability of small and larger molecules. However, there was no opening for a 40 kDa molecule to pass.

4.3.2.4. D-amino acid derivative of trictide is not effective.

Substitution of physiological L-amino acids with non-physiological D-amino acids might decrease the substrate recognition and binding affinity by proteolytic enzymes (Di, 2015) and may increase stability of respected peptide. For that reason, a trictide with D-conformation was synthesized. Initial experiments were executed with higher concentrations than used for L-trictide such as 200 and 300 µM. Even those high concentrations did not cause any drop of TER or any barrier opening activity (Fig. 4.8A). Likewise paracellular permeability of 10 kDa molecules did not increase due to the incubation with D-trictide (Fig. 4.8B).

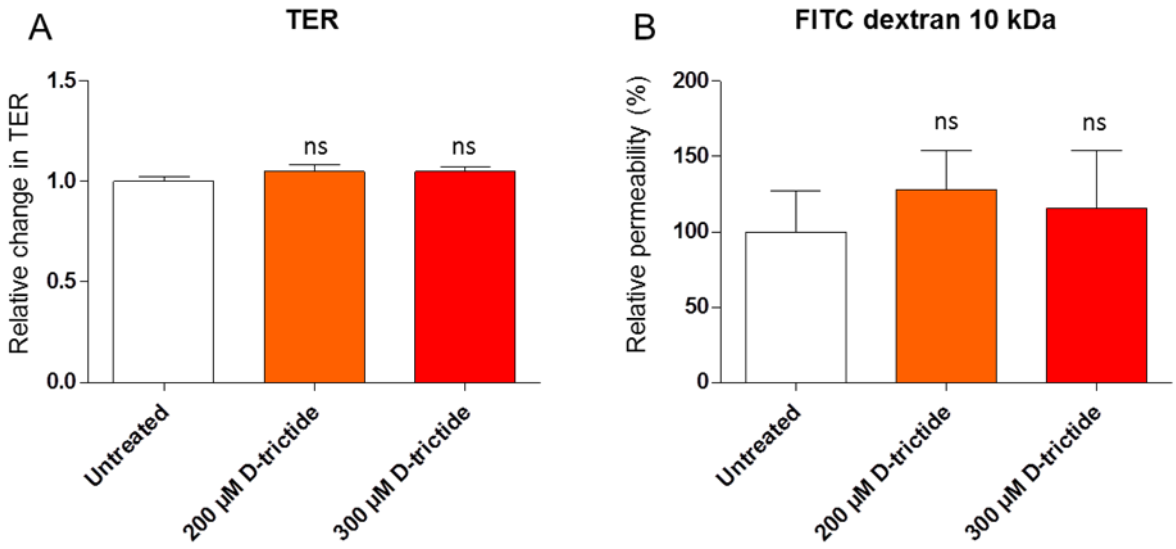

Fig. 4.8 D-amino acid trictide (D-trictide) does not have an effect on transcellular barrier tightness of human colon carcinoma epithelial cells. **(A)** Transepithelial electrical resistance (TER) **(B)** Paracellular permeability of FITC (fluorescein isothiocyanate) Dextran 10 kDa. **(A-B)** Values were related to substance-free medium (untreated). Total incubation time: 16 h. One-way ANOVA test was applied prior to Dunnett's comparison *post hoc* test. Mean±SEM, n=3, ns: non-significant, versus untreated control.

4.3.2.5. Trictide affects bicellular and tricellular tight junction proteins

In order to be acquainted with alterations at protein level and to investigate how individual TJ proteins were affected by trictide, immunocytochemistry was applied. It was stimulating to examine alterations of Occl and Tric together due to their compensating regulation over each other (Raleigh et al., 2010) Occl-Cldn1 and Tric-Cldn1 co-stainings were selected due to information in the literature that affirms the contribution of Cldn1 to the enrichment of Occl and Tric at cell-cell contacts (Cording et al., 2013). Tric-LSR co-staining was included considering that both LSR and Tric molecules are required for normal tTJ formation and barrier integrity (Masuda et al., 2011). As described in detail in chapter 4.3.2.1, 150 µM trictide was the active concentration in barrier opening of Caco-2 cells. But at cellular level, we observed that this concentration was altering localization of TJ proteins too drastically and making it impossible to observe small modifications of individual proteins (Fig. 4.9). That is why mainly 100 µM of trictide was applied as a milder concentration during the following experiments.

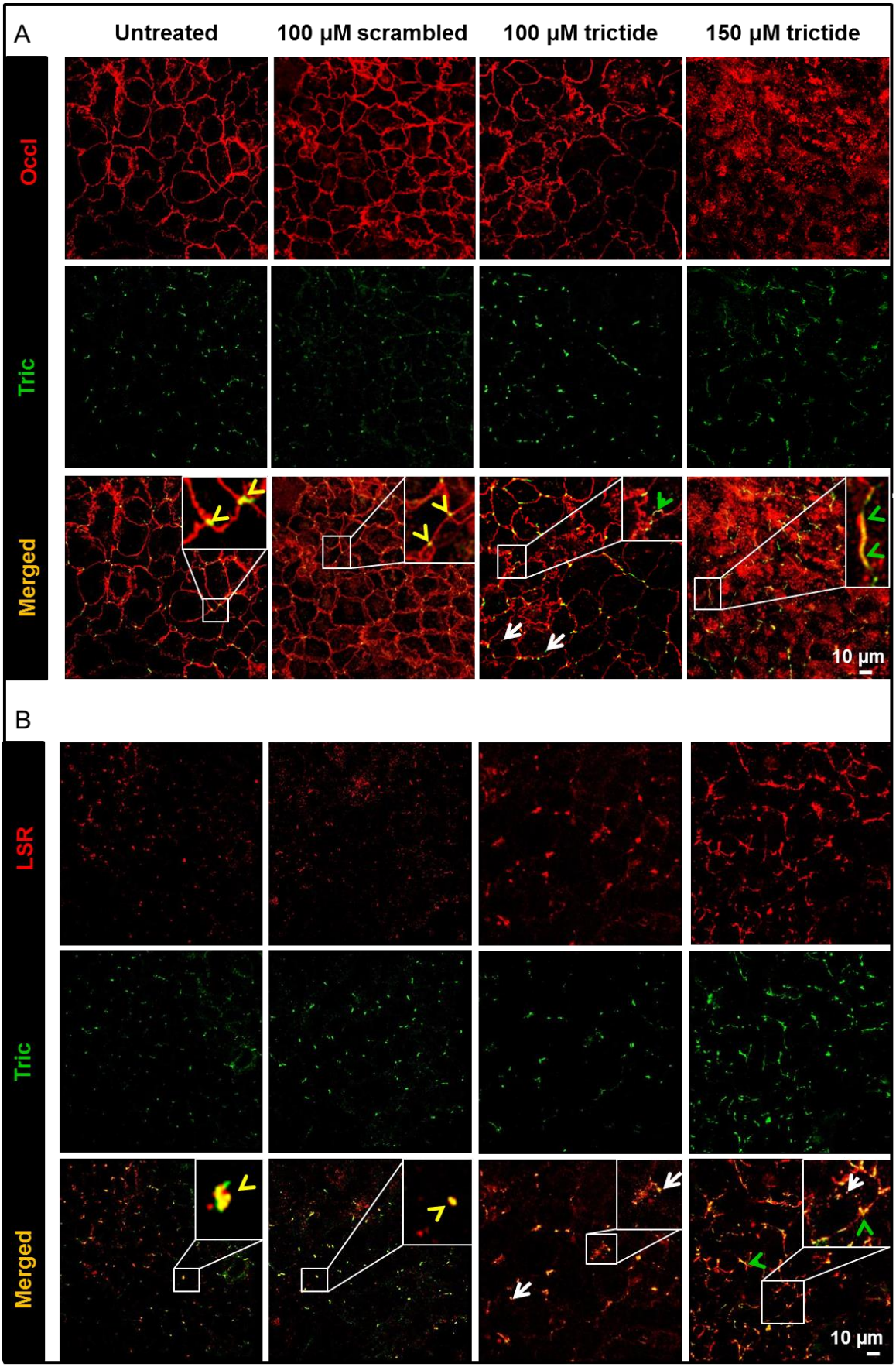

Fig. 4.9 See figure legend on the next page.

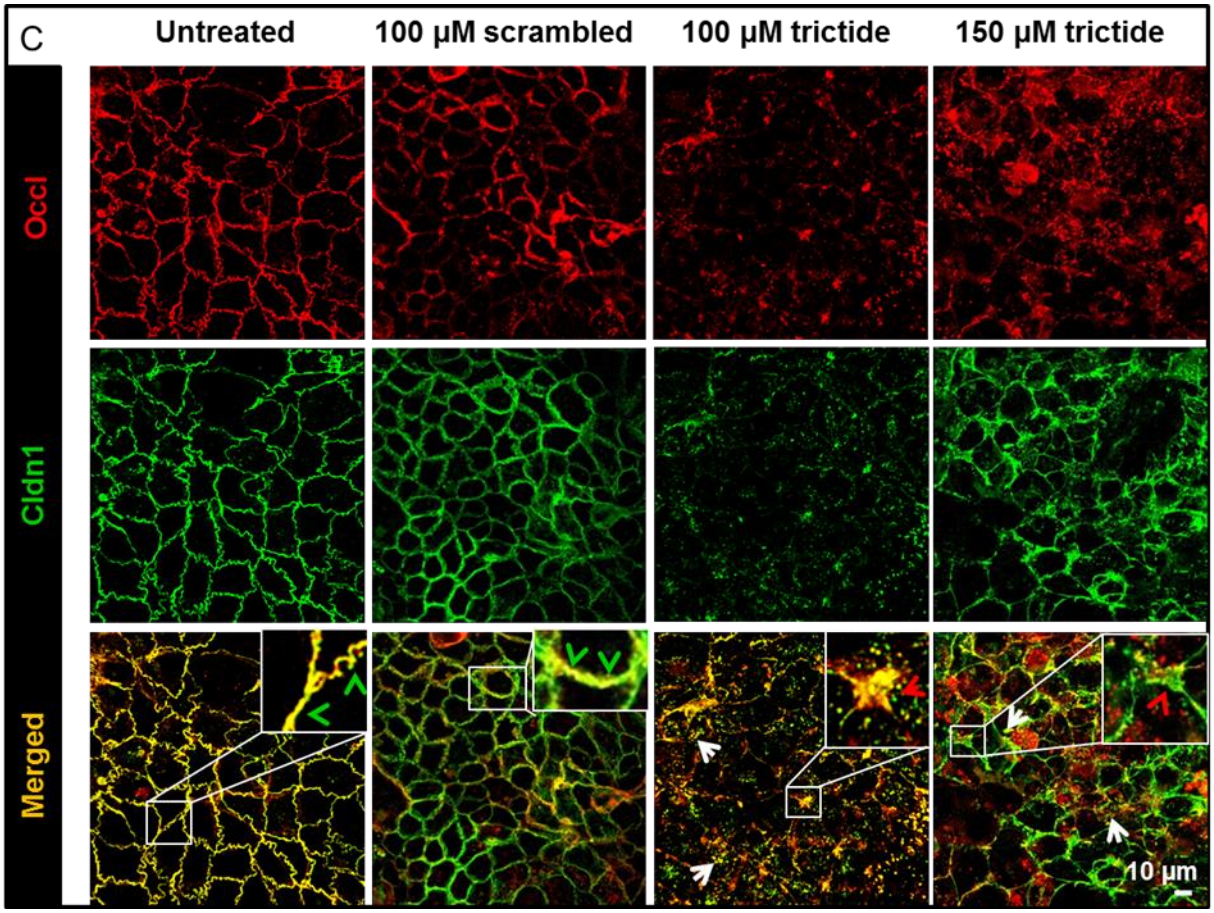

Fig. 4.9 Proteins related to the tricellular tight junctions are strongly affected by 16 h treatment with trictide. (Continuation of A and B from page 11) Human epithelial colorectal adenocarcinoma cells were grown until confluency and then incubated with peptide-free (untreated), scrambled peptide and trictide containing medium. Z-stack images were taken by confocal laser scanning microscopy and maximum intensity Z-projection method was performed. **(A)** Occludin (Occl) and tricellulin (Tric) co-stainings: In the untreated and scrambled trictide treated sample, Tric was localized to tricellular tight junctions (tTJs) (yellow arrowheads), whereas Occl was localized to bicellular tight junctions (bTJs). After 100 µM trictide treatment, Occl and Tric were internalized (white arrows). Tric localization was extended to bTJs after both 100 and 150 µM trictide treatments (green arrowheads). **(B)** Lipolysis-stimulated lipoprotein receptor (LSR) and Tric co-stainings: In the untreated and scrambled trictide treated sample, Tric and LSR localized exclusively to tTJs (yellow arrowheads). Trictide addition led to co-internalization of Tric and LSR (white arrows), and to extended signals of Tric and LSR towards bTJs (green arrowheads). **(C)** Occl and claudin-1 (Cldn1) co-stainings: In the untreated and scrambled trictide treated sample, Cldn-1 and Occl localized exclusively to bTJs (green arrowheads). After trictide treatment, Cldn-1 and Occl co-internalized (white arrows), and concentrated signals appeared around tTJs (red arrowhead).

In untreated samples, Tric localizes as a dot-like structure where 3-cells come together, while Occl localizes mainly at cell borders where 2-cells meet (Fig. 4.9A, yellow arrowheads). After treatment with 100 µM trictide for 16 h, immunocytochemical stainings revealed discontinuous Occl staining and elongated Tric staining through bicellular plasma membrane (Fig. 4.9A, green arrowheads).

LSR and Tric signals of untreated and scrambled trictide treated samples were observed as yellow dots at tricellular contacts (Fig. 4.9B, yellow arrowheads). Samples labelled with LSR and Tric exhibited co-internalization of both proteins (white arrows) and signals extending from tTJs to bTJs when cells were administered with 100 µM or 150 µM trictide (Fig. 4.9B, green arrowheads).

In untreated samples, Occl and Cldn1 co-stainings showed yellow co-localizing signals along cell-cell contacts (Fig. 4.9C, green arrowheads). Only with scrambled trictide, the green signal was more abundant than the yellow signal that indicates reduction of Occl and increase of Cldn1. The distribution of Occl and Cldn1 along the entire cell surface was different. The reason for that is Caco-2 cells growing upwards in various degrees, resulting in variable cell heights. These variations cause maximum intensity projected Z-stacks to reveal different amounts of Occl and Cldn1 at different levels. After 100 µM trictide, Cldn1 remained near the tricellular area (Fig. 4.9C, red arrowhead) and Cldn1 signal was reduced at bicellular area. Occl was dispersed discontinuously throughout bTJs, and proteins were co-internalized after 100 and 150 µM of trictide (Fig. 4.9C, white arrows).

To sum up, 100 µM of scrambled trictide did not cause considerable changes to the typical localization of Tric, LSR, Occl, and Cldn1 (Fig. 4.9A, B, C, second column). After treatment with 150 µM trictide, alterations in the localization of these TJ proteins were intensified due to the presence of the greater concentration of the peptide (Fig. 4.9A, B, C, fourth column). In this chapter, it was confirmed that the mechanism of trictide affecting cell barrier integrity also modifies localization of tricellular and bicellular TJ proteins.

4.3.2.6. Trictide mainly causes down-regulation of tricellulin and occludin

The remarkable effect of trictide on barrier integrity and increase of permeability of the barrier raised the question of what happens at expression levels of TJ proteins. Therefore, mRNA expressions of TAMPs, LSR, Cldn1, Cldn5 and ZO-1 were analyzed by qRT-PCR in Caco-2 cells (Table.S2). mRNA values ($2^{\Delta Ct}$) (see chapter 3.2.8.1) of proteins expressed in untreated controls were: Tric ($12\pm0.7\bullet10^{-3}$), Occl ($18\pm3\bullet10^{-3}$), MD3 ($7\pm0.7\bullet10^{-4}$), LSR ($16\pm2\bullet10^{-3}$), Cldn1 ($4\pm0.1\bullet10^{-3}$), Cldn5 ($30\pm6\bullet10^{-7}$), and ZO-1 ($7\pm1\bullet10^{-3}$).

Thus, incubation with 150 µM trictide decreased mRNA expression of several TJ proteins significantly compared to untreated control. As expected, trictide reduced Tric mRNA down to 43±10%. Even though there is no similarity found between human marveld3

(MD3) and scrambled peptide, MD3 mRNA was reduced by both scrambled trictide (51±6%) and trictide (37±8%). Cldn1 expression was decreased to 58±10%; Cldn5 expression was similarly decreased (60±13%) by trictide (Fig. 4.10A). The latter result directed trictide investigation to work on a cell line with higher Cldn5 expression level because Caco-2 cells do not express high levels of Cldn5 (see chapter 4.3.3.3).

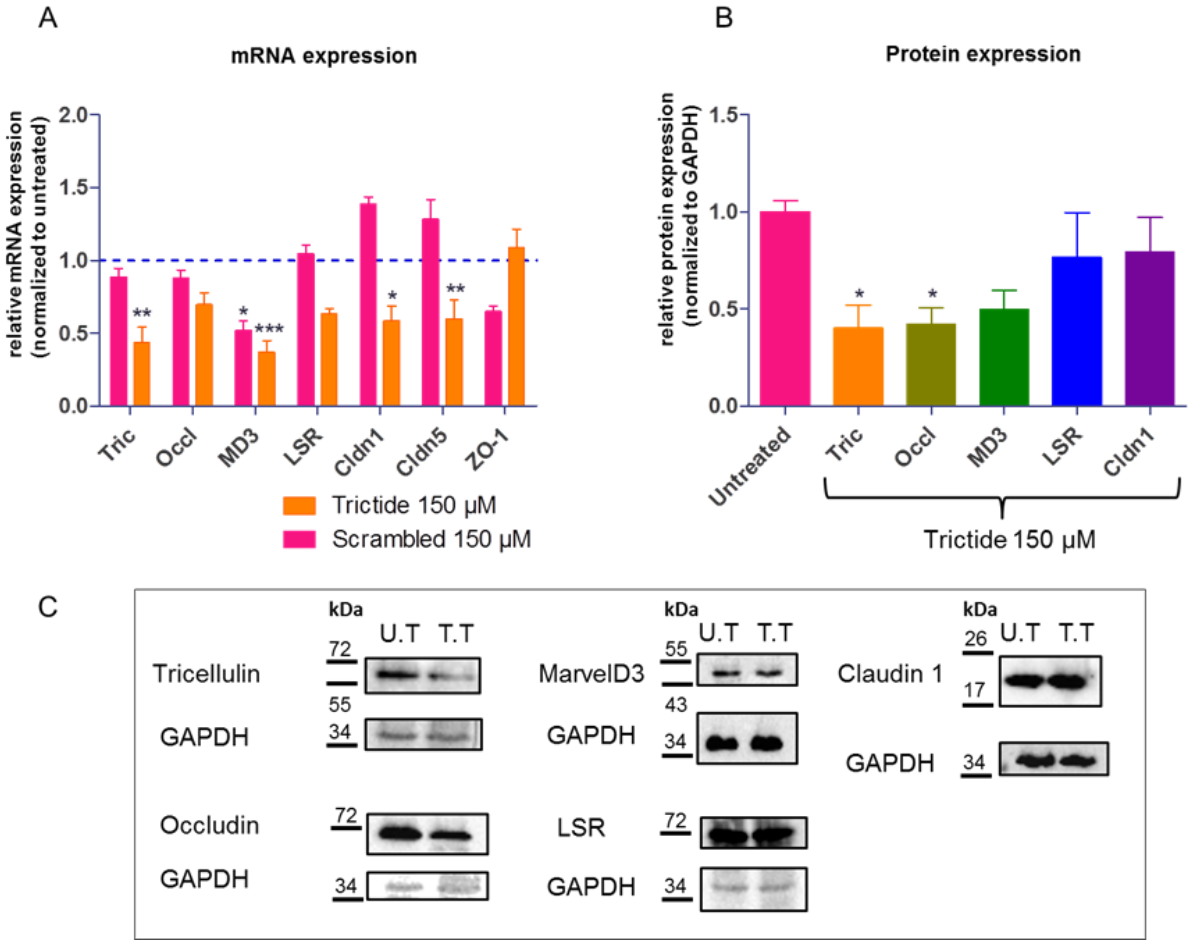

Fig. 4.10 Trictide down-regulates expression of tricellulin, marvelD3, occludin and claudins in human colon carcinoma epithelial cells. (A) Effect on messenger RNA (mRNA) of designated proteins upon trictide and scrambled trictide treatment compared to untreated control ($2^{\Delta\Delta Ct}$) (blue dotted line). mRNA normalized to β-actin (Actb) ($\Delta Ct = {}_{Ctjunction\ protein} - Ct_{actin}$); Ct, Cycle threshold; total incubation time, 16 h; two-way ANOVA test was applied prior to Bonferroni's comparison *post hoc* test; mean±SEM; n=10; * $P \leq 0.05$, ** $P \leq 0.01$, *** $P \leq 0.001$ versus untreated control. **(B)** Effect on tight junction protein expressions upon trictide treatment compared to peptide-free medium (untreated). Expression levels were determined by Western blotting followed by densitometry analysis of protein band intensities. Expression levels were normalized to GAPDH (Glyceraldehyde 3-Phosphate Dehydrogenase) and compared to untreated control. Total incubation time, 16 h; one-way ANOVA test was applied prior to Dunnett's comparison *post hoc* test; mean±SEM; n ≥5; * $P \leq 0.05$ versus untreated control. **(C)** Examples of Western blotted TJ protein bands were given. Expected protein sizes are: tricellulin (Tric), 64 kDa; occludin (Occl), 65 kDa; marvelD3 (MD3), 45 kDa; anti-lipolysis stimulated lipoprotein receptor (LSR), 71.4 kDa; claudin-1 (Cldn1), 23 kDa. U.T, untreated; T.T, 150 µM trictide treated; 30 µg protein/ well was loaded.

Protein expressions of TAMPs, LSR and Cldn1 were measured to examine whether mRNA changes were reflected in protein quantities. As a result of 150 µM trictide administration, Tric expression decreased to 40±11% and Occl expression decreased to 42±8%. The rest of the proteins exhibited expression levels such as: MD3 (50±10%), LSR (77±22%) and Cldn1 (80±18%) (Fig. 4.10B). Only Tric and Occl were down-regulated significantly compared to the untreated control samples, and stated effects can be also observed in the given protein bands (Fig. 4.10C).

4.3.3. Effect of trictide on claudin-5 rich endothelial cells forming blood-brain barrier

In chapter 4.3.2.6, it was stated that Cldn5 mRNA expression of Caco-2 cells was affected by trictide treatment. Thus, trictide investigations were performed with mouse brain endothelial cells (bEnd.3) expressing high Cldn5 amount. Unfortunately, bEnd.3 cells express limited numbers of TJ proteins in high amounts such as: Occl, Cldn5, Cldn12 (Berndt, 2017). That is why it was not possible to investigate interplay between Cldn5 and Tric.

4.3.3.1. Trictide weakens the paracellular barrier of mouse brain endothelial cells

The ECIS measurements in Fig. 4.11 showed TER change relative to the untreated sample plotted against the time, starting with peptide addition. Effects of each condition were statistically calculated compared to untreated cells. Before treatment, all cells reached a stable TER of 1077.8±44.4 $\Omega \cdot cm^2$ (n=4). Untreated control cells showed TER of 1503.7±206.5 $\Omega \cdot cm^2$ after 21 h of administration. 50 µM trictide (95±9%) and scrambled trictide (98±7%) had no effect on TER during the administration time.

Significant effect of 100 µM trictide on TER started at 9 h (75±8%) and developed further at 10 h (66±9%) and 11 h (58±1%). At the end of the incubation time TER was decreased to 16±1%. On the other hand, 75 µM trictide decreased TER gradually and significantly starting from 14 h (62±3%) and decreased further at 15 h (57±3%), 16 h (51±2%), 17 h (46±2%) and 18 h (42±2%) of incubation (Fig. 4.11).

Trictide was known to open epithelial cell barriers after 16 h of incubation (see chapter 4.3.2.1). Investigations with endothelial cell barrier confirmed that trictide reduced

transcellular resistance significantly from 9 h with 100 µM and from 14 h with 75 µM of trictide.

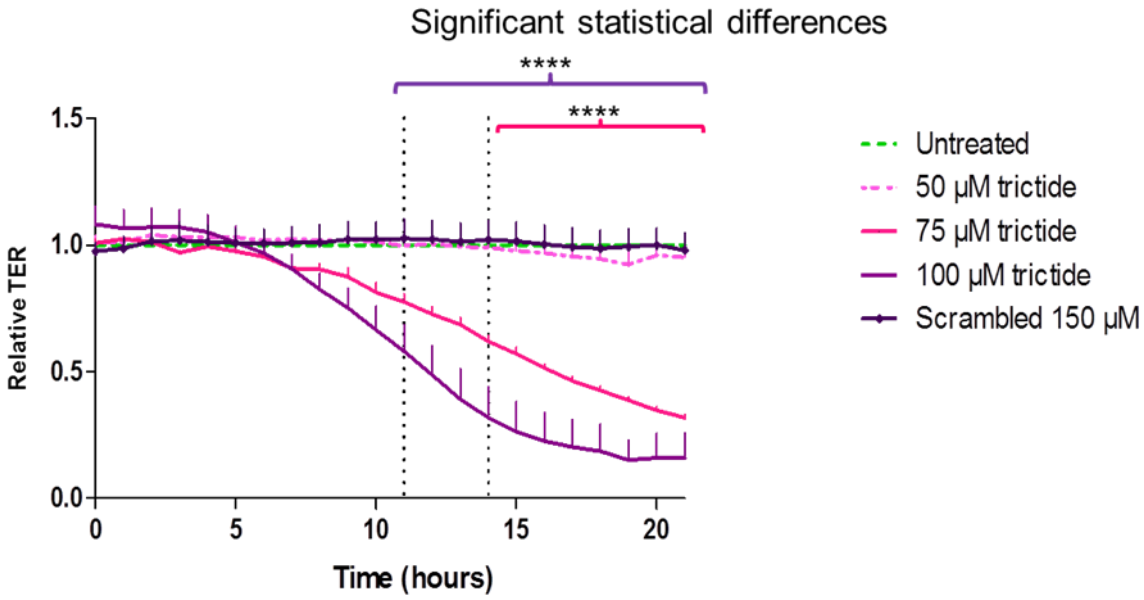

Fig. 4.11 Trictide weakens the paracellular barrier of mouse brain endothelial cells starting from 9 h of incubation. Effect on transcellular electrical resistance (TER) upon 50-100 µM trictide and 150 µM scrambled trictide administration compared to peptide-free medium (untreated). Measurements were done by electric cell-substrate impedance sensor. The graph initiated with peptide administration; total incubation time, 21 h; dotted lines, time points of statistically significant changes; two-way ANOVA test was applied prior to Bonferroni's comparison *post hoc* test; mean±SEM; n=4; ****P ≤ 0.0001 versus untreated control.

4.3.3.2. Up to 75 micromolar, trictide is not cytotoxic for mouse brain endothelial cells

In order to measure cell viability after peptide treatment, neutral red uptake assay was used. The bEnd.3 cells were incubated with peptide-free medium (untreated) and a variety of trictide concentrations. Scrambled trictide was used as negative and 0.01% triton X-100 containing medium was used as positive control. Thus, cell viability values were observed for: 50 µM (118±10%), 75µM (98±10%), 100 µM (50±23%) and 150 µM of trictide (13±4%), 150 µM of scrambled trictide (124±12%), and 0.01% triton X-100 (10±3%) (Fig. 4.12). Even though Triton X-100 concentration was maintained 10 times less compared to experiments with Caco-2 cells, much lower cell viability was detected. Taken together, 75 µM trictide was not cytotoxic within the duration of the experiment (16 h), and bEnd.3 cells were more sensitive for trictide administration. For further studies, 75 µM trictide was chosen as working concentration.

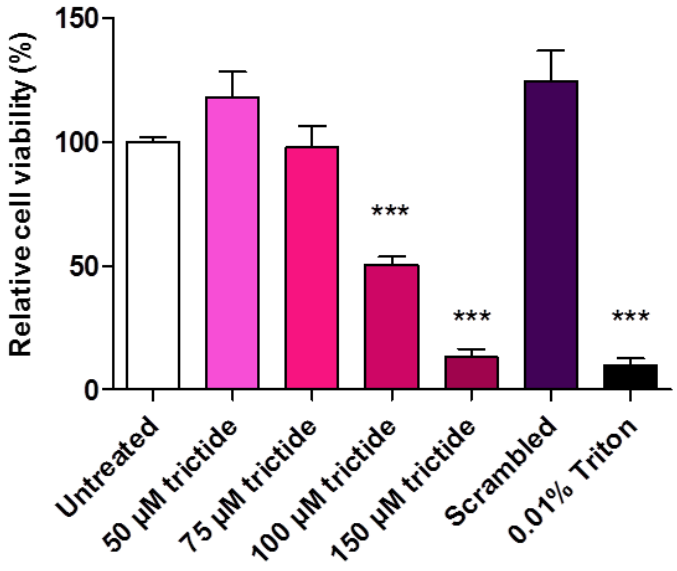

Fig. 4.12 ≤75 µM trictide is not cytotoxic for mouse brain endothelial cells (bEnd.3). Effect on cell viability upon 50-150 µM trictide, 150 µM scrambled trictide (negative control), and 0.01% Triton X-100 (positive control) treatment compared to peptide-free medium (untreated). Cell viability was measured with neutral red uptake assay. Total incubation time, 16 h; one-way ANOVA test was applied prior to Dunnett's comparison *post hoc* test; mean±SEM; n=7; *** P < 0.001 versus untreated control.

4.3.3.3. Trictide down-regulates claudin-1, lipolysis stimulated lipoprotein receptor and occludin in mouse brain endothelial cells

The mode of action of trictide affecting individual junctional proteins and leading to disruption of barrier integrity was not fully understood. mRNA expressions of Tric, Cldn5, Cldn1, LSR, ZO-1, Occl and Cldn25 were analyzed upon 75 µM trictide and 100 µM scrambled trictide administration compared to peptide-free medium (untreated) (Table S3). mRNA investigations of TJ proteins were started with 100 µM trictide concentration (Fig. S5) but reduced to 75 µM due to better cell viability. Cldn25 was included as a non-barrier forming control because it does not exhibit classical claudin TJ function with barrier tightening (Ohnishi et al., 2017). To date there is no information about interaction between Cldn25 and Tric available.

Incubation with 75 µM trictide significantly decreased mRNA expression of Cldn1 (36±8%), LSR (26±4%) and Occl (50±6%) (Fig. 4.13A). In fact, bEnd.3 cells expressed only a few junctional proteins in high levels, with exemplary delta Ct values ($2^{\Delta Ct}$) such as Cldn5 ($12\pm1\cdot10^{-2}$), Cldn25 ($1.5\pm0.2\cdot10^{-3}$), Occl ($5\pm0.7\cdot10^{-3}$) and ZO-1 ($21\pm0.8\cdot10^{-3}$). Tric is the lowest expressed protein ($4.6\pm1.1\cdot10^{-6}$). Cldn1 ($8\pm1.6\cdot10^{-6}$) and LSR ($9\pm1\cdot10^{-5}$)

exhibited greater expression compared to Tric but were still expressed less compared to Cldn5, Cldn25, Occl and ZO-1.

Protein expression level of Cldn5 upon 75 µM trictide application was tested to inspect whether mRNA change was reflected by protein amount and compared to untreated control. Cldn5 was up to 177±75% up-regulated, but this effect was insignificant due to high variation among samples (Fig. 4.13B). An example of analyzed protein bands can be observed in figure 4.13C.

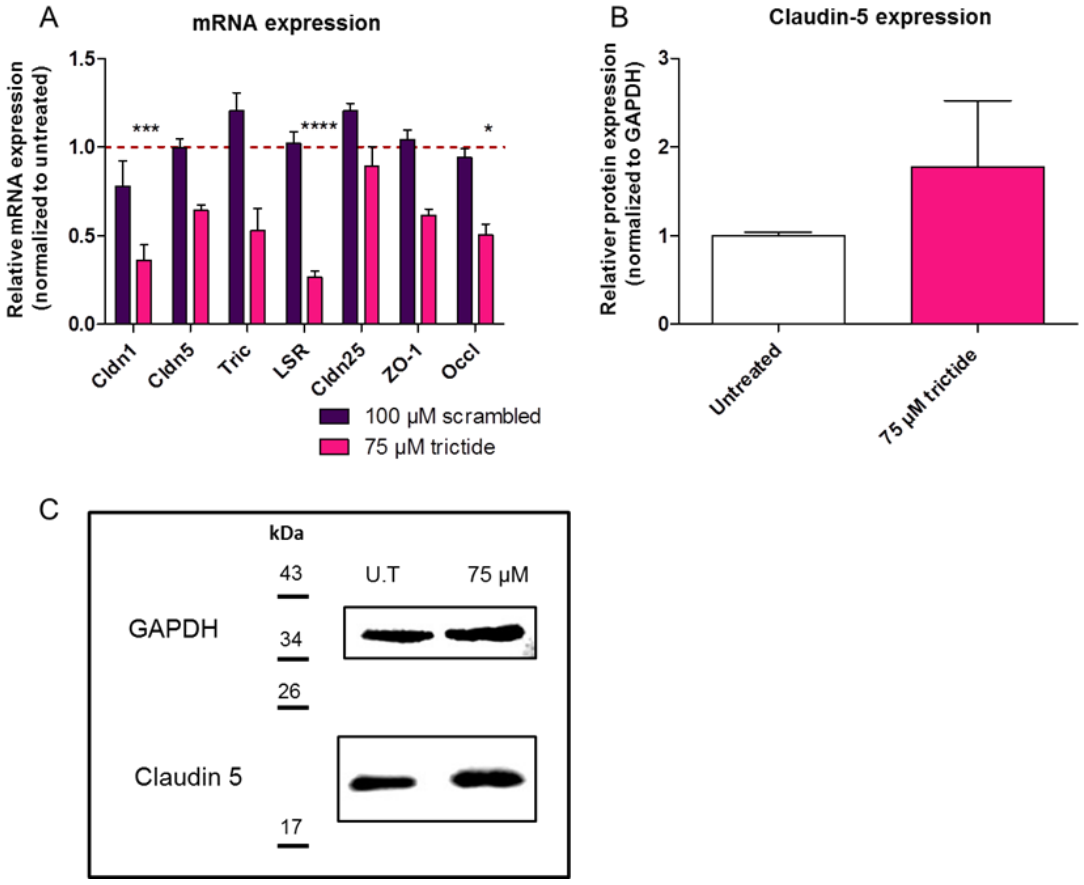

Fig. 4.13 Trictide down-regulates mRNA expression of claudin-1, LSR and occludin in mouse brain endothelial cells. (A) Effect on messenger RNA (mRNA) of designated proteins; upon trictide and scrambled trictide treatment compared to untreated control ($2^{\Delta\Delta Ct}$) (red dotted line). mRNA normalized to β-actin (Actb) ($\Delta Ct = Ct_{junction\ protein} - Ct_{actin}$); Ct, Cycle threshold; total incubation time, 16 h; two-way ANOVA test was applied prior to Bonferroni's comparison post hoc test; mean±SEM; n≥8; * $P \leq 0.05$, *** $P \leq 0.001$, ****$P \leq 0.0001$ versus untreated control. **(B)** Effect on claudin-5 (Cldn5) expressions upon trictide treatment compared to peptide-free medium (untreated). Expression levels were determined by Western blotting followed by densitometry analysis of protein band intensities. Expression levels were normalized to GAPDH (glyceraldehyde 3-phosphate dehydrogenase) and compared to untreated control. Total incubation time, 16 h; student's t-test was applied prior to Mann Whitney *post hoc* test; mean±SEM; n=4. **(C)** Examples of Western blotted Cldn5 (22 kDa) protein bands were given. Cldn1, claudin-1; Tric, tricellulin; LSR, anti-lipolysis stimulated lipoprotein receptor; Cldn25, claudin-25; ZO-1, *zonula occludens* protein-1; Occl, occludin; U.T, untreated; 75 µM trictide treated.

4.3.3.4. Trictide concentrates claudin-5 and ZO-1 around tricellular contacts

It was demonstrated that trictide affects endothelial cell barrier and down-regulates several TJ proteins (chapter 4.3.3.1). Cldn5 is of specific interest for trictide administration in brain endothelial cells because of its status as the highest expressed TJ protein and the main paracellular tightener. The localization changes were displayed after 16 h of 75 or 100 µM trictide treatments (Fig. 4.14). Cells treated with peptide-free medium and 75 µM scrambled trictide containing medium were included as negative control. Cells were labelled with anti-Cldn5 (TJ marker) and anti-ZO-1 (junctional marker) antibodies. Both 75 and 100 µM trictide concentrations were included to visualize gradual effect of the peptide.

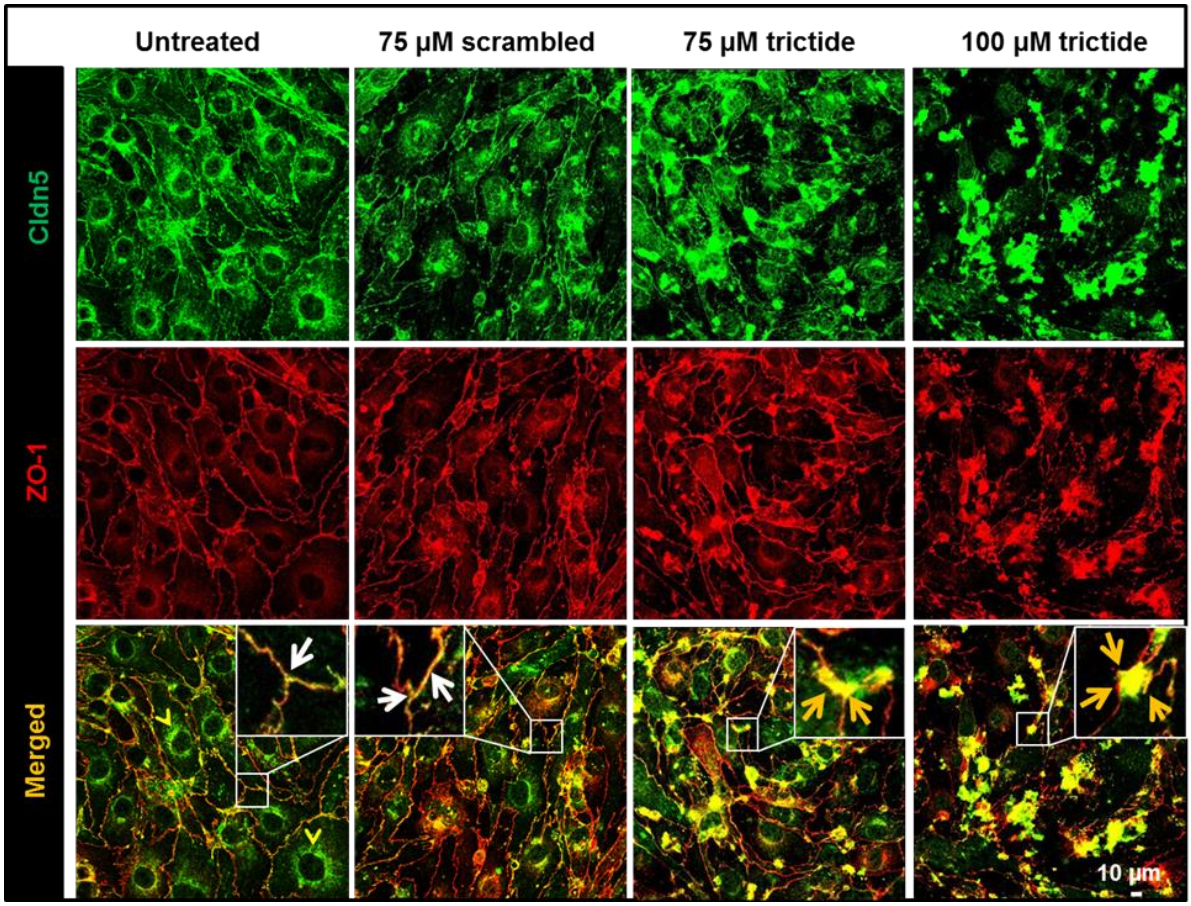

Fig. 4.14 Claudin-5 (Cldn5) and *zonula occludens* protein-1 (ZO-1) are enriched close to tricellular area after trictide treatment. Mouse brain endothelial cells (bEnd.3) were grown until confluency and then incubated with peptide-free (untreated), scrambled and trictide containing medium. Z-stack images were taken by confocal laser scanning microscopy and maximum intensity Z-projection method was performed. **Untreated cells:** Cldn5 localized at bicellular contacts (white arrow) and intracellularly (yellow arrowheads). ZO-1 also localized at bicellular contacts. **75 µM scrambled trictide:** No major changes were observed. Cldn5 and ZO-1 located at bicellular contacts (white arrow). **75 µM trictide:** Cldn5 was clustered around tricellular contacts (yellow arrows) and ZO-1 was still localizing at bicellular contacts. **100 µM trictide:** Cldn5 and ZO-1 were localized stronger around tricellular area (yellow arrows). Incubation time, 16 h; enlarged images, 4x magnification; 40x objective.

Untreated samples showed staining at bicellular contacts for both Cldn5 (green) and ZO-1 (red) (Fig. 4.14, white arrow). Cldn5 antibody also showed intracellular staining around cell nucleus. After scrambled trictide (75 µM) treatment, signals were dominantly observed at bicellular contacts (Fig. 4.14, white arrows). In the 75 µM trictide treated samples, bicellular localization of Cldn5 was reduced and green signal was redistributed to concentrate around tricellular contacts (Fig. 4.14, red arrows). At those points, the signal manifested itself yellow due to the fact that ZO-1 protein also moved close to tricellular contacts. 100 µM trictide caused greater alterations compared to 75 µM. The staining of Cldn5 as well as ZO-1 at bicellular contacts was severely reduced. A greater part of the signals was concentrated as a yellow signal around tricellular areas (Fig. 4.14, yellow arrows).

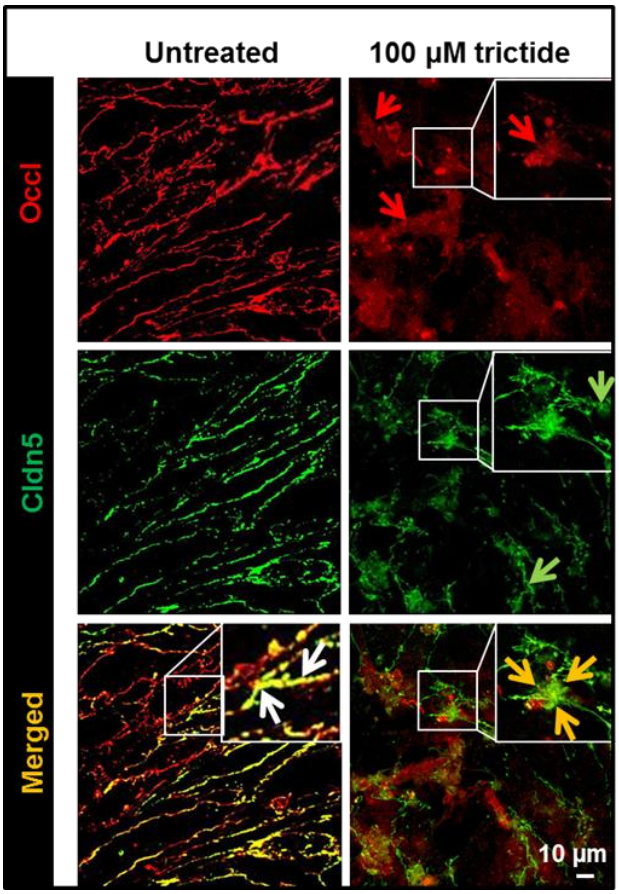

Fig. 4.15 Claudin-5 (Cldn5) and occludin (Occl) are internalized and enriched close to tricellular area after trictide treatment. Mouse brain endothelial cells (bEnd.3) were grown until confluency and then incubated with peptide-free (untreated) and trictide containing medium. Z-stack images were taken by confocal laser scanning microscopy and maximum intensity Z-projection method was performed. **Untreated cells:** Cldn5 and Occl localized at bicellular and tricellular contacts (white arrows). **100 µM trictide:** both Cldn5 (green arrows) and Occl (red arrows) were internalized and observed at subcellular areas. Cldn5 and Occl were redistributed from bicellular contacts to intracellular area and clustered around tricellular contacts (yellow arrows). Incubation time, 16 h; enlarged images, 4x magnification; 63x objective.

Modifications of Cldn5 and Occl localizations were further observed after trictide administration. Untreated cells exhibited sharp staining of Cldn5 (green) and Occl (red) at bicellular contacts that overlapped also at tricellular contacts (Fig. 4.15, white arrows). After 100 µM trictide treatment, Occl was highly internalized and detected also at subcellular areas (Fig. 4.15, red arrows) that were likewise close to tricellular contacts (Fig. 4.15, yellow arrows). Although Cldn5 was internalized to a lesser degree compared to Occl, it can be still found at bicellular contacts (Fig. 4.15, green arrows). Just like Cldn5 and ZO-1 stainings, Cldn5 and Occl signals were concentrated around some tricellular contacts.

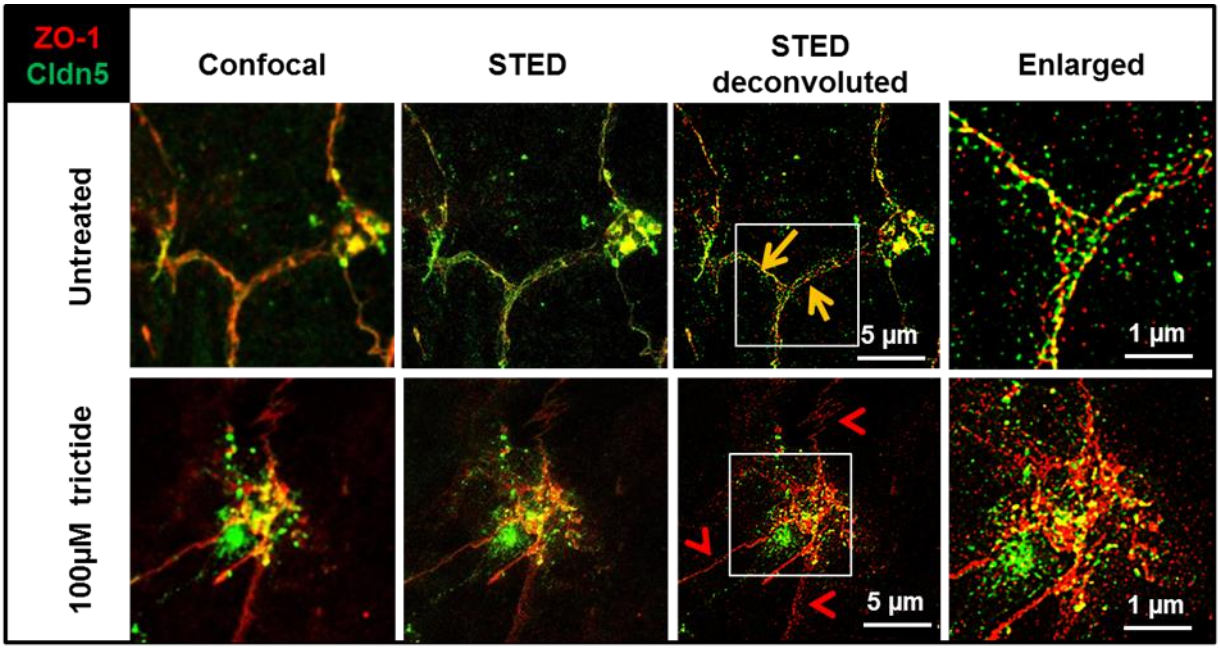

Fig. 4.16 Claudin-5 (Cldn5) is concentrated around tricellular area after trictide treatment. Mouse brain endothelial cells (bEnd.3) were grown until confluency and then incubated with peptide-free (untreated) and trictide containing medium. Individual cell contacts were imaged using confocal microscopy and STED super-resolution microscopy. The deconvoluted STED image showed further background reduction. **Untreated cells:** Cldn5 and ZO-1 localized at bicellular and tricellular contacts (yellow arrows). **100 µM trictide:** Cldn5 and ZO-1 were clustered around tricellular contacts (enlarged). ZO-1 could also be observed at bicellular contacts (red arrowheads). Incubation time, 16 h; enlarged images, zoom: 6.0; 100x objective.

The opening of the mouse endothelial cell barrier was clearly demonstrated according to results in chapter 4.3.3.1. But it was not yet understood if the barrier was open exclusively at tricellular or additionally at bicellular areas. However, immunocytostainings of trictide administered bEnd.3 cells showed clear modification of localization for Cldn5, ZO-1 and

Occl as they tend to concentrate around the tricellular contacts. To comprehend detailed structure of the tricellular area, images with stimulated emission depletion (STED) super-resolution microscopy were taken. The cells were treated with 100 µM trictide-containing and peptide-free medium (untreated).

Untreated cells showed typical localization of Cldn5 and ZO-1 at bicellular junctions. Confocal microscopy pictures of Cldn5 (green) and ZO-1 (red) showed overlapping signals (orange-like) along the plasma membrane. However, STED images enabled to present distinct signals of Cldn5 and ZO-1 at cell contacts. Deconvoluted STED images further decreased the background noise at bicellular contacts and demonstrated organization of individual junctional proteins (Fig. 4. 16, yellow arrows).

Consequently, 100 µM trictide treated cells revealed reduced signal of Cldn5 at the plasma membrane and formation of clustering Cldn5 signals at the periphery of tricellular contacts. ZO-1 signal remained at bicellular contacts (Fig. 4. 16, red arrowheads). Deconvoluted STED images revealed an opening in the centre of the tricellular region. This strong modulation of highly barrier forming TJ protein Cldn5 indicates opening of endothelial cell barriers tricellularly.

4.3.4. Tricellulin knockdown confirms the tricellulin dependent function of trictide

As a control experiment, TER and the permeability for FD4 were investigated in Tric knockdown cells. Thus, human colon epithelial adenocarcinoma cell line HT 29/B6 was transfected with either a vector containing shRNA sequence targeting Tric (shTric) or the empty vector. Two clones of shTric were used: shTric20= 20% and shTric50 = 50% of initial tricellulin expression (Fig. 4.16C). Cells were seeded on filters and treated with 150 µM trictide or 150 µM scrambled trictide for 24 h. Cells transfected with the empty vector and administered with scrambled trictide constructed the control group.

Cells transfected with the empty vector and treated with trictide showed significant decrease of TER compared to the scrambled trictide treatment. The shTric50 clone also displayed significant decrease of TER after trictide, compared to scrambled trictide administration. However, the shTric20 clone did not demonstrate any difference in TER between trictide and scrambled trictide applications (Fig. 4.17A). In this case, the cell

barrier was already leaky due to only 20% of Tric expression, and therefore trictide had no additional effect on the barrier in the absence of Tric.

Trictide treatment significantly increased the paracellular permeability of the cells transfected with the empty vector compared to scrambled trictide treatment. Both scrambled trictide administered shTric50 and shTric20 clones were permeable for 4 kDa molecule, compared to the control group. Trictide increased the permeability of both clones only slightly (Fig. 4.17B). In conclusion, the shTric50 and shTric20 Tric knockdown clones showed decreased TER down to 50% and 25%, thus underlining the importance of Tric in cellular barrier tightness. Moreover, Tric knockdown clones show that the effect of trictide depends on the presence of Tric

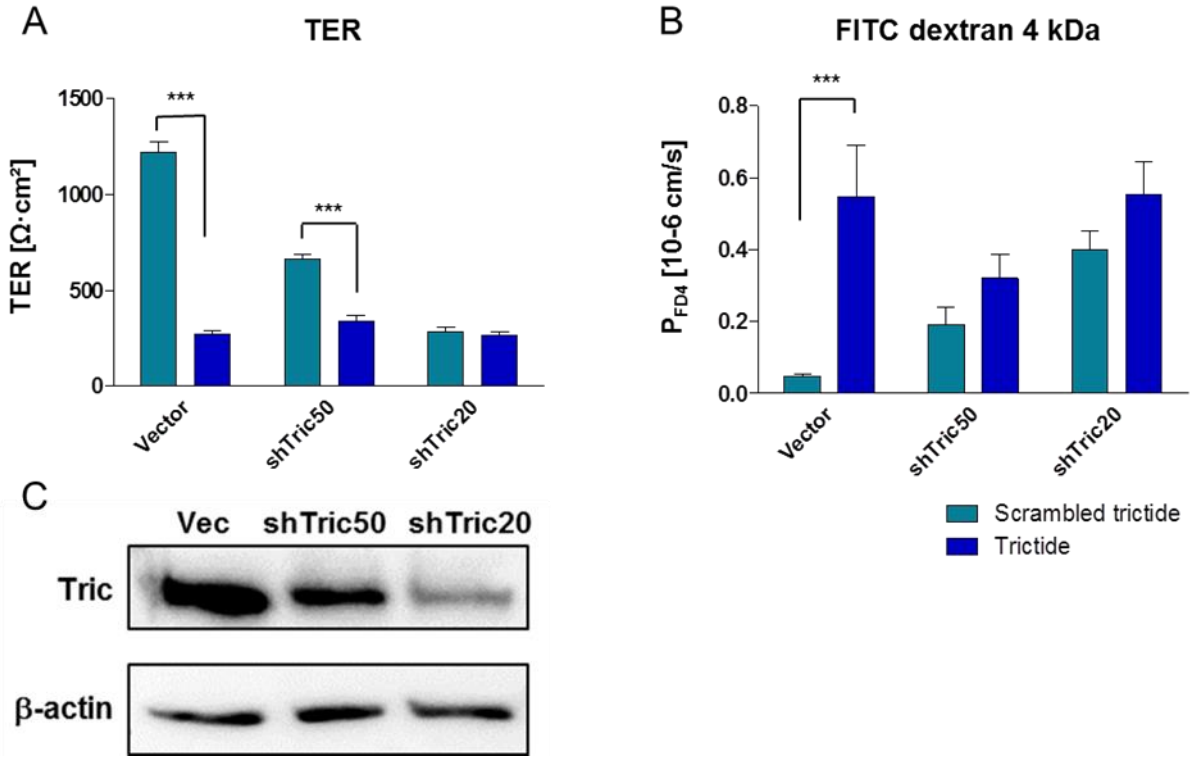

Fig. 4.17 Tricellulin (Tric) knockdown cells confirmed that trictide function depends on the presence of Tric. Human colon epithelial adenocarcinoma cells (HT 29/B6) were transfected with vector containing a sequence for short hairpin RNA (shRNA) that targeted Tric (shTric) or the empty vector. Cells were seeded on filters and apically treated with 150 µM trictide or scrambled trictide for 24 h. **(A)** Transcellular electrical resistance (TER) of cells after peptide administrations **(B)** Permeation of 4-kDa FITC (fluorescein isothiocyanate) dextran (FD4) after peptide treatments (basolateral determination of FD4 concentrations at 0, 20, 40, 60 and 120 min). **(C)** Vec, empty vector transfected cells; shTric50/shTric20, clones showing 50%/20% Tric expression. Two-way ANOVA test was applied prior to Bonferroni's comparison *post hoc* test; mean±SEM; n=6. *** $P \leq 0.001$ versus scrambled trictide (control peptide). Experiments were performed in collaboration with Dr. Susanne Krug (Institute of Clinical Physiology, Charite, Berlin).

4.3.5. Effect of trictide on Madin-Darby canine kidney and human embryonic kidney cells

Since HEK cells are embryonic cells, they do not express TJs. Hence, experiments conducted with HEK cells enable analysis of proteins without interference from other TJ proteins. Fluorescence resonance energy transfer (FRET) assay was used to determine the *cis*-interactions for different TJ proteins and to define specific binding sites of trictide at the molecular level. MDCK-II cells express TJ proteins endogenously and form a paracellular barrier. They were used to examine interactions between Tric-Tric after trictide administration. MDCK-II cells were also ideal for STED due to their homogenous propagation over microscopic cover glasses that reduced background and uneven deposition of cells.

4.3.5.1. Trictide affects tight junction protein-protein interactions

The association of TJ proteins along the plasma membrane is termed *cis*-interaction. To study this association, FRET efficiencies between CFP and YFP-labelled proteins were measured. Possible alterations of interactions between TJ proteins caused by 50 µM trictide and 50 µM scrambled trictide treatments in comparison to the peptide-free medium in HEK cells after 24 h were investigated. Subsequently, FRET efficiencies were measured by LSM microscopy (Fig. 4.18).

The strong bicellular homophilic *cis*-interaction of Cldn1 was not changed by either the scrambled peptide or trictide (Cording et al., 2013). Similarly, bicellular heterophilic *cis*-interactions for Cldn1–Occl and Cldn1-MD3, that do not involve Tric, were not affected. As expected, *cis*-interactions in Tric-containing protein combinations were reduced by trictide. The *cis*-interaction of Cldn1 with Tric was disrupted by 50%; Tric with MD3 completely disappeared after incubation with trictide (Fig. 4.18 B). Fluorescent images of cell-cell contacts between co-transfected Tric and Cldn1 expressing cells showed localization of both proteins at bicellular contacts after peptide administrations (Figure 4.18A). It is usual to observe Tric at bicellular area in the TJ protein transfected HEK cell systems (Cording et al., 2013).

Occl localization was strongly affected from trictide application in Caco-2 cells (see chapter 4.3.2.5). In order to examine this effect, Occl-Occl FRET efficiencies were

measured after trictide and scrambled trictide. Accordingly, the data showed that homophilic *cis*-interaction of Occl decreased to 47% after trictide treatment compared to untreated control (Fig. 4.18B).

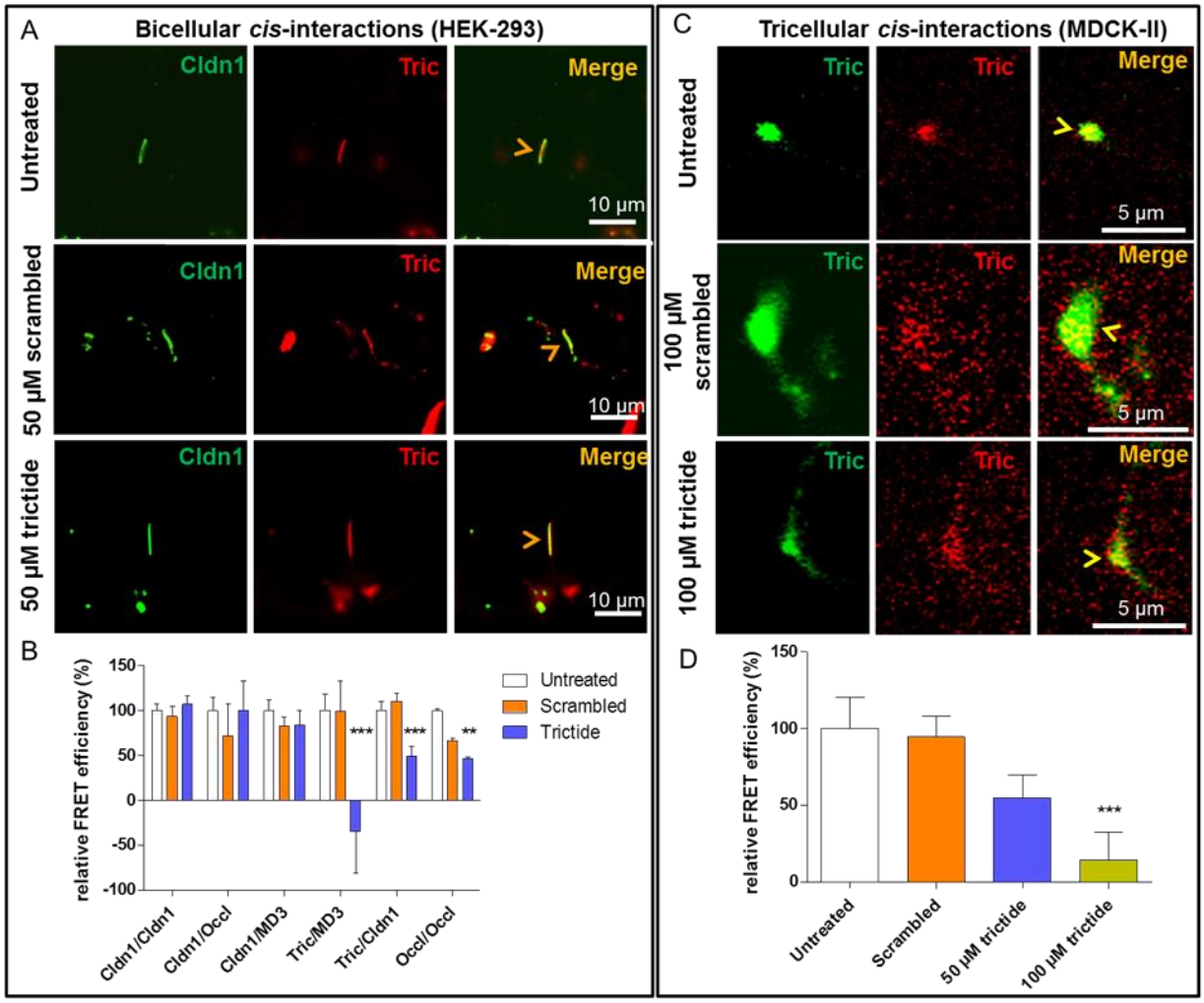

Fig. 4.18 Trictide interferes with protein interactions of tricellulin (Tric) and with Occl (occludin)-Occl association (**A)** Human embryonic kidney (HEK-293) cells transiently expressing Claudin-1 (Cldn1)-YFP and CFP-Tric were treated with peptide free, scrambled trictide or trictide-containing medium. Both proteins localized at bicellular contacts (orange arrowheads). (**B)** *cis*-Interactions of homo- and heterophilic protein combinations as determined by fluorescence resonance energy transfer (FRET) in co-transfected HEK cells after treatment with 50 µM of trictide or scrambled trictide. The protein pairs were transfected as YFP- and CFP-fusion proteins, respectively. **(C)** Co-transfected Madin-Darby canine kidney cells (MDCK-II) transiently expressing CFP- and YFP-Tric treated with scrambled trictide or trictide; the proteins were localized at tricellular contacts (yellow arrowheads). Due to overexpression of Tric, signals were also observed in cytosol. **(D)** Trictide treatment leads to a loss of Tric-Tric *cis*-interaction, as demonstrated by FRET in co-transfected MDCK-II cells. **(B-D)** MD3, marvelD3; YFP/CFP, yellow/cyan fluorescent protein; total incubation time, 24 h; one-way ANOVA test was applied prior to Dunnett's comparison *post hoc* test; mean±SEM; n=19; ** $P \leq 0.01$, *** $P < 0.001$ versus untreated control.

Homophilic *cis*-interactions of Tric were measured at tTJs in co-transfected MDCK-II cells. Tric mostly localized to the tTJs and showed relatively strong FRET signals (11.6±2.3) (Fig. 4.18C). 50 µM trictide decreased the homophilic tricellular Tric *cis*-interaction to 55% while 100 µM trictide reduced it to 14% (Fig. 4.18D). Consequently, Tric containing homophilic and heterophilic *cis*-interactions and Occl-Occl *cis*-interactions was significantly affected by trictide administration.

4.3.5.2. Super resolution microscopy revealed opening of the tricellular sealing tube

To understand the detailed structure of the tricellular junctions, STED super-resolution microscopy was applied on MDCK-II cells. This method also enabled us to detect alterations in the assembly of TJ proteins after trictide treatment.

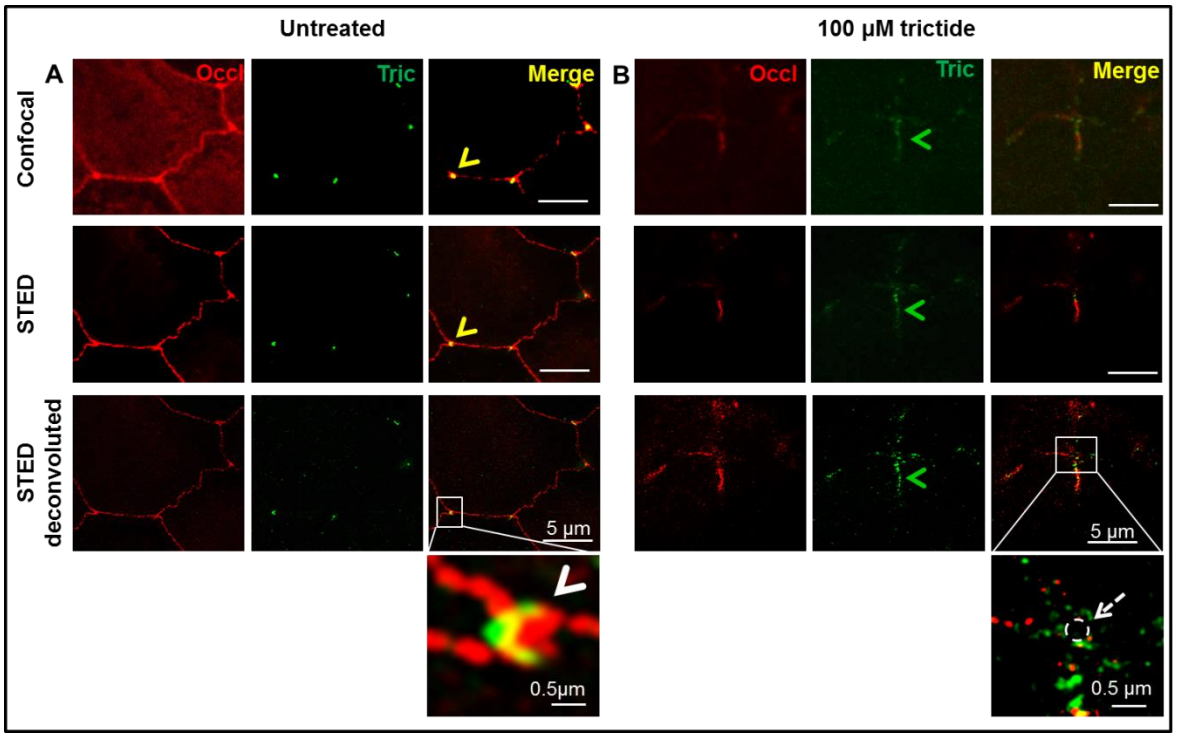

Fig. 4.19 Trictide treatment opens tricellular tight junctions by removing tricellulin (Tric) and occludin (Occl) from the tricellular cell contact area. (**A)** Madin-Darby canine kidney (MDCK-II) cells immunostained against Occl and Tric. Individual cells were imaged using confocal microscopy (top) and stimulated emission depletion (STED) super-resolution microscopy (middle); the deconvoluted STED images showed further background reduction (bottom). The enlargement (white box, merge) suggests only partially co-localized Tric and Occl signals (white arrowhead). Under control conditions, Tric localized at tricellular junctions (yellow arrowheads). (**B)** MDCK-II cells were treated with trictide. Tric spread out to the bicellular tight junctions (green arrowheads) and left a tricellulin-free area (white dotted arrow and circle, enlarged merge). Incubation time, 16 h; enlarged images, zoom: 6.0; 100x objective.

Untreated cells exhibited typical localization of Occl at bicellular and Tric at tricellular junctions. Confocal microscopy pictures of Occl (red) and Tric (green) showed yellow points at tricellular junctions (Fig. 4.19A, yellow arrowheads). These could be interpreted as co-localization of both proteins at tTJs (Fig. 4.19A, upper row). However, STED pictures showed cell junctions with less background, and it was possible to detect TJ proteins aligning along the cell membrane with 50 nm resolution (Fig. 4.19A, middle row). Deconvoluted STED images further decreased the background noise at tricellular junctions and demonstrated that Tric and Occl co-localized only partially at tTJs (Fig. 4.19A, lower row). Tric stands in the center and Occl surrounds it from three bicellular contact ends (Fig. 4.19A, enlarged image, white arrowhead).

100 µM trictide treated cells revealed elongated signals of Tric from tTJs to bTJs in confocal images (green arrowheads) (Fig. 4.19B, upper row). STED, in particular deconvoluted images, revealed a Tric-free area in the center of the tricellular region (Fig. 4.19B, enlarged image, white dashed circle and arrow). The absence of Tric suggests that tricellular sealing tube is open and could enable paracellular passage of molecules through tricellular contact. It also supports the argument that trictide binds Tric and affects tricellular area preferentially. However, we should also consider other mechanisms like internalization and down-regulation of Tric as potentially leading to localization changes.

4.3.5.3. Trictide redistributes occludin from bicellular junctions progressively during 15 h of incubation

Our objective was to observe the time course of cellular modifications caused by trictide and fluorescently labelled TAMRA-trictide. Spin disk confocal microscopy was used for live-cell imaging in long-term time-lapse. This technique is useful for imaging fluorescence samples for longer durations without being bleached. Therefore YFP-Occl transfected MDCK-II cells were used to emphasize cellular borders with TJ marker protein Occl. This enabled us to track the effect of trictide without using any other marker that might disturb the monolayer after long-lasting treatment.

Untreated cells maintained continuous and linear cell membrane and tricellular contacts throughout the experiment (Fig. 4.20A, yellow arrows). 100 µM of trictide caused disruption and redistribution of Occl at cellular borders. Occl signals were reduced at some bicellular contacts and enriched at others where 3-cells are come together in 6 h and 9 h

images (Fig. 4.20B, white arrowheads). Between 12 h and 15 h, it became clear that YFP-Occl signal was weakened at bicellular contacts progressively and finally enriched intracellularly (Fig. 4.20B, white arrows).

Cells administered with 10 µM TAMRA-trictide containing medium had two different fluorescent signals: YFP-Occl (green) and TAMRA-trictide (red). This combination allowed the investigation of peptide's mode of action by comparison of the influence on cellular borders and peptide's localization. The lesser concentration was used to avoid saturated fluorescence intensity of TAMRA and to maintain TJ visibility before Occl is removed from the cell junctions. It was observed that starting from 6 h of peptide treatment, YFP-Occl signal deteriorated at tricellullar contacts (Fig. 4.20C, dotted circles), and these areas (central-tube like) were filled with fluorescently labelled trictide (Fig. 4.20D, red arrows). From 12 h, the effect on cell contacts was further expanded to 2-cell contacts that caused accumulation of TAMRA-trictide in greater amounts up to 2 µm deep submembranously. After 15 h of treatment, fluorescent peptide was localizing intracellularly around most of the bicellular contacts and causing disappearance of cell contacts.

The internalization and enrichment of Occl protein around tricellular contacts after trictide was presented in chapter 4.3.3.4. Furthermore it was found that Occl expression is significantly down-regulated consequent to trictide administration. So the outcome of this live-cell imaging (Fig. 4.20) is in accordance with previous chapters and enabled us to acquire more information about the mode of action. Trictide first affects tTJs, then starts transfer of TJ proteins to bicellular contacts, and finally causes internalization of proteins. Even though trictide's binding mechanism is not fully understood, it evidently disturbs association of TJ proteins in a way that alters their localization and affects the integrity of bi- and tricellular junctions.

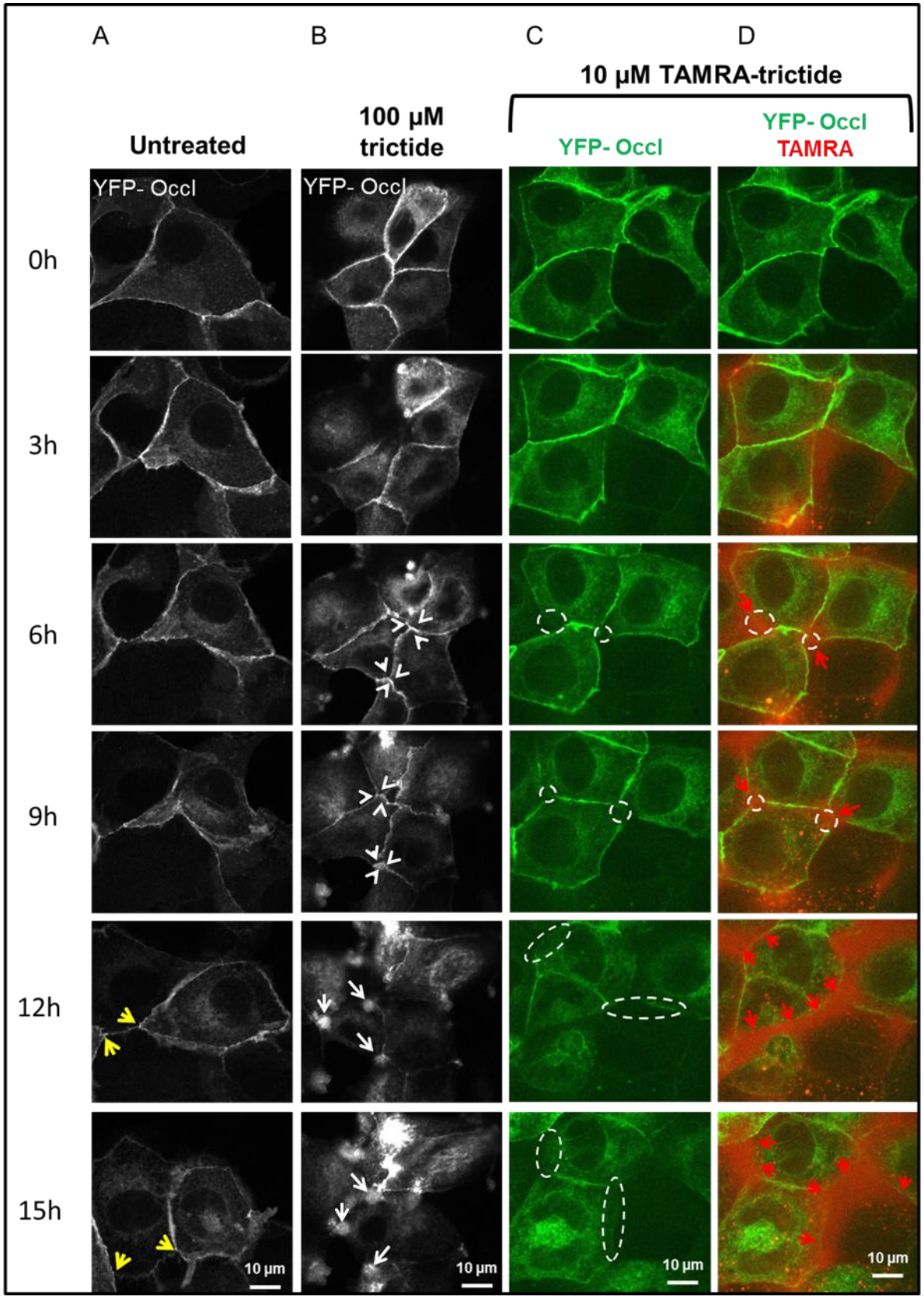

Fig. 4.20 See figure legend on the next page.

4.20 Live-cell imaging for 15 h reveals that trictide and TAMRA-trictide alter localization of occludin and cause its redistribution from 2-cell contacts to cytosol. YFP-Occl (occludin with yellow fluorescent protein) transfected MDCK-II (Madin-Darby Canine Kidney) cells were treated with peptide-free medium, trictide and TAMRA-trictide. First image (0 h) was taken before the treatment. Every 15 min, an image was taken to record each condition. Cells were kept in a 10% CO_2 controlled environment at 37 ºC. **(A)** Untreated cells have continuous and sharp cellular borders (yellow arrows). **(B)** 100 µM trictide caused disappearance of Occl from bicellular contacts and enrichment around tricellular area (white arrow heads); and starting from 12 h, relocalization to cytosol begins under the cell membrane (white arrows). **(A-B)** Black and white was used to create better contrast for images with single channel. **(C)** YFP-Occl signals observable alterations at cellular borders. From 6h, tricellular contacts were the first to disappear gradually (dotted circles). **(D)** Merged images of YFP and TAMRA signals. At 3 h, TAMRA signal was observed particularly at 3-cell contacts. At 6 h, some tricellular contacts became invisible (dotted circles) and these zones were filled with TAMRA signal (red arrows). This effect increased in time and, starting from 12 h on, a greater amount of TAMRA signal was localized at cellular contacts (red arrows), which caused complete loss of some 3-cell borders (dotted circles) as well as submembranous uptake.

4.3.6. *In vivo* effect of trictide

4.3.6.1. Trictide can be detected in mouse blood plasma up to 48 hours

Before starting *in vivo* use of trictide, its degradation curve was obtained to study how long trictide is stable in mouse blood. Blood plasma contains peptidases that play a role in peptide stability (Di, 2015). In order to investigate the half-life of peptide, TAMRA-trictide (3.1 kDa) was dissolved in mouse blood plasma at 37 °C and incubated for 48 h. TAMRA fluorescence was observed at about 10 kDa band of the protein marker and at the bottom of the gel (Fig. 4.21A). A possible reason is that the samples were separated with the gradient SDS-PAGE gel, and 10 kDa was the smallest size of that protein marker.

After densitometry analysis of bands on SDS-PAGE gel, 2 h, 4 h, 8 h, 12 h, 13 h, 24 h and 48 h samples have respectively shown 82%, 68%, 59%, 50%, 42%, 30% and 14% of fluorescence intensity. Taken together, TAMRA-trictide's half-life in blood plasma was detected as 12 ± 1.9 h (Fig. 4.21B). 4 h and 24 h time points were chosen for further *in vivo* experiments because of the *in vitro* effect observed at 16 h and in order to check the effect of trictide in a prolonged interval.

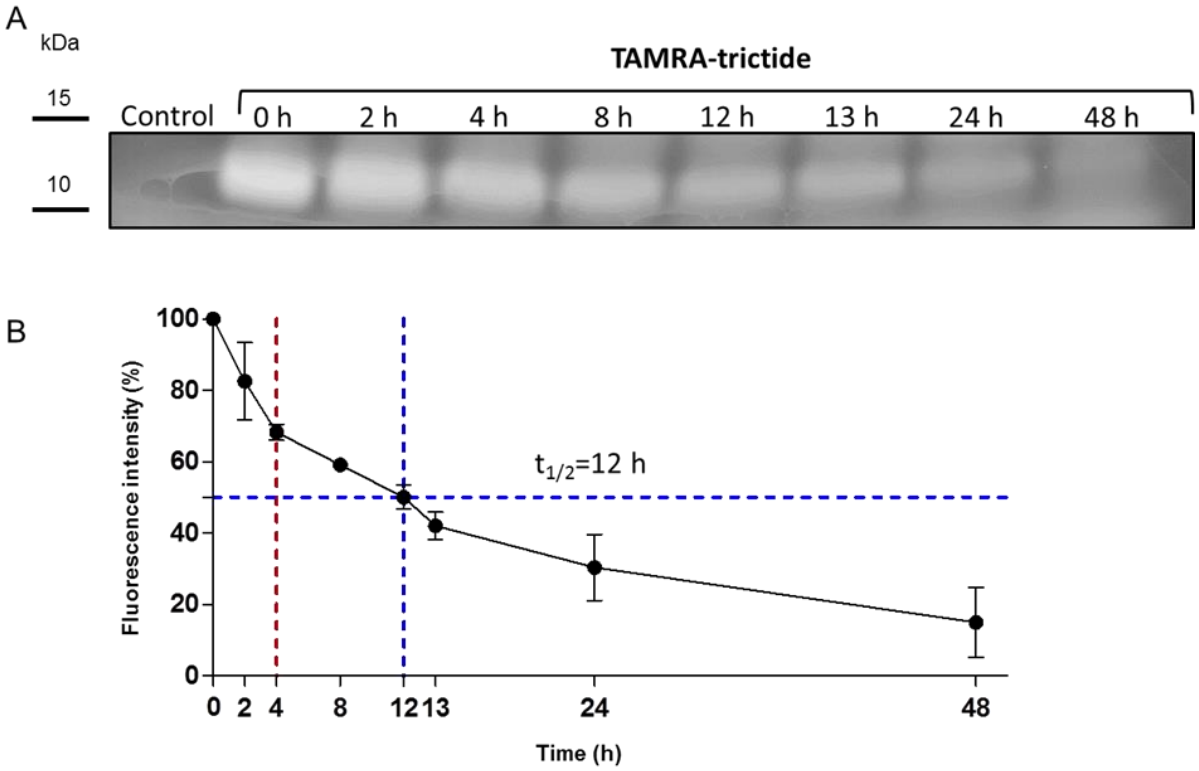

Fig. 4.21 TAMRA-trictide (human) has a half-life of 12 h in mouse blood plasma. 10 µM of TAMRA-trictide was dissolved in mouse blood plasma and incubated at 37 ºC up to 48 h. **(A)** Fluorescence image of gradient SDS-PAGE gel bands pertaining to the indicated incubation times. First sample was blood plasma without fluorescent peptide (negative control). Bands were observed close to the level of 10 kDa marker protein. **(B)** Fluorescence intensity of bands was assessed by densitometry analysis. Dashed blue line indicates half-life of the peptide at about 12 h. Red line indicates intensity of a 4 h sample that was preferentially selected for the experiments described in the following chapters. Values were relative to the 0 h sample (as 100% of fluorescence intensity); mean ± SEM; n=3.

4.3.6.2. Junction proteins in mouse brain and kidney are highly affected by trictide

Brain and kidney barriers were both essential targets to be examined when the effect of trictide was tested as a potential drug enhancer. The primary objective was to measure changes in several junctional proteins at mRNA level. For this purpose, 800 µM trictide (3.6 µmol/kg dissolved in phosphate-buffered saline) or phosphate-buffered saline (control group) was administered (100 µl/22 g mice) to mice which were sacrificed after 4 h or 24 h. Absolute mRNA expressions ($2^{\Delta Ct}$ values) of the junction proteins are given in Table 26 and Table S4.

Table 26. Messenger RNA (mRNA) expression of untreated mouse brain and kidney

Absolute mRNA expressions ($2^{\Delta Ct}$)	Brain	Kidney
Tric	$13\pm3\cdot10^{-5}$	$32\pm1\cdot10^{-4}$
LSR	$68\pm7\cdot10^{-5}$	$47\pm3\cdot10^{-4}$
Occl	$10\pm0.4\cdot10^{-4}$	$68\pm2\cdot10^{-4}$
Cldn5	$39\pm1\cdot10^{-4}$	
ZO-1	$8\pm1\cdot10^{-3}$	$7.9\pm0.2\cdot10^{-3}$
Cldn12	$34\pm3\cdot10^{-4}$	
Cldn25	$67\pm2\cdot10^{-4}$	$42\pm2\cdot10^{-4}$
MD3		$19\pm1\cdot10^{-5}$
Cldn1		$44\pm1\cdot10^{-4}$

mRNA normalized to β-actin (Actb) ($\Delta Ct = Ct_{junction\ protein} - Ct_{actin}$); Ct, Cycle threshold; mean ± SEM; n ≥4; Tric, tricellulin; LSR, lipolysis stimulated lipoprotein receptor; Occl, occludin; Cldn5, claudin-5; ZO-1, *zonula occludens* protein 1; Cldn12, claudin-12; Cldn25, claudin-25; MD3, marvelD3; Cldn1, claudin-1.

In brain, 24 h after trictide administration, Cldn5 was up-regulated compared to 4 h after application (1.75 fold) and control group (1.4 fold). Tric was also up-regulated after 24 h compared to 4 h after application (1.9 fold) and control group (1.7 fold). On the other hand, LSR was down-regulated after 4 h of treatment compared to control group (58±5%) (Fig. 4.22A).

In kidney, Tric expression was reduced to 65±5% after 4 h and to 32±1% 24 h after trictide injections. MD3 expression was decreased to 38±9% 24 h after trictide administration. This effect was highly significant compared to both 4 h (94±8%) and control group mRNA levels. ZO-1 mRNA was first up-regulated 1.3 fold (131±11%) at 4 h, then down-regulated (94±1%) 24 h after the treatment (Fig. 4.22B). Cldn25 mRNA was expressed in kidney at almost the same level as in the brain (Table 26). Cldn25 was down-regulated to 58±1% 24 h after the injections, and this down-regulation is statistically significant compared to 4 h after application (97±9%) and control group (Fig. 4.22B). The data of mRNA expressions suggests that trictide has a time-dependent gradual effect at mRNA level. Due to the strong alterations of important barrier-forming TJ proteins (Tric, Cldn5 and LSR), barrier properties of mouse brain, kidney and liver were investigated after trictide injections.

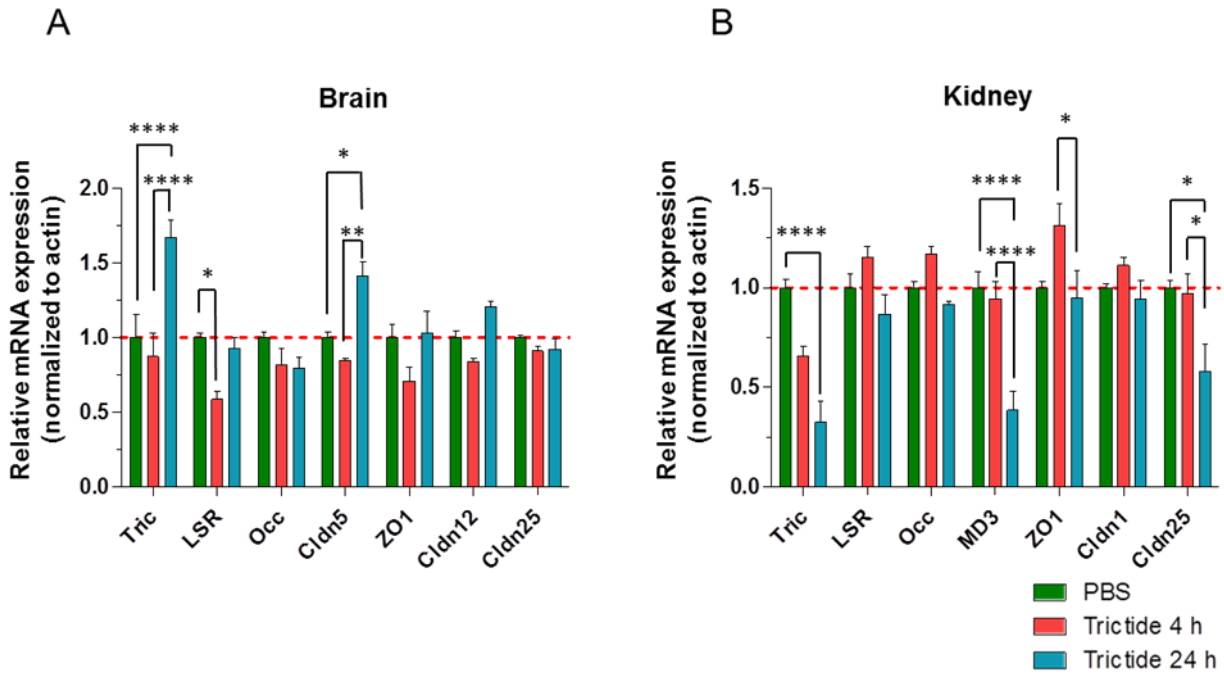

Fig. 4.22 Trictide causes up-regulation of tricellulin (Tric) and claudin-5 (Cldn5), down-regulation of lipolysis stimulated lipoprotein receptor (LSR) in brain. Trictide causes down-regulation of Tric, marvelD3 (MD3), *zonula occludens* protein 1 (ZO1) and claudin-25 (Cldn25) in kidney. Effect on messenger RNA (mRNA) of designated proteins ($2^{\Delta\Delta Ct}$); upon 800 µM of trictide (3.6 µmol/kg) compared to phosphate-buffered saline (PBS) (red dotted line) intravenous injections (100 µl/ 22 g mouse). 4 h and 24 h after the administrations, animals were sacrificed and their brains and kidneys were isolated and prepared for quantitative real-time polymerase chain reaction. (**A)** mRNA expression of junction proteins in trictide administered mouse brain. **(B)** mRNA expression of junction proteins in trictide injected mouse kidney. mRNA normalized to β-actin (Actb) ($\Delta Ct = Ct_{junction\ protein} - Ct_{actin}$); Ct, Cycle threshold; Cldn12, claudin-12; Cldn1, claudin-1; two-way ANOVA test was applied prior to Bonferroni's comparison *post hoc* test; mean ± SEM; n≥4; * P ≤ 0.05, ** P ≤ 0.01, ****P ≤ 0.0001 versus PBS control.

4.3.6.3. Trictide does not change Na-fluorescein uptake of kidney and liver, while uptake in brain tends to be enhanced

Tric was found to be highly expressed in mouse liver and kidney but low in brain (chapter 4.1). Thus, *in vivo* experiments were performed to explore trictide's effect on barrier properties of brain, liver and kidney. PBS or 800 µM of Trictide (3.6 µmol/kg) was administered to mice (100 µl/22 g mice) intravenously. After 4 h of peptide injection, mice were injected again intravenously with Na-fluorescein (0.5 mmol/kg, 100 µl/22 g) and afterwards perfused for ~10 min. The graphs below show comparison between Na-fluorescein uptake of kidney, liver and brain taken from trictide or PBS injected animals (Fig. 4.23).

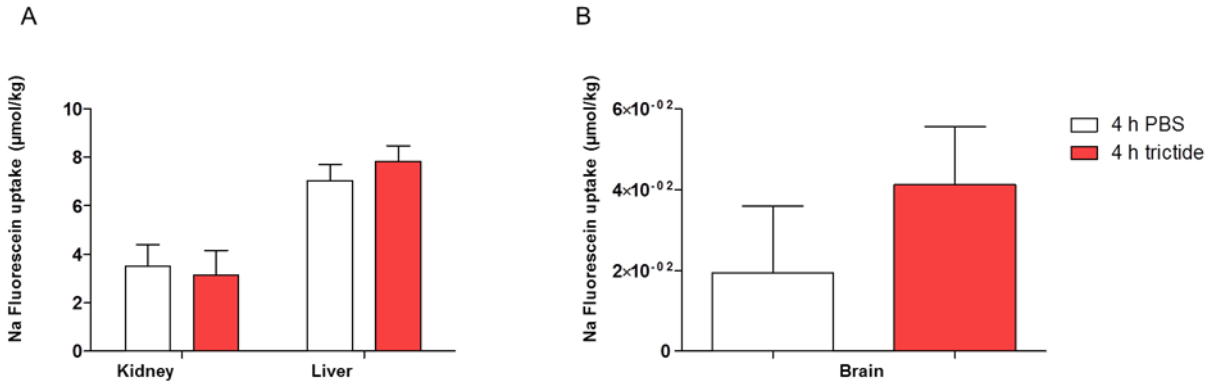

Fig. 4.23 Na-fluorescein uptake of kidney and liver does not change 4 h after trictide administration, but uptake in brain tends to be higher. 800 µM of trictide (3.6 µmol/kg) was injected (100 µl/22 g mice) intravenously and 4 h later the fluorescent dye Na-fluorescein (376 Da; 0.5 mmol/kg, 100 µl/22 g mice) was injected. (**A)** Na-fluorescein uptake in mouse kidney after trictide and phosphate-buffered saline (PBS) injection. **(B)** Na-fluorescein uptake in brain. Na-fluorescein was dissolved in PBS and treatments with only PBS were taken as untreated control. Absolute amount of Na-fluorescein molecule was given as µmol/kg. Student's t-test was applied prior to Mann-Whitney's *post hoc* test versus PBS control. Mean ± SEM, n=9.

In the kidney of trictide and phosphate-buffered saline (PBS) applied animals, we detected 3.5±1 µmol/kg and 4±1 µmol/kg of Na-fluorescein, respectively. In the liver of trictide and PBS administered animals, Na-fluorescein was detected as 8±0.6 µmol/kg and 7±0.7 µmol/kg, respectively. The liver was more permeable for Na-fluorescein compared to the kidney. Neither kidney nor liver showed significant changes of Na-fluorescein levels as a result of trictide injections when compared to PBS (Fig. 4.23A).

The microvessels of brains of the PBS administered animals were tighter and 200 times more impermeable by Na-fluorescein than kidney. In brain of the trictide and PBS applied animals, 0.05±0.01 µmol/kg and 0.02±0.015 µmol/kg of Na-fluorescein was detected, respectively (Fig. 4.23B). Brain uptake of Na-fluorescein in trictide injected animals demonstrated an increase, but due to high variation among data sets, this effect was statistically insignificant. Collectively, trictide tended to open the cerebral barriers for small molecules. However, more experiments would be necessary to confirm the tendency.

4.3.6.4. Claudin-5 and occludin are altered in brain capillaries after trictide administration

Further information on TJ protein amount and localization was necessary to understand the functional consequences of trictide treatment. Brains of 800 µM trictide (3.6 µmol/kg) and

PBS injected mice were cut as thin cryosections and labelled with anti-Cldn5, Tric, Occl and ZO-1 antibodies. Brain capillaries were imaged by STED microscopy to enable observation of changes, especially at 3-cell junctions on a molecular level.

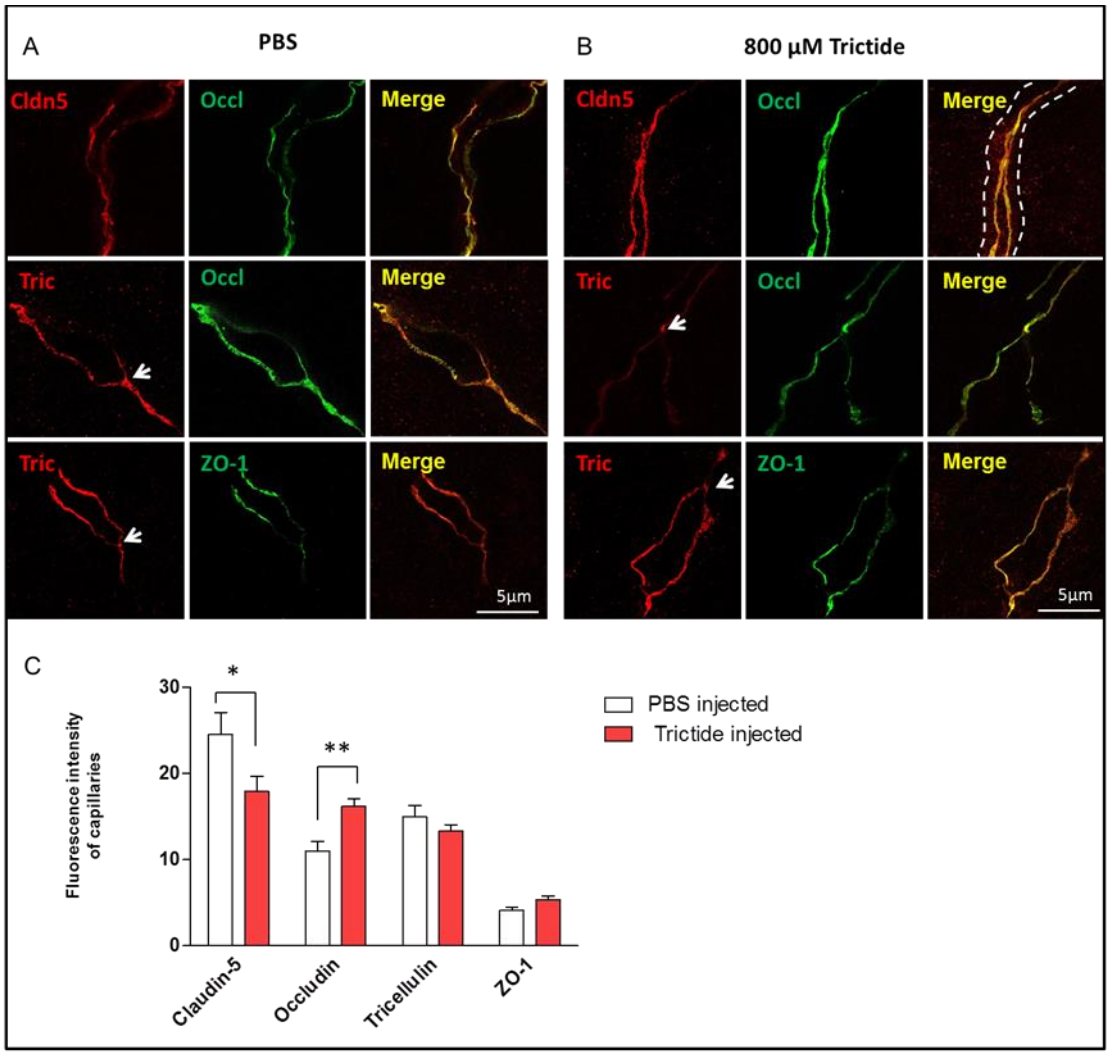

Fig. 4.24 Trictide injections caused slight alterations at the localization of claudin-5 (Cldn5) and tricellulin (Tric), and significant changes of the fluorescence intensity of Cldn5 and occludin (Occl) proteins. (A) Immunofluorescent STED images of brain capillary of phosphate-buffered saline (PBS) injected mice (control group). **(B)** Immunofluorescent STED images of brain capillaries after 800 µM (3.6 µmol/kg) trictide treatment. Tric weakened at tricellular junctions and Cldn5 became poriferous. White arrows, Tric enrichment at tricellular contacts; dashed lines, representative capillary border; 8 µm brain cryosections; zoom: 6.0; 100x objective. **(C)** Fluorescence intensities of brain capillaries from PBS vs. 800 µM trictide injected mice. Cldn5 was down- and Occl was up-regulated after trictide administration. Tric showed tendency of down-regulation. Zonula occludens protein-1, ZO-1; incubation time after injections, 4 h; measurements were performed with ImageJ; two-way ANOVA test was applied prior to Bonferroni's comparison post hoc test; mean±SEM; n=6-16; * $P \leq 0.05$, ** $P \leq 0.01$ versus PBS control.

Cldn5 was included as dominant TJ marker of the BBB and ZO-1 as general cell-cell contact marker in order to confirm the structures displayed in the images as a brain capillary (Fig. 4.24A). No greater changes of the localization of Cldn5, ZO-1 and Occl were observed in the brain capillaries of the trictide group. However, the fluorescence intensity of Cldn5 and Occl appeared slightly altered in the 2-cell junctions. The Cldn5 intensity was weakened and the contact line seemed to become poriferous (Fig. 4.24B). Tric signal was not only visible in tricellular but also at bicellular junctions (Fig. 4.24A). It was possible to distinguish specific Tric signal at tricellular junctions also after trictide administration. Nevertheless, decline of Tric signal occurred in 3-cell junctions after trictide treatment in some slices (Fig. 4.24B, white arrows).

Since visual examination of microscopy images was insufficient to prove up- or down-regulations of the latter proteins, fluorescence intensities of brain capillaries were quantified for Tric, Cldn5, Occl, and ZO-1. According to that analysis, Cldn5 signal was reduced and Occl signal increased significantly in brain capillaries of trictide injected mice. Tric tended towards reduction, while ZO-1 tended to increase (Fig. 4.24C).

Although trictide has a 12 h half-time in blood plasma (Fig. 4.21B), trictide injections did not significantly increase permeability of brain, kidney and liver barriers (Fig. 4.23). In addition, there were significant mRNA expression alterations of Cldn5 and Tric in brain, and of Tric, MD3 and Cldn25 in kidney at 4 h and 24 h after trictide injections (Fig. 4.22). For further *in vivo* studies, more experimentation is necessary; barrier permeability and protein expressions should be more carefully studied approximately 12 h after the administration.

4.3.7. Trictide structure is predicted as a β-sheet formed by two β-strands with surface-exposed aromatic residues.

In order to understand trictide's key structural components for its barrier opening function, trictide and scrambled trictide were analyzed with CD spectroscopy. The spectra were compared with reference spectra (Yang et. al., 1986) in order to determine the proportion of secondary structural elements. On the other hand, 3D structure models of peptides were obtained and verified by the peptide structure prediction program (PEP-FOLD).

Trictide and scrambled trictide mostly showed β–sheet followed by random coil propensity in phosphate buffer. Moreover, in micelles of SDS a pronounced β–sheet conformation was found for both trictide and scrambled trictide. TFE favored a weak α-helical secondary structure propensity, which was not different for trictide and scrambled trictide at representative wavelengths (Fig. 4.25A). Accordingly, the molar ellipticity (Θ) did not exhibit a statistically significant difference from characteristic ellipticity minimum (217 nm for β-sheet, 208 and 222 nm for α-helix).

A

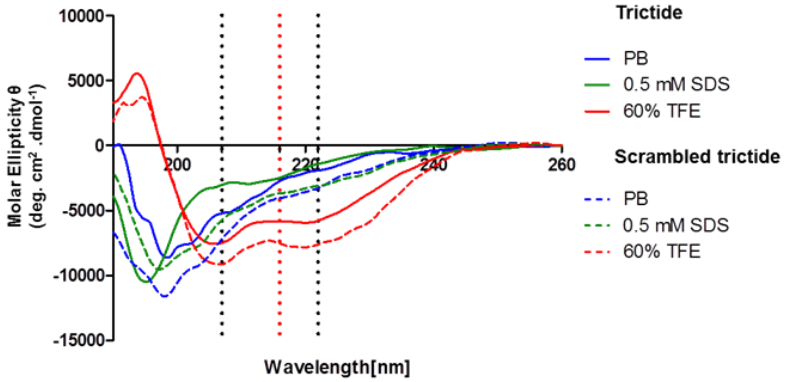

B

Secondary structure prediction (%)

Trictide

Propensity:	random	β-sheet	α-helix	β-turn
PB	36 ± 4	55 ± 5	0	9 ± 1
SDS	35 ± 2	53 ± 3	0	12 ± 1
TFE	35 ± 3	46 ± 8	11 ± 1	9 ± 5
PEP-FOLD	33	50	0	17

Scrambled trictide

Propensity:	random	β-sheet	α-helix	β-turn
PB	37 ± 12	54 ± 18	0	9 ± 6
SDS	39 ± 4	43 ± 17	3 ± 5	12 ± 7
TFE	37 ± 5	33 ± 12	17 ± 1	13 ± 4
PEP-FOLD	54	46	0	0

Fig. 4.25. Trictide has mainly the potential to form β-sheet. (A) Circular dichroism spectrograms of trictide (50 µM) and scrambled trictide (50 µM) in different solvents. Random coil propensity of the peptides in 10 mM phosphate buffer (PB) (pH 7.4). β-sheet propensity of trictide in PB with 0.5 mM sodium dodecyl sulfate (SDS) [minimum at 216 nm (red dotted line). Helical propensity of trictide in PB with 60% 2.2.2-trifluoroethanol (TFE) (two minima expected between 207-222 nm (black dotted lines)], respectively. **(B)** CD spectroscopy data (mean±SEM; n=6) and prediction of secondary structural elements by PEP-FOLD. Abbreviations and conditions as in **(A)**. CD spectroscopy was executed in collaboration with Christian Staat and Sophie Dithmer.

Structural prediction analysis of trictide by CD spectroscopy revealed high β-sheet propensity in phosphate buffer (55%) combined with unstructured random domains (36%). Conditions promoting β-sheet formation (0.5 mM SDS) did not increase the propensity of peptide to form β-sheet (53%) or unstructured (35%) elements. TFE, an agent which supports α-helix formation in peptides, only slightly increased the α-helix content from 0 to 11±1%, indicating a very low α-helical potential of trictide (Fig. 4.25B left). The

prediction of secondary structural elements by 3D model of trictide with the highest thermodynamic stability showed a large β-sheet fraction (50%) accompanied by unstructured segments (33%), just like predictions obtained from CD spectroscopy (Fig.4.25B).

Scrambled trictide also displayed high β-sheet content in phosphate buffer (54%) combined with random domains (37%). SDS buffer affected the scrambled trictide affinity to form β-sheet (43%) or unstructured (39%) elements. The α-helix content of scrambled trictide was also as low as trictide and did not increase significantly by TFE (Fig. 4.25B).

Taken together, trictide's β-sheet and random domains propensity obtained from CD spectroscopy was comparable to PEP-FOLD modeling. Molecular modeling of the scrambled trictide with the PEP-FOLD program revealed a remarkably greater amount of randomly arranged amino acids, a lower percentage of β-sheets, and no β-turns when compared to the trictide structure. α-Helices were not predicted, neither in trictide nor in the scrambled trictide model. Thus α-helice is not an essential factor for the structure of the trictide, but β-sheet is important. Since β-sheet is not a discriminating factor, it was not clear how the β-strands need to be arranged to enable its function.

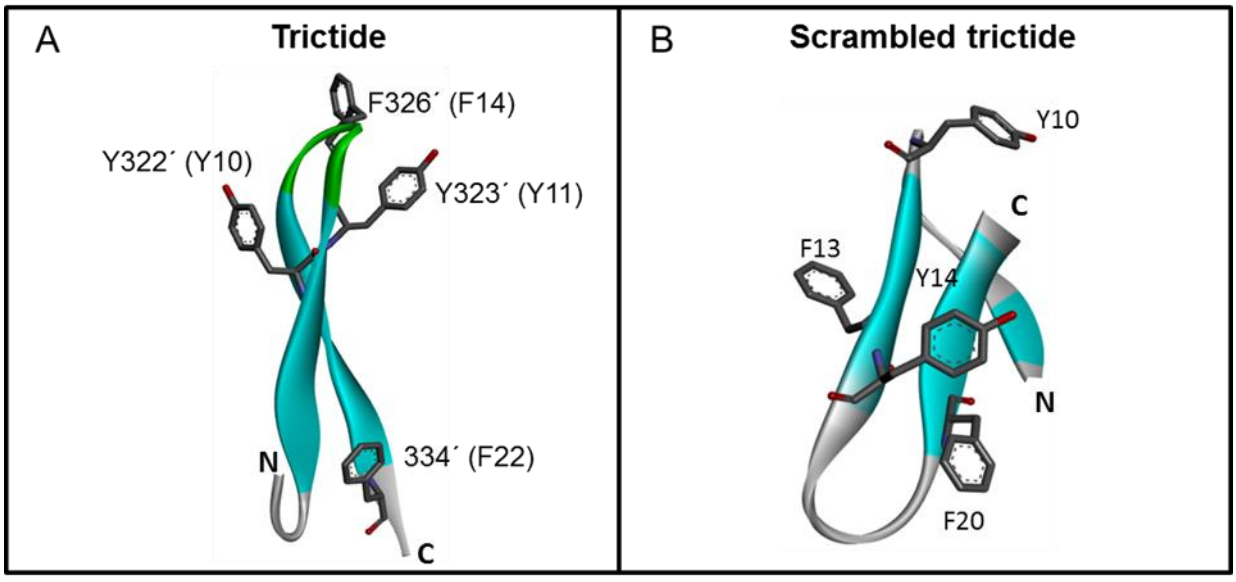

Fig. 4.26 Trictide structure is predicted as a β-sheet formed by two β-strands with surface-exposed aromatic residues. (A) PEP-FOLD model of trictide with the highest thermodynamic stability based on circular dichroism spectroscopic measurements. More than 50% of trictide showed β-sheet propensity of two β-strands (light blue) connected by a β-turn (green); the aromatic amino acids were localized sidewise of β-sheet. **(B)** The PEP-FOLD model of the scrambled peptide exhibited three β-strands compared to trictide with two β-strands, no β-turn, and a greater amount of random structuring. (A, B) F13, -14, -20, -22, Y10, -11, and -14 correspond to the amino acid positions in the respective peptide.

The importance of aromatic residues in *trans*-interaction for TJ proteins was previously revealed for Cldn5 ECL2 (Piontek et al., 2008b). Aromatic amino acids such as F14 and Y11 were concentrated at the β-turn of the trictide molecule, with outward directed side chains. Two further aromatic amino acids (Y10, F22) locate at the surface of the β-sheet or in its close proximity. The β-sheet is formed by two β-strands resulting in an elongated conformation (Fig. 4.26A). Secondary structure modeling of the scrambled trictide showed that the aromatic amino acids are randomly distributed along the peptide. Three β-strands form a more compact β-sheet compared to trictide (Fig. 4.26B). The outward directed aromatic amino acids are the most important structural difference between trictide and scrambled trictide. This may account for trictide's efficiency.

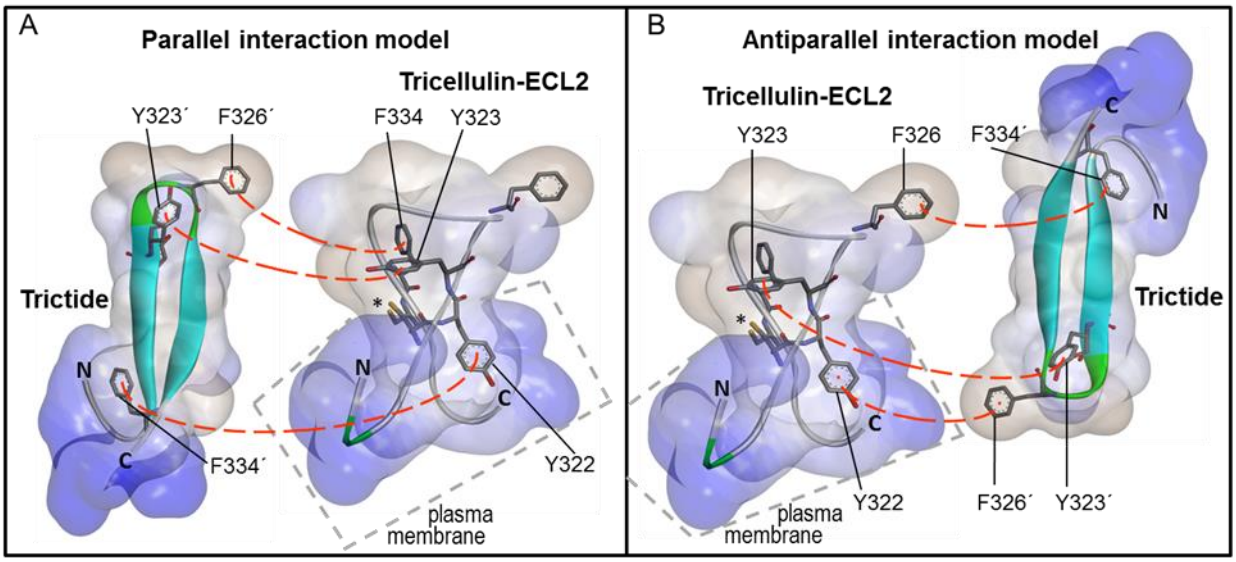

Fig. 4.27 Potential aromatic binding mechanisms of trictide to the human tricellulin (Tric) extracellular loop two (ECL2). (A) Parallel interaction model proposing binding of Y323'-Y323 and F326' (trictide) with F334 (Tric ECL2) while F334' (trictide) binds to Y322**. (B)** Antiparallel interaction model proposing binding of Y323-Y323', Y322 (Tric ECL2)-F326' (trictide) and F326 (Tric ECL2)-F334' (trictide). Blue, hydrophilic surface; brown, hydrophobic surface; asterisk, disulfide bridge between yellow thiol residues. Molecular modeling was executed in collaboration with Jimmi Cording.

Two alternative mechanisms of trictide association with the ECL2 of Tric are shown in Fig. 4.27. In a parallel interaction mode, the aromatic residues Y323´, F326´ and F334´ in trictide form a hydrophobic surface at one side of the peptide structure. The postulated structure of the Tric-ECL2 exhibits a complementary hydrophobic surface formed by Y322, Y323 and F334 (Fig. 4.27A). Alternatively, Y323´, F326´and F334´ of trictide might bind in an antiparallel interaction mode to the hydrophobic binding surface at the Tric-ECL2 structure (Y322, Y323 and F326) (Fig. 4.27B).

To conclude, prediction of secondary structural elements did not point out important differences, but 3D modeling of the peptides highlighted the importance of tertiary structure and positions of aromatic amino acids.

4.3.8. Single substitutions of aromatic residues in tricellulin extracellular loop 2 do not alter localization of tricellulin.

The structure of trictide obtained from the molecular modelling approach, taken together with the ECL2 model of Tric, indicated the essential role of ECL2 aromatic amino acids in Tric. This prompted us to consider these amino acids as potential binding determinants.

Aromatic residues in ECL2 region of Cldn5 were proven to play a major role in Cldn5's *trans*-interactions and enrichment at Cldn5-contacts (Piontek et al., 2008b). In addition, Tyr and Phe (Y322, Y323, F326, F334) residues of Tric ECL2 were highly conserved among vertebrate species (human, chimpanzee, orangutan, bovine, rat, mouse, xenopus) (Cording et al., 2015). In order to examine individual contributions of Y322, F326 and F334 amino acids into *trans*-interaction of Tric, single amino acids were exchanged by hydrophobic Ala or Ile residues (Fig. 4.28A). Localization pattern of substituted recombinant Tric was inspected by live-cell imaging (Fig. 4.28B).

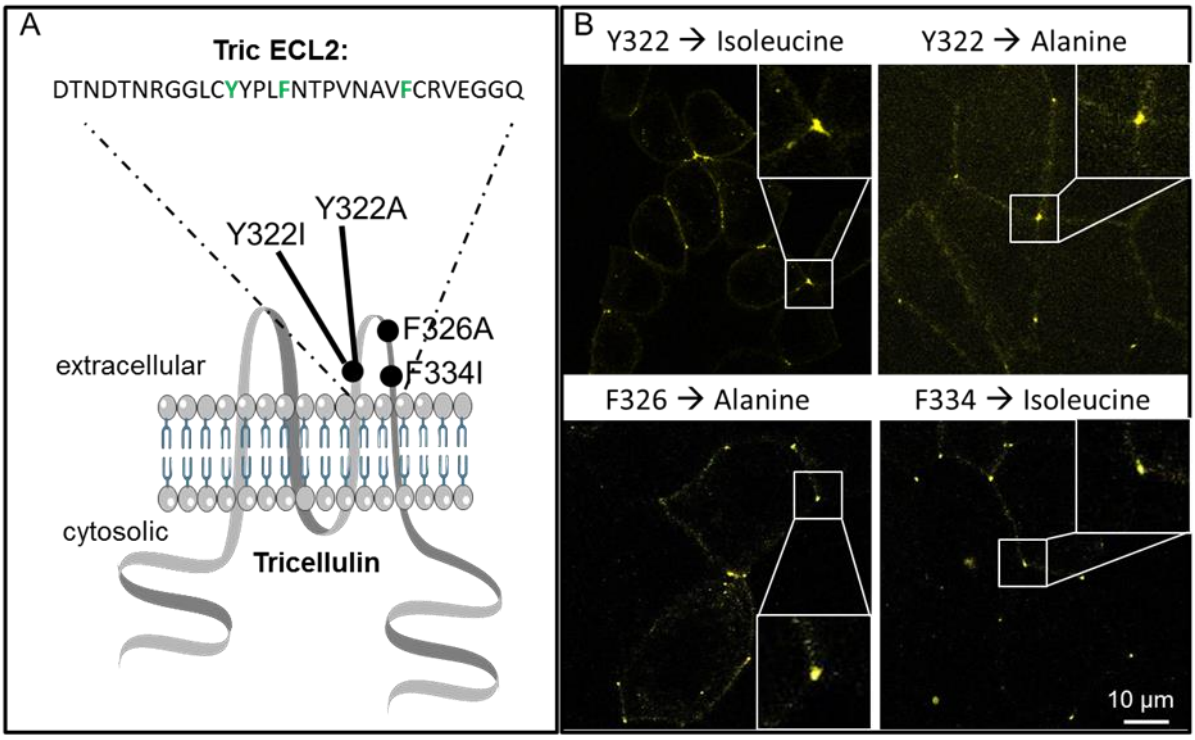

Fig. 4.28 Tricellulin (Tric) extracellular loop 2 (ECL2) mutations do not change Tric's tricellular localization. (A) Schematic illustration of Tric, sequence of Tric ECL2 and location of single aromatic amino acid mutations. **(B)** Madin-Darby canine kidney cells (MDCK-II) transiently expressing YFP-Tric that was modified by single amino acid exchange at Y322, F326, F334. Mutations did not change tricellullar localization of Tric. YFP, yellow fluorescent protein, enlarged images, 4x magnification; 63x objective.

Because MDCK-II cells express Tric endogenously, typical Tric localization at tricellular contacts was observed between wild-type YFP-Tric transfected cells (Fig. 4.18C). Study of localization of YFP-Tric substitutes (Y322I, Y322A, F326A, F334I) revealed that Tric could still localize at tricellular contacts with its typical dot-like appearance. Replacement of aromatic residues did not alter typical Tric localization (Fig. 4.28B). Further investigations of *trans*-interactions and paracellular tightness of cells expressing substituted recombinant Tric are required in order to fully understand the contributions of those aromatic residues to paracellular barrier tightening.

4.3.9. Homophillic tricellulin interactions are mediated by its C-terminal tail

The cytosolic C-terminal tail takes part in homophilic *cis*-interactions of Tric (Westphal, 2010). We therefore analyzed the binding between human Tric and recombinant N-terminally His-tagged C-terminal tail of human Tric (204 amino acids, 24 kDa) before and

after trictide administration. The purified protein was incubated with Caco-2 cell lysate for a co-immunoprecipitation assay. The eluted fraction of the bound proteins was analyzed by Western Blot. The blot was cut into two pieces. The upper part ≥ 55 kDa was incubated with anti-Tric antibody due to the larger size of the protein (64 kDa); the lower part was incubated with anti-His antibody (Fig. 4.29).

The existence of N-terminally His-tagged C-terminal tail of human Tric (Tric C-term) construct was confirmed by recognition of anti-His antibody at the expected size (blue box, Fig 4.29). Furthermore, binding of the Tric C-term to full length Tric within the cell lysate was displayed by recognition of anti-Tric antibody (red box, Fig. 4.29). Co-immunoprecipitation data proved that homophilic binding of Tric occurs also via its C-terminal tail in addition to the extracellular domain (see chapter 4.3.5.1, Fig. 4.18D). The protein band surrounded by green box was observed in between 55 and about 40 kDa and interpreted as dimer of the Tric C-term construct. This dimer was observed in the upper part of the blot incubated with anti-Tric antibody that was designed to recognize C-terminal tail of Tric. The control lane contained only Tric C-term construct without cell lysate, and therefore no protein band was observed. No considerable change in the amount of bound protein fractions (Tric + Tric C-term) was observed consequent to trictide treatment (Fig. 4.29). However, it is essential to conduct more experiments to draw a conclusion about this effect.

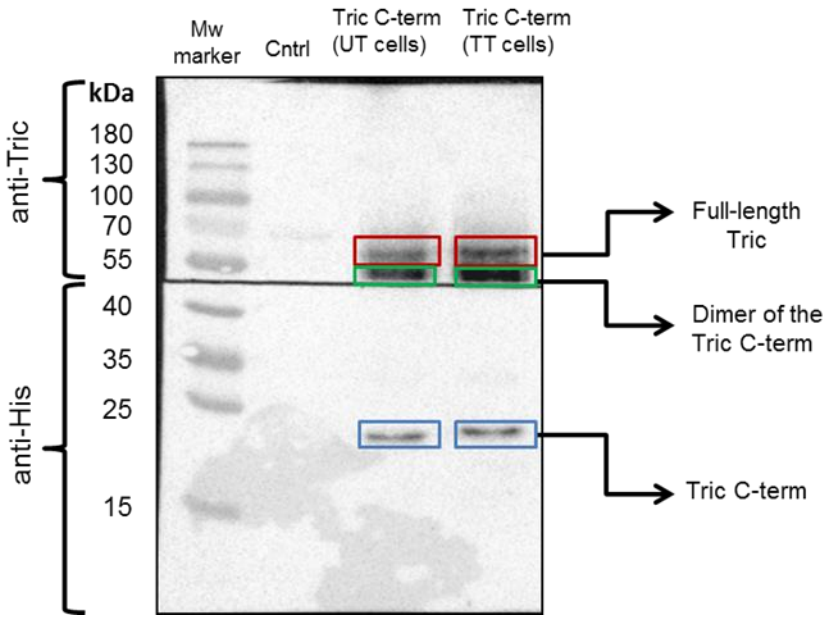

4.29 Tricellulin (Tric) binds to Tric with its C-terminal tail. Recombinant N-terminally His (polyhistidine)-tagged C-terminal tail of human Tric (Tric C-term) was incubated with human colon carcinoma epithelial cells for 2 h and purified by co-immunoprecipitation method. Control (Cntrl) lane includes only Tric C-term construct and no cell-lysate. Mw, molecular weight; UT, untreated cell lysate; TT, 150 μM trictide treated cell lysate; incubation time with trictide, 16 h. Upper part of the blot incubated with anti-Tric antibody, lower part of the blot incubated with anti-His antibody. Red box, full-length Tric (64 kDa); green box, dimer of the Tric C-term (48 kDa); blue box, Tric C-term (24 kDa).

5. DISCUSSION

Tricellulin is a tight junction protein that mostly localizes at the tricellular tight junctions and constitutes a cellular barrier by restricting passage of macromolecules through the paracellular pathway (Ikenouchi et al., 2005; Krug et al., 2009). The ECL2 region of Tric is known to be involved in *trans*-association of two Tric proteins and extracellular binding of three Tric proteins at tTJs. A Tric ECL2 derived peptide called “trictide” was designed to modulate the tricellular structure, hence the paracellular tightness. Before trictide was developed, all peptide-based strategies for opening barriers were based on the modulation of bTJ proteins. Therefore this thesis focuses on revealing tricellular organization of TJ proteins and altering this organization to increase paracellular permeability.

5.1. TRICELLULIN DETECTED MOSTLY IN EPITHELIAL TISSUE DOMINANT ORGANS

In previous studies, the Tric expression profile among several mice organs was investigated (Ikenouchi et al., 2005; Raleigh et al., 2010). Analysis of Tric mRNA expression in mice organs enabled us to compare epithelial versus endothelial dominant organs. Additionally, Tric expression in brain is compared to the rest of the covered organs including different parts of small intestine and colon.

We found that colon is the highest Tric expressing organ and brain is one of the low Tric expressing endothelial dominant organs. When Tric was identified for the first time, it was found to be expressed in epithelial-derived tissues excessively (Ikenouchi et al., 2005; Schlüter et al., 2007). They detected high Tric expression especially in small intestine, kidney and lung. It was expressed at medium level in liver and at much lower level in testis and brain. Those results are consistent with the findings of this thesis, except the fact that parts of small intestine expressed at lower degrees compared to liver according to our examinations. Ikenouchi et al. (2005) used northern blotting whereas in this thesis qRT-PCR has been used for Tric profiling. Thus, variances might be caused by different

methods or other factors like sex and age differences etc. On the other hand, Raleigh and his colleagues (2010) used two different techniques to analyze mouse Tric in different organs. Chip-based analysis of transcript profiles demonstrated the highest Tric expression in kidney, stomach, liver and lung, relatively. Semi-quantitative RT-PCR showed the highest Tric expression in colon and jejunal epithelium (Raleigh et al., 2010). Tric expression in brain was mostly found at low levels in both studies (Ikenouchi et al., 2005; Raleigh et al., 2010). Their results were also consistent with the results of our study, which investigated Tric expression within mouse organs. Moreover, the greater part of our investigation is constituted on the stated value of Caco-2 cells as high Tric expressing cell models (Raleigh et al., 2010).

Cerebral capillary endothelial cells contain TJs that seal between neighboring cells to form a continuous blood vessel. The volume of capillary and endothelial cell constitutes around 1% and 0.1% of the whole brain tissue volume, respectively (Pardridge et al., 1990). Due to low percentage of capillary endothelial cells throughout the brain, expressions of TJ proteins within brain capillaries cannot be abundant. Even though Tric is detected in low levels in the whole brain, it is expressed higher in the peripheral nervous system compared to the central nervous system, according to mRNA analysis and immunohistostainings (Kikuchi et al., 2010). Tric was detected by immunofluorescence stainings of different frozen mice organ sections (Iwamoto et al., 2014). In mouse cerebrum and cerebellum, both Tric and LSR were observed at triendothelial contacts (Iwamoto et al., 2014). On the other hand, Mariano and her colleagues (2013) observed Tric localizing at cell membrane including both bicellular and tricellular regions, nuclear and perinuclear areas of cultured endothelial cells, and also co-localizing with Cldn5 in brain microvessels (Mariano et al., 2013). The latter result is similar to our findings because Tric is observed at bicellular contacts and co-localizing with Occl and Cldn5 in mouse brain capillaries. In addition, we demonstrated localization of Tric at tTJs extending through Z-direction. In human brain microvessels, we observed Tric and LSR more precisely at tricellular contacts similar to previous findings (Iwamoto et al., 2014; Sohet et al., 2015). It is not possible to make a clear statement about Tric localization due to different results of *ex vivo* immunostainings of human and mouse brain. However, many factors determine the quality of an immunostaining; like antibody specificity and cross reactivity, low protein expression and background vs. noise ratio that might affect the results. Taken together, the results of this

experiment are consistent with previous results and can be improved when considering said factors.

5.2. TRICTIDE OPENS CELL BARRIERS AND IMPROVES THE PASSAGE OF IONS AND MACROMOLECULES

In previous studies, TJ peptidomimetics were only derived from Cldns or Occl and targeted to open the cellular barrier at bTJs. It was demonstrated that Cldn peptides have potential to modulate bTJ structure and paracellular barrier (Dithmer et al., 2017; Staat et al., 2015; Zwanziger, Hackel, et al., 2012). For the first time with this study, we focus on opening paracellular barrier at tricellular contacts. Thus, Tric has been selected as a target because it was the first TJ protein discovered at tTJ which contributes to paracellular tightness (Ikenouchi et al., 2005; Krug et al., 2009). Trictide does not show any homology to parts of other TJ proteins. That is why, trictide is assumed to bind Tric more specifically at a certain region of the TJ mainly the tTJs. On the other hand, there is limited knowledge of pathways and mechanisms behind transcriptional regulation of Tric (see chapter 1.3.2.3) which makes it difficult to evaluate the acquired data.

The ECL parts of two opposing TJ proteins were known to play role in *trans*-interactions (Piontek et al., 2008). Similarly, Cys residues in Tric's ECL2 are found to be involved in its *trans*-interactions (Cording et al., 2015). As first-step of trictide, a recombinant protein was produced from the ECL2 region of human Tric fused with the purification tag MBP. MBP-Tric ECL2 opens the human colorectal adenocarcinoma cell (Caco-2) barrier for ions and causes localization changes of TJ proteins. Occludin is observed at submembranous region and internalized within intracellular vesicles. Tric is also internalized, mostly together with Occl and shifted to bicellular area. These effects are detected progressively depending on the increasing concentration of the construct. It is unlikely to see a clear effect on Occl because an earlier experiment showed that Occl and Tric do not interact directly (Raleigh et al., 2010). This effect is further investigated by measuring *cis*-interactions between TJ proteins and their expression levels (see chapter 5.3).

Recombinant protein MBP-Tric ECL2 has provided promising results regarding the modulation of TJ proteins and opening of a cell barrier. This is the reason why trictide (2.7 kDa), a chemically synthesized peptide, has been designed from the ECL2 part of human $Tric_{313–336}$. Using a synthetic peptide is preferred to a recombinant protein because it is cheaper, more reproducible, and allows for easier pharmaceutical applications.

In order to investigate functional alterations like barrier opening and permeability for ions and macromolecules, and to use a homologous human system for the human trictide, Caco-2 cells with high Tric expression were used primarily (Berndt, 2017). In previous studies, peptides were applied for 24-48 h (Dithmer et al., 2017; Sauer et al., 2014; Staat et al., 2015; Zwanziger, Hackel, et al., 2012). We incubated the cells with trictide for 16 h because significant effects were obtained at this time. Trictide has a concentration-dependent effect on both epithelial and endothelial cell lines. The encompassed concentrations are also tested for cytotoxicity. For Caco-2 cells, 150 µM of trictide is the preferred working concentration because this concentration increases ion permeability significantly without causing cytotoxicity. Previous studies also used similar concentrations *in vitro* such as 200 µM (Staat et al., 2015) and 100 to 300 µM (Zwanziger, Hackel, et al., 2012) of Cldn1; and 300 µM of Cldn5 (Dithmer et al., 2017) peptidomimetics. The working concentration of Cldn5 peptide was also not cytotoxic, similar to trictide (Dithmer et al., 2017).

The trictide effect is also sequence specific because scrambled trictide does not change any of the barrier properties. The permeability is increased for molecules up to 10 kDa in addition to ions. This finding is consistent with that of previous studies undertaken without peptidomimetics or other treatments. These results proved that Tric selectively tightens for molecules 4 to 10 kDa (Krug et al., 2009). Hereby we show that by altering Tric's function, molecules with 0.4 and 10 kDa are able to pass through central sealing tube while much bigger sizes (≥40 kDa) cannot. The minimum radius of tTJ central sealing tube was estimated as 5 nm, (Staehelin, 1973) and the Stokes radius of 10 kDa molecules is 2.3 nm (Staehelin, 1973). Therefore, a 10 kDa molecule can permeate through tTJ central sealing tube. Earlier studies using Caco-2 cells and markers of identical size (0.4 and 10 kDa) reported similar significant increase in paracellular permeability for those markers in addition to ions (Staat et al., 2015; Zwanziger, Hackel, et al., 2012).

Interestingly, we saw that 100 µM of trictide decreases permeability compared to untreated control. ECIS measurements also support this finding with slowly increasing TER of 100 µM trictide. The same effect is observed with 50 µM trictide at filter experiments. Taken together, a threshold concentration between 50 and 100 µM of trictide is assumed to be effective. Cells' recovery from trictide is analyzed by ECIS. We observed that after 21 h of exposure to trictide (at 47 h), medium is exchanged and the decreasing slope of TER changes to an increasing slope. This reversal can be interpreted as cell recovery.

D-amino acid derivative of trictide is also considered in this study. Non-physiological D-amino acids are proven to be degraded slower compared to L-amino acids because of their reverse conformation (Di, 2015; Werle et al., 2006). Besides, my colleagues obtained stronger barrier opening with D-amino acid derivative of a Cldn5 peptidomimetic *in vivo* (Dithmer et al., 2017). Unfortunately, we did not see any effect of D-trictide *in vitro,* even when double concentrations of trictide were administered. D-trictide was therefore excluded from *in vivo* experiments. The reason for non-functioning D-trictide could be an improperly formed tertiary structure. This may be clarified by CD spectroscopy experiments in the future.

Trictide causes alteration of Cldn5 mRNA expression in Caco-2 cells (see chapter 5.3), which prompted *in vitro* investigations of endothelial cells. Cldn5 is expressed in a much lower amount in Caco-2 cells (Table S2) compared to mouse brain endothelial cells (Table S3). Besides, it is important to understand the potential of trictide at blood-brain barrier focused applications. Therefore, once trictide's efficacy was determined, it was administered to mouse brain endothelial cells and barrier propertiesafter trictide has been investigated. Trictide opens the endothelial cell barrier with 75 µM and 100 µM concentrations starting from 9 h of incubation. When mouse brain endothelial cells were treated with Cldn5 (300 µM) derived peptides, the TER was reduced to a steady-state after 24 h (Dithmer et al., 2017). In addition, toxicity tests of Cldn5 derived peptides displayed higher viability compared to trictide, which exhibits cell toxicity starting from 100 µM. Taken together with the cell cytotoxicity results, it can be stated that the therapeutic window of trictide is much narrower compared to Cldn5 derived peptides. 50 µM of trictide does not have an effect, while 100 µM is highly toxic for cells. The working concentration of Cldn5 derived peptides is also four times higher than trictide without any cytotoxicity. Scrambled trictide is non-functioning and also not cytotoxic at all.

Earlier, LSR, Tric and Occl were knocked down to reveal their involvement in barrier formation and possible interplays between Tric-Occl and LSR-Tric (Ikenouchi et al., 2005; Ikenouchi et al., 2008; Masuda et al., 2011). According to our research, the tightness of cell barrier decreases with decreasing Tric expression as it was stated at the discovery of Tric (Ikenouchi et al., 2005). So trictide does not cause an additional effect on that already leaky barrier, and the effect of trictide depends on the presence of Tric.

5.3. TRICTIDE MODULATES LOCALIZATION AND EXPRESSION OF TRICELLULIN AND OTHER TIGHT JUNCTION PROTEINS

Our investigations of barrier functions revealed the fact that both epithelial and endothelial cell barriers open after trictide administration. However, it is important to recognize which molecular modulations cause this aperture in order to understand the contribution of individual TJ proteins in barrier formation and the mechanism of barrier opening. There are two scenarios that may explain the process through which trictide binds to Tric. The first scenario assumes that trictide binds to the ECL2 part of Tric and specifically interferes with the *trans*-interactions between the proteins that form tTJs (Cording et al., 2015). The trictide influences the barrier function and eases paracellular passage of compounds through epithelial and endothelial monolayers. Previous research asserts that after synthesis, Tric-Occl complexes are transported together to the edges of elongating bicellular junctions and get separated when tricellular contacts are formed (Westphal et al., 2010). Thus, the second scenario suggests that trictide binds to Tric ECL2 at bicellular contacts just after synthesis and before it reaches tricellular contacts. Therefore our experiments were designed to visualize localization of several TJ proteins and test their expression at mRNA and protein levels.

We observed that in epithelial cells, Tric is elongated from tTJs to bTJs. This effect is similar to what is observed under pathological conditions like hypoxia (Cording et al., 2015). Either by disturbing *trans*-interactions between the ECL2 parts of Tric or by being bound to Tric before reaching tTJs, trictide disrupts trimerization and destabilizes tricellular contacts. Interestingly, Occl is highly affected by trictide treatments. The typical bicellular signal of Occl is decreased, and the degree of internalization is increased. The

expression of both mRNA and protein is also down-regulated. It was previously stated that Occl is highly dynamic at cell membrane. External factors like temperature and the amount of cholesterol at cell membrane affect the mobile fraction of Occl. Thus, the membrane fluidity is important for Occl and determines barrier function in parallel (Shen et al., 2008). In order to understand trictide's effect on Occl, we conducted FRET analysis to test whether Occl-Occl *cis*-interactions are affected. According to FRET, Occl-Occl interactions are highly affected and results are consistent with microscopic investigations. Nevertheless it was stated in previous studies that Occl and Tric do not bind directly (Raleigh et al., 2010). That is why we assume that this must be an indirect effect like the previously revealed interplay between Occl and Tric (Ikenouchi et al., 2008). Occl transfected MDCK-II cells are treated with trictide and observed live with spin-disk microscopy for 15 h. Consequently, we found that Occl is moved towards tTJs progressively. At 12 h, internalization is visible especially from tricellular contacts. The internalization increases over time and bicellular signal is severely decreased. The current investigation also tests fluorescently labelled TAMRA-trictide. As expected, TAMRA signal is concentrated at tricellular area and loss of Occl signal overlaps with increasing TAMRA signal. Based on these data, a claim can be made that the peptide acts first at tTJ, which is then followed by bTJ, and interferes with the membrane fluidity of Occl - a determiner of barrier properties.

In epithelial cells, LSR is also elongated from tTJs to bTJs acting together with Tric. Previously, LSR was reported to interact with Tric directly or indirectly through its cytoplasmic domain. In addition, Tric knockdown cells did not show any alteration at localization of LSR (Masuda et al., 2011). However, in our study Tric has changed its localization after trictide that might have caused LSR to elongate towards bTJs together. LSR expression at mRNA level is also highly affected by trictide treatment just like Tric.

Cldn1 and Cldn5 are known to improve enrichment of Occl and Tric at cell–cell contacts (Cording et al., 2013). We observed that Cldn1 is translocated to tricellular contacts and led to a concentrated signal around tricellular area as a result of peptide administration. Furthermore, it is highly internalized and down-regulated at mRNA level. In previous studies, it was observed that a Cldn1 derived peptide similarly reduces membrane-localization of Cldn1(Mrsny et al., 2008). FRET analysis shows that Cldn1-Tric interactions are significantly decreased, whereas Cldn1-Cldn1 interactions remain constant

after trictide. Cldn5 is examined with endothelial cells due to high expression levels. Just like Cldn1, Cldn5 signal is decreased at bTJs but increased around tTJs and extremely internalized. Cldn5 mRNA is 40% down-regulated in epithelial cells and 35% decreased in endothelial cells. Detection of Cldn1 and Cldn5 at tricellular contacts can be explained either by compensatory mechanisms (Cording et al., 2015; Breitkreuz-Korff, 2018) or shift of TJ proteins to unstabilized tricellular area.

The mRNA of ZO-1 is not affected by trictide in epithelial cells and only insignificantly decreased in endothelial cells. It is not expected to see a vast effect of trictide on ZO-1 protein. However, we observed that ZO-1 is also internalized and lessened at bicellular contacts. In addition, STED images confirmed that typical localization of ZO-1 is disturbed and, additionally, ZO-1 is assembled like a circle at tricellular contacts. Similar results are obtained with STED images of Tric and Occl proteins in MDCK-II cells. Both results can be interpreted as a confirmation of the opening of unstabilized tricellular contacts, which increase permeability of small and large molecules.

FRET measurements confirmed that generally Tric involving protein-protein interactions are affected by trictide except Occl-Occl interactions, which are possibly affected indirectly by compensatory mechanisms (Ikenouchi et al., 2008). This strengthens the argument that Tric is specifically modulated directly from trictide applications. Nevertheless, other TJ proteins are also found to change their localization and down-regulate their expression as a result of an indirect or direct trictide influence. The reason for these modulations is not completely understood.

To sum up, both scenarios are supported by the acquired data, such as elongated signals at tTJs, disturbed TJ signals at bTJs, and unstabilized tricellular contacts. Indeed, microscopic investigations revealed the fact that tricellular area is preferentially and highly affected by trictide. Moreover, Tric is modulated at every expression level, and trictide's action depends on Tric's presence. Most of the affected proteins have direct or indirect relations with Tric, except Occl. It is also important to acquire more information about transcriptional regulation of TJ proteins in order to explain down and up-regulations of their mRNA appropriately.

5.4. TRICTIDE DOES NOT MODULATE PROPERTIES OF TISSUE BARRIERS CONSIDERABLY

During *in vitro* studies, concentration and incubation time are optimized, and the effect of peptide is examined using various methods. Our objective was to test the drug passage through tissue barriers of several organs. Trictide is administered via intravenous injections to avoid the first-pass effect that greatly reduces a drug's concentration before it reaches systemic circulation. We selected the highest dose (800 µM) that is soluble without a solubility enhancer. The administered dose is well tolerated by the animals, weight gain continues, no behavioral differences are observed compared to control group, and no edema are observed. Trictide increases the permeability significantly after 16 h *in vitro*. However, the proteolytic degradation by plasma proteins plays an additional role in blood stability and exposure time of the peptide (Werle & Föger, 2018). *Ex vivo* peptide stability tests within blood plasma demonstrated that peptide is still detectable up to 48 h, and its half-life endures approximately 12 h. Therefore, exposure time is expected between 4 h to 24 h. Unlike in previous studies (Sauer et al., 2014; Zwanziger, Hackel, et al., 2012), exposure time is kept shorter in order to observe a short-term effect (4 h) in addition to a long-term effect (24 h) . On account of the plasma half-life being determined *ex vivo*, the further metabolic and excretion processes responsible for elimination of the peptides are not considered (Diao & Meibohm, 2013).

After 4 h and 24 h of injections, mRNA expression of several TJ proteins is investigated in the organ of interest (brain) and the organ with higher Tric expression (kidney). TJ proteins are selected and grouped for different organs according to their expression levels. In brain, Cldn5 and Tric are highly up-regulated after 24 h of trictide injections, compared to the PBS control. These two proteins are important because Cldn5 is the dominant TJ protein in BBB, and Tric is the target protein of trictide. Interestingly, both proteins are slightly down-regulated after 4 h as a short-term effect. LSR is also significantly down-regulated after 4 h. We expected to see *in vivo* effect of trictide much earlier compared to *in vitro*, considering previous studies (Dithmer et al., 2017). Tric, Cldn1, Cldn5 (in colonic epithelial cells) and LSR, Cldn1, Occl (in mouse endothelial cells) are down-regulated after trictide administrations (16 h) during the *in vitro* experiments. When *in vivo* and *in vitro* results are compared in the sense of exposure time, it is notable that 4 h of exposure

time after peptide injections has a similar influence on mRNA expressions of TJ proteins with 16 h of peptide incubation. The overexpression of Cldn5 and Tric found after 24 h of trictide can be an indicator of compensatory mechanism between TJ proteins. Similar mechanisms are observed between Cldn1-Cldn3 (Breitkreuz-Korff, 2018), Tric-Occl (Cording et al., 2015; Ikenouchi et al., 2008) and Tric-LSR (Masuda et al., 2011). On the other hand, previous studies demonstrated that when Cldn1 targeting peptides were injected into perineurium, the permeability of small and macromolecules was enhanced and Cldn1 was down-regulated even after 48 h (Sauer et al., 2014; Zwanziger, Hackel, et al., 2012). Since the outcomes of both *in vivo* peptidomimetics are different, the reason behind Cldn5 and Tric up-regulations cannot be totally understood.

In kidney, Tric and MD3 are down-regulated gradually from 3 h to 24 h of trictide exposure. Tric is highly expressed in mouse kidney as well as in colon (see chapter 4.1). Therefore, it is reasonable to state that Tric and MD3 are affected in a similar way as during *in vitro* experiments. Besides, the effect of trictide on a high Tric expressing organ is quite comparable to the findings of previous peptidomimetic studies (Dithmer et al., 2017; Sauer et al., 2014; Zwanziger, Hackel, et al., 2012). Taken together, these findings show that trictide affected kidney in a more progressive and consistent way, and much earlier, which can be explained by the peptide's water-soluble characteristic.

Cldn25 is a recently discovered TJ protein and known to be expressed in brain cerebellum abundantly (Ohnishi et al., 2017). Cldn25 is used as a control protein in our mRNA examinations because its sequence is not similar to Tric, (Berndt, 2017) and to date there is no information about the interaction of Cldn25 and Tric. Surprisingly, Cldn25 is not affected by trictide in brain, yet it is significantly down-regulated after 24 h of trictide exposure in kidney. The expression level of Cldn25 in different organs is unknown, and that is why we are interested by prospects of future studies on Cldn25 expression in kidney.

The most important part of *in vivo* investigation is fluorescent uptake of the tissue barriers after trictide. Therefore, animals were injected with Na-fluorescein (376 Da) after 4 h of trictide injections. The preliminary tests at 4 h and 24 h intervals did not reveal any meaningful difference. A significant effect was obtained at the 4 h interval in previous studies (Dithmer et al., 2017). Hence, we continued with 4 h injections for the uptake tests.

Na-fluorescein uptake of kidney and liver is not enhanced by trictide injections. Brain has a tendency to increase the uptake after trictide administration, but the effect is insignificant due to high variability among datasets. Nevertheless, by increasing the number of experiments and by applying further optimizations, trictide's potential for increasing BBB permeability can be revealed to a greater extent. C5C2, a Cldn5 peptide, was also administered intravenously at nearly the same dosage (3.5 µmol/kg). The D-amino acid derivative of C5C2 triggered the strong barrier opening and significant increase of the brain uptake (Dithmer et al., 2017). Another peptide derived from Cldn5 is also administered intravenously (2.9 µmol/kg). Evaluations have determined that this peptide increases Na-fluorescein uptake of brain only if it is applied three times: at 0 h, 18 h and 21 h (Breitkreuz-Korff, 2018). Thus, the applications of trictide can be optimized similarly in order to enhance the brain's Na-fluorescein uptake.

The brain sections of trictide injected animals have been prepared for microscopic investigations. There were no major alterations in the localization of TJ proteins on brain microvessels that can be spotted visually. Similarly, the immunohistochemical stainings of brain cryosections of mice treated with Cldn5 derivative did not show a clear peptide-mediated effect on Cldn5 localization in the TJs (Breitkreuz-Korff, 2018). However, the Cldn5 signal of brain microvessels from the trictide injected group is detected as more porous, and total fluorescence is quantified as weaker compared to that of the PBS group. Furthermore, the tricellular localization of Tric on brain capillaries is slightly decreased after trictide injection. Surprisingly, the total fluorescence of Occl is quantified as intensifying significantly in trictide injected animal brains. Unfortunately, immunohistochemical stainings of trictide injected brain sections cannot provide much information. More evident changes can be observed within 24 h trictide exposed animal brains. Since brain is the only organ that shows a tendency of increasing Na-fluorescein uptake, it was stimulating to examine possible TJ protein modulations in brain. And yet, the data obtained do not confirm proper functional or visual alterations *in vivo*.

5.5. DETERMINATION OF TRICTIDE'S SECONDARY STRUCTURE AND INTERACTION WITH TRICELLULIN

The structure of trictide is proposed by CD spectroscopy and molecular modeling as an elongated β-sheet composed of two β-strands with aromatic residues located at the surface of the peptide. The scrambled peptide exhibits three β-strands in a more compact organization and with numerous randomly structured sequence fragments. The aromatic amino acids are positioned in a totally different orientation compared to the trictide structure. The notable difference between the two structures can be the reason of the lack of efficacy of the scrambled peptide. Earlier studies have described how trans-interactions between ECLs of Cldns are mediated by hydrophobic interactions of aromatic amino acids; we suggest a similar binding mechanism for trictide (Krause et al., 2008; Suzuki et al., 2014).

The sequence of trictide was not modified to optimize its function like the Cldn5 derived peptidomimetic (C5C2). When the α-helical propensity of C5C2 is reduced by C-terminal truncation, this reduction remarkably eliminates barrier-opening function. Distinct from Tric ECL2 and trictide binding mechanism, hydrogen bond association was proposed between ECL2 of Cldn5 and C5C2 (Dithmer et al., 2017).

Like trictide, Cldn1 derived peptide has mostly β-sheet propensity, which is important for its function (Zwanziger, Hackel, et al., 2012). The conserved aromatic residues among classical claudins (Piehl et al., 2010); Phe and Tyr are suggested as binding elements between Cldn1 ECL2 and the peptide (Suzuki et al., 2014, Staat, doctoral dissertation 2015). Similarly, the highly conserved amino acids of Tric ECL2, among vertebrate species, (Cording et al., 2015) are understood to play a role in trictide association

In order to confirm this mechanism, the aromatic core amino acids of Tric ECL2 are exchanged one by one with amino acids, which are again hydrophobic and smaller in size. MDCK-II cells are transfected with those recombinant proteins. The typical localization of Tric remains unchanged, which suggests complete *trans*-interactions between ECL2s and stable tricellular contacts. Further investigation of the barrier properties of Tric ECL2 mutated cells is necessary to understand binding mechanism better. Instead of exchanging aromatic core amino acids individually, all four of them, or different combinations of these

four amino acids, can be replaced. Until now only the C-terminal coiled-coil domain part of Tric crystal structure has been revealed (Schuetz et al., 2017). Additional data relevant to Tric's 3D structure will stimulate this line of scientific inquiry.

In earlier studies, the structure of Tric ECL2 did not show considerable secondary structure elements (Cording et al., 2015). The structure of Tric ECL2 and trictide has been modelled by different methods. The detected differences should be caused by the missing disulfide bond in trictide. The docking model presents two possible binding mechanisms, considering that the interactions occur between the hydrophobic surfaces. These binding mechanisms may explain the disruption of tricellular *trans*-interactions and the opening of the paracellular cleft observed in super-resolution STED microscopy and permeation measurements.

6. CONCLUSION

Tricellulin (Tric) is a tricellular tight junction (TJ) protein that establishes a barrier by sealing the intercellular cleft between tricellular cell-cell contacts. We have only limited information about the exact structure, function and transcriptional regulation of Tric. This study was conceived in order to better understand the contribution of Tric and other TJ proteins to the formation of the tricellular contact and maintenance of the proper barrier function.

Trictide, a synthetic peptide derived from the second extracellular loop of Tric, has been developed to affect Tric for modulating paracellular tightness to initiate temporary opening of cell barriers. The functional, structural and molecular changes caused by the peptide have been examined in order to understand its mode of action and its potential for pharmacological use. With this work, for the first time tricellular TJs are targeted by using Tric peptidomimetics for a transient opening.

When all functional and molecular alterations are considered together, it can be stated that trictide administration opens the cellular barrier transiently for small molecules and macromolecules until 40 kDa, concentration- and time-dependently. Furthermore, the disruption of tricellular contacts is revealed by various microscopy techniques such as laser scanning confocal, gated stimulated emission depletion (STED) and spin disk confocal microscopy. So it has became clear that destabilization of tricellular contact organization takes place together with the barrier opening.

However, the molecular alterations at tricellular contacts may not be the only reason for the trictide-induced barrier opening. Because occludin (Occl) - a bicellular TJ protein - is shown to be highly internalized at the cell membrane, it is down-regulated at both mRNA and protein level and the homophilic *cis*-interaction of Occl is highly decreased after trictide. Since there is no information to date about direct interaction between Tric and Occl, trictide's influence on Occl is assumed as an indirect or unspecific effect. Additionally, MD3, LSR, Cldn1 and Cldn5 are down-regulated at mRNA but not at protein level. Therefore, they are not considered as direct targets. Considering long-term (15 h) live-cell screening of trictide displaying initial decomposition of cell junctions at tricellular

contacts, the alteration of other tricellular or bicellular TJ proteins should be a secondary effect.

The determined working concentration of the peptide was not toxic for cells. Since the therapeutic window of trictide is relatively narrow, concentrations between 125 and 150 µM would be worth for further investigations of the barrier opening activity.

Trictide has been implemented into *in vivo* experiments in order to modulate tissue barriers. We only observed a tendency of increased intake of small molecules into the brain. *In vivo* investigation of trictide still needs further optimization of administration as well as for the modification of the peptide. To optimize the pharmacokinetic profile of trictide and to minimize its recognition by peptidases, the peptide should be PEGylated or modified by fatty acids. The use of D-amino acids has been another option to increase trictide's stability and availability in the blood. However, D-trictide does not efficiently alter barrier properties, most probably due to its conformational problems.

Moreover, trictide should be modified, as successfully applied in previous studies for claudin peptidomimetics (Dithmer et al., 2017) for instance by extension. Moreover, basic amino acids such as arginine, histidine and lysine should be introduced, which is known to enhance cell penetration of the peptide and gain admission into the cell (Madani et al., 2011). Most importantly, aromatic amino acids that are proposed to form the binding core should be exchanged to prove their importance in trictide's efficacy.

Due to its unique structure and function, Tric is expressed among all tissue barriers of all organs, unlike Cldn5, which is abundantly expressed only in a few organs, for instance in the capillaries of the brain. As Tric appears in ubiquitary distribution in all barriers, systemic administration is impossible to modulate a specific barrier selectively. Therefore, local administration is recommended. A drug combined with trictide could be given directly to the artery of a certain organ, like intra-arterial use of some chemotherapeutics in treating retinoblastoma (Yamane et al., 2004). The opening of the tissue barrier and the facilitated uptake of a certain drug by trictide will provide advantages in treatment protocols. Trictide's usage in tissues with tighter barriers like the brain and eye is particularly beneficial. Because by facilitating intracellular uptake of the drug, the dose of the drug could be lowered and drug efficacy could be increased.

The general relevance of this dissertation is found in its novel revelations about molecular modifications of the addressed TJ proteins triggered by trictide-induced Tric modulation. The barrier opening for molecules smaller than 40 kDa and destabilization of tricellular contacts is the proof of mechanism that trictide interferes with the interaction between the opposing extracellular regions of Tric contributing to the paracellular tightness. We propose trictide as a drug enhancer to increase the permeability of TJ-based tissue barriers and thereby effectuate a general drug-delivery strategy.

REFERENCES

Abbott, N. J. (2013). Blood-brain barrier structure and function and the challenges for CNS drug delivery. *Journal of Inherited Metabolic Disease*, *36*(3), 437–449. https://doi.org/10.1007/s10545-013-9608-0

Alexandre, M. D., Jeansonne, B. G., Renegar, R. H., Tatum, R., & Chen, Y. H. (2007). The first extracellular domain of claudin-7 affects paracellular Cl- permeability. *Biochemical and Biophysical Research Communications*, *357*(1), 87–91. https://doi.org/10.1016/j.bbrc.2007.03.078

Amasheh, S., Meiri, N., Gitter, A. H., Schöneberg, T., Mankertz, J., Schulzke, J. D., & Fromm, M. (2002). Claudin-2 expression induces cation-selective channels in tight junctions of epithelial cells. *Journal of Cell Science*, *115*(Pt 24), 4969–4976. https://doi.org/10.1242/jcs.00165

Amasheh, S., Schmidt, T., Mahn, M., Florian, P., Mankertz, J., Tavalali, S., … Fromm, M. (2005). Contribution of claudin-5 to barrier properties in tight junctions of epithelial cells. *Cell and Tissue Research*, *321*(1), 89–96. https://doi.org/10.1007/s00441-005-1101-0

Asma Nusrat, G. Thomas Brown,Jeffrey Tom, Alex Drake, Tam T.T. Bui, Cliff Quan, and R. J. M. (2005). Multiple Protein Interactions Involving Proposed Extracellular Loop Domains of the Tight Junction Protein Occludin. *Molecular Biology of the Cell*, *16*(8), 1725–1734. https://doi.org/10.1091/mbc.E04

Balda, M. S., Gonzalez-Mariscal, L., Matter, K., Cereijido, M., & Anderson, J. M. (1993). Assembly of the tight junction: The role of diacylglycerol. *Journal of Cell Biology*, *123*(2), 293–302. https://doi.org/10.1083/jcb.123.2.293

Bazzoni, G. (2004a). Endothelial Cell-to-Cell Junctions: Molecular Organization and Role in Vascular Homeostasis. *Physiological Reviews*, *84*(3), 869–901. https://doi.org/10.1152/physrev.00035.2003

Bazzoni, G. (2004b). Endothelial Cell-to-Cell Junctions: Molecular Organization and Role in Vascular Homeostasis. *Physiological Reviews*, *84*(3), 869–901. https://doi.org/10.1152/physrev.00035.2003

Beeman, N. E., Baumgartner, H. K., Webb, P. G., Schaack, J. B., & Neville, M. C. (2009). Disruption of occludin function in polarized epithelial cells activates the extrinsic pathway of apoptosis leading to cell extrusion without loss of transepithelial resistance. *BMC Cell Biology*, *10*(1), 85. https://doi.org/10.1186/1471-2121-10-85

Bellmann, C., Schreivogel, S., Günther, R., Dabrowski, S., Schümann, M., Wolburg, H., & Blasig, I. E. (2014). Highly conserved cysteines are involved in the oligomerization of occludin-redox dependency of the second extracellular loop. *Antioxidants & Redox Signaling*, *20*(6), 855–67. https://doi.org/10.1089/ars.2013.5288

BERNDT, P. (2017). *Claudins and tight junction-associated MARVEL proteins at the blood-brain barrier – contribution to paracellular barrier formation*. (Doctoral dissertation). Retrieved from https://refubium.fu-berlin.de/handle/fub188/8149

Blasig, I., Bellmann, C., Cording, J., & Vecchio, G. (2011). Occludin protein family: oxidative stress and reducing conditions. *Antioxidants & Redox*. Retrieved from /citations?view_op=view_citation&continue=/scholar%3Fhl%3Den%26as_sdt%3D0,5%26scilib%3D1&citilm=1&citation_for_view=PD5Opp4AAAAJ:u5HHmVD_uO8C&hl=en&oi=p

Brandsch, M., Knütter, I., & Bosse-Doenecke, E. (2008). Pharmaceutical and pharmacological importance of peptide transporters. *The Journal of Pharmacy and Pharmacology*, *60*(5), 543–585. https://doi.org/10.1211/jpp.60.5.0002

Breitkreuz-Korff, O. (2017) *Charakterisierung und Modulation von Claudinen zur Öffnung der Blut-Hirn-Schranke* (Doctoral dissertation). Retrieved from https://refubium.fu-berlin.de/bitstream/handle/fub188/4165/Dissertation_Olga_Breitkreuz-Korff.pdf?sequence=1

Buck, M. (1998). Trifluoroethanol and colleagues: cosolvents come of age. Recent studies with peptides and proteins. *Quarterly Reviews of Biophysics*, *31*(3), 297–355.

Burgess, A., & Hynynen, K. H. (2014). Drug delivery across the blood-brain barrier using focused ultrasound. *Expert Opinion on Drug Delivery*, *11*(5), 711–721. https://doi.org/10.1517/17425247.2014.897693

Campbell, M., Nguyen, A. T. H., Kiang, A.-S., Tam, L. C. S., Gobbo, O. L., Kerskens, C., … Humphries, P. (2009). An experimental platform for systemic drug delivery to the retina. *Proceedings of the National Academy of Sciences of the United States of America*, *106*(42), 17817–22. https://doi.org/10.1073/pnas.0908561106

Chaplin, D. D. (2010). Overview of the immune response. *Journal of Allergy and Clinical Immunology*, *125*(2 SUPPL. 2), S3–S23. https://doi.org/10.1016/j.jaci.2009.12.980

Chung, N. P., Mruk, D., Mo, M. Y., Lee, W. M., & Cheng, C. Y. (2001). A 22-amino acid synthetic peptide corresponding to the second extracellular loop of rat occludin perturbs the blood-testis barrier and disrupts spermatogenesis reversibly in vivo.

Biology of Reproduction, *65*(5), 1340–1351. https://doi.org/10.1095/biolreprod65.5.1340

Citi, S., & Cordenosi, M. (1998). Tight junction proteins. *Biochim. Biophys. Acta*, *1448*, 1–11.

Colegio, O. R., Van Itallie, C. M., McCrea, H. J., Rahner, C., & Anderson, J. M. (2002). Claudins create charge-selective channels in the paracellular pathway between epithelial cells. *American Journal of Physiology. Cell Physiology*, *283*(1), C142–C147. https://doi.org/10.1152/ajpcell.00038.2002

Cording, J., Arslan, B., Staat, C., Dithmer, S., Krug, S. M., Krüger, A., … Haseloff, R. F. (2017). Trictide, a tricellulin-derived peptide to overcome cellular barriers. *Annals of the New York Academy of Sciences*, *1405*(1), 89–101. https://doi.org/10.1111/nyas.13392

Cording, J., Berg, J., Käding, N., Bellmann, C., Tscheik, C., Westphal, J. K., … Blasig, I. E. (2013). In tight junctions, claudins regulate the interactions between occludin, tricellulin and marvelD3, which, inversely, modulate claudin oligomerization. *Journal of Cell Science*, *126*(Pt 2), 554–64. https://doi.org/10.1242/jcs.114306

Cording, J., Günther, R., Vigolo, E., Tscheik, C., Winkler, L., Schlattner, I., … Blasig, I. E. (2015). Redox Regulation of Cell Contacts by Tricellulin and Occludin: Redox-Sensitive Cysteine Sites in Tricellulin Regulate Both Tri- and Bicellular Junctions in Tissue Barriers as Shown in Hypoxia and Ischemia. *Antioxidants & Redox Signaling*, *0*(0), 150608093200004. https://doi.org/10.1089/ars.2014.6162

Corrêa, D. H. a, Ramos, C. H. I., & Correa, D. (2009). The use of circular dichroism spectroscopy to study protein folding, form and function. *African J Biochem Res*, *3*(5), 164–173. https://doi.org/not available

Czulkies, B. A., Mastroianni, J., Lutz, L., Lang, S., Schwan, C., Schmidt, G., … Papatheodorou, P. (2016). Loss of LSR affects epithelial barrier integrity and tumor xenograft growth of CaCo-2 cells. *Oncotarget*, *8*(23), 37009–37022. https://doi.org/10.18632/oncotarget.10425

Dai, T., Jiang, K., & Lu, W. (2018). Liposomes and lipid disks traverse the BBB and BBTB as intact forms as revealed by two-step Förster resonance energy transfer imaging. *Acta Pharmaceutica Sinica B*, *8*(2), 261–271. https://doi.org/10.1016/j.apsb.2018.01.004

Denker, B. M., & Nigam, S. K. (1998). Molecular structure and assembly of the tight

junction. *Am J Physiol*, *274*(1 Pt 2), F1-9. Retrieved from http://www.ncbi.nlm.nih.gov/entrez/query.fcgi?cmd=Retrieve&db=PubMed&dopt=Citation&list_uids=9458817

Di, L. (2015). Strategic approaches to optimizing peptide ADME properties. *The AAPS Journal*, *17*(1), 134–43. https://doi.org/10.1208/s12248-014-9687-3

Diao, L., & Meibohm, B. (2013). Pharmacokinetics and Pharmacokinetic--Pharmacodynamic Correlations of Therapeutic Peptides. *Clinical Pharmacokinetics*, *52*(10), 855–868. https://doi.org/10.1007/s40262-013-0079-0

Dithmer, S., Staat, C., Müller, C., Ku, M. C., Pohlmann, A., Niendorf, T., … Winkler, L. (2017). Claudin peptidomimetics modulate tissue barriers for enhanced drug delivery. *Annals of the New York Academy of Sciences*, *1397*(1), 169–184. https://doi.org/10.1111/nyas.13359

Dokmanovic-Chouinard, M., Chung, W. K., Chevre, J.-C., Watson, E., Yonan, J., Wiegand, B., … Leibel, R. L. (2008). Positional Cloning of "Lisch-like", a Candidate Modifier of Susceptibility to Type 2 Diabetes in Mice. *PLoS Genetics*, *4*(7), e1000137. https://doi.org/10.1371/journal.pgen.1000137

E.PALADE, M. G. F. and G. (1963). JUNCTIONAL COMPLEXES IN VARIOUS EPITHELIA. *The Journal of Cell Biology*, *17*, 375–412. https://doi.org/10.1083/jcb.17.2.375

El Maghraby, G. M., Barry, B. W., & Williams, A. C. (2008). Liposomes and skin: From drug delivery to model membranes. *European Journal of Pharmaceutical Sciences*, *34*(4–5), 203–222. https://doi.org/10.1016/J.EJPS.2008.05.002

Elizabeth McNeil, Christopher T. Capaldo, and I. G. M. (2006). Zonula Occludens-1 Function in the Assembly of Tight Junctions in Madin-Darby Canine Kidney Epithelial Cells. *Molecular Biology of the Cell*, *17*(2), 1922–1932. https://doi.org/10.1091/mbc.E05

Everett, R. S., Vanhook, M. K., Barozzi, N., Toth, I., & Johnson, L. G. (2006). Specific modulation of airway epithelial tight junctions by apical application of an occludin peptide. *Molecular Pharmacology*, *69*(2), 492–500. https://doi.org/10.1124/mol.105.017251

F. Lacaz-Vieira1, M.M.M. Jaeger2, P. Farshori3, B. K. (1999). Small Synthetic Peptides Homologous to Segments of the First External Loop of Occludin Impair Tight Junction Resealing. *Membrane Biology*, *168*, 289–297.

https://doi.org/10.1007/s00232-001-0030-4

Fanning, A. S., & Anderson, J. M. (2013). Regulate the Assembly of Cellular Junctions, 113–120. https://doi.org/10.1111/j.1749-6632.2009.04440.x.Zonula

Fanning, A. S., Jameson, B. J., Jesaitis, L. A., & Anderson, J. M. (1998). The tight junction protein ZO-1 establishes a link between the transmembrane protein occludin and the actin cytoskeleton. *Journal of Biological Chemistry*, *273*(45), 29745–29753. https://doi.org/10.1074/jbc.273.45.29745

Fukumatsu, M., Ogawa, M., Arakawa, S., Suzuki, M., Nakayama, K., Shimizu, S., … Sasakawa, C. (2012). Shigella targets epithelial tricellular junctions and uses a noncanonical clathrin-dependent endocytic pathway to spread between cells. *Cell Host and Microbe*, *11*(4), 325–336. https://doi.org/10.1016/j.chom.2012.03.001

Furuse, M., Fujita, K., Hiiragi, T., Fujimoto, K., & Tsukita, S. (1998). Claudin-1 and -2: Novel integral membrane proteins localizing at tight junctions with no sequence similarity to occludin. *Journal of Cell Biology*, *141*(7), 1539–1550. https://doi.org/10.1083/jcb.141.7.1539

Furuse, M., Furuse, K., Sasaki, H., & Tsukita, S. (2001). Conversion of zonulae occludentes from tight to leaky strand type by introducing claudin-2 into Madin-Darby canine kidney I cells. *Journal of Cell Biology*, *153*(2), 263–272. https://doi.org/10.1083/jcb.153.2.263

Furuse, M., Hata, M., Furuse, K., Yoshida, Y., Haratake, A., Sugitani, Y., … Tsukita, S. (2002). Claudin-based tight junctions are crucial for the mammalian epidermal barrier: A lesson from claudin-1-deficient mice. *Journal of Cell Biology*, *156*(6), 1099–1111. https://doi.org/10.1083/jcb.200110122

Furuse, M., Hirase, T., Itoh, M., Nagafuchi, A., Yonemura, S., Tsukita, S., & Tsukita, S. (1993). Occludin: A novel integral membrane protein localizing at tight junctions. *Journal of Cell Biology*, *123*(6 II), 1777–1788. https://doi.org/10.1083/jcb.123.6.1777

Furuse, M., Itoh, M., Hirase, T., Nagaftichi, A., Yonemura, S., Tsukita, S., & Tsukita, S. (1994). Direct association of occludin with ZO-1 and its possible involvement in the localization of occludin at tight junctions. *Journal of Cell Biology*, *127*(6 I), 1617–1626. https://doi.org/10.1083/jcb.127.6.1617

Furuse, M., Sasaki, H., & Tsukita, S. (1999). Between Tight Junction Strands. *Cell*, *147*(4), 891–903.

Giepmans, B. N. G., & Moolenaar, W. H. (1998). The gap junction protein connexin43

interacts with the second PDZ domain of the zona occludens-1 protein. *Current Biology*, *8*(16), 931–934. https://doi.org/10.1016/S0960-9822(07)00375-2

Gopal, R., Park, J. S., Seo, C. H., & Park, Y. (2012). Applications of Circular Dichroism for Structural Analysis of Gelatin and Antimicrobial Peptides, 3229–3244. https://doi.org/10.3390/ijms13033229

Grauel, M. K., Maglione, M., Reddy-Alla, S., Willmes, C. G., Brockmann, M. M., Trimbuch, T., … Rosenmund, C. (2016). RIM-binding protein 2 regulates release probability by fine-tuning calcium channel localization at murine hippocampal synapses. *Proceedings of the National Academy of Sciences*, *113*(41), 11615–11620. https://doi.org/10.1073/pnas.1605256113

Greene, C., & Campbell, M. (2016). Tight junction modulation of the blood brain barrier: CNS delivery of small molecules. *Tissue Barriers*, *4*(1). https://doi.org/10.1080/21688370.2015.1138017

Greenfield, N., & Fasman, G. D. (1969). Computed Circular Dichroism Spectra for the Evaluation of Protein Conformation. *Biochemistry*, *8*(10), 4108–4116. https://doi.org/10.1021/bi00838a031

Guillemot, L., Paschoud, S., Pulimeno, P., Foglia, A., & Citi, S. (2008). The cytoplasmic plaque of tight junctions: A scaffolding and signalling center. *Biochimica et Biophysica Acta - Biomembranes*, *1778*(3), 601–613. https://doi.org/10.1016/j.bbamem.2007.09.032

Gumbiner, B., Lowenkopf, T., & Apatira, D. (1991). Identification of a 160-kDa polypeptide that binds to the tight junction protein ZO-1. *Proceedings of the National Academy of Sciences of the United States of America*, *88*(8), 3460–4. https://doi.org/10.1073/pnas.88.8.3460

Gumbiner, B. M. (1993). Breaking through the tight junction barrier. *The Journal of Cell Biology*, *123*(6), 1631 LP-1633. Retrieved from http://jcb.rupress.org/content/123/6/1631.abstract

Günzel, D., & Yu, A. S. L. (2013). *Claudins and the modulation of tight junction permeability. Physiological reviews* (Vol. 93). https://doi.org/10.1152/physrev.00019.2012

Higashi, T., Katsuno, T., Kitajiri, S. I., & Furuse, M. (2015). Deficiency of angulin-2/ILDR1, a tricellular tight junction-associated membrane protein, causes deafness with cochlear hair cell degeneration in mice. *PLoS ONE*, *10*(3).

https://doi.org/10.1371/journal.pone.0120674

Higashi, T., Tokuda, S., Kitajiri, S. -i., Masuda, S., Nakamura, H., Oda, Y., & Furuse, M. (2013). Analysis of the “angulin” proteins LSR, ILDR1 and ILDR2 - tricellulin recruitment, epithelial barrier function and implication in deafness pathogenesis. *Journal of Cell Science*, *126*(16), 3797–3797. https://doi.org/10.1242/jcs.138271

Hou, J., Renigunta, A., Yang, J., & Waldegger, S. (2010). Claudin-4 forms paracellular chloride channel in the kidney and requires claudin-8 for tight junction localization. *Proceedings of the National Academy of Sciences of the United States of America*, *107*, 18010–18015. https://doi.org/10.1073/pnas.1009399107

Ikenouchi, J., Furuse, M., Furuse, K., Sasaki, H., Tsukita, S., & Tsukita, S. (2005). Tricellulin constitutes a novel barrier at tricellular contacts of epithelial cells. *The Journal of Cell Biology*, *171*(6), 939–45. https://doi.org/10.1083/jcb.200510043

Ikenouchi, J., Sasaki, H., Tsukita, S., Furuse, M., & Tsukita, S. (2008). Loss of occludin affects tricellular localization of tricellulin. *Molecular Biology of the Cell*, *19*(11), 4687–93. https://doi.org/10.1091/mbc.E08-05-0530

Ikenouchi, J., Umeda, K., Tsukita, S., Furuse, M., & Tsukita, S. (2007). Requirement of ZO-1 for the formation of belt-like adherens junctions during epithelial cell polarization. *Journal of Cell Biology*, *176*(6), 779–786. https://doi.org/10.1083/jcb.200612080

Itoh, M., Morita, K., & Tsukita, S. (1999). Characterization of ZO-2 as a MAGUK family member associated with tight as well as adherens junctions with a binding affinity to occludin and α catenin. *Journal of Biological Chemistry*, *274*(9), 5981–5986. https://doi.org/10.1074/jbc.274.9.5981

Iwamoto, N., Higashi, T., & Furuse, M. (2014). Localization of angulin-1/LSR and tricellulin at tricellular contacts of brain and retinal endothelial cells in vivo. *Cell Structure and Function*, *39*(1), 1–8. https://doi.org/10.1247/csf.13015

Jennek, S., Mittag, S., Reiche, J., Westphal, J. K., Seelk, S., Dörfel, M. J., … Huber, O. (2017). Tricellulin is a target of the ubiquitin ligase itch. *Annals of the New York Academy of Sciences*, *1397*(1), 157–168. https://doi.org/10.1111/nyas.13349

Kamitani, T., Sakaguchi, H., Tamura, A., Miyashita, T., Yamazaki, Y., Tokumasu, R., … Tsukita, S. (2015). Deletion of Tricellulin Causes Progressive Hearing Loss Associated with Degeneration of Cochlear Hair Cells. *Scientific Reports*, *5*(December), 1–12. https://doi.org/10.1038/srep18402

Katahira, J., Inoue, N., Horiguchi, Y., Matsuda, M., & Sugimoto, N. (1997). Molecular cloning and functional characterization of the receptor for Clostridium perfringens enterotoxin. *The Journal of Cell Biology*, *136*(6), 1239–47. https://doi.org/10.1083/jcb.136.6.1239

Kenworthy, A. K. (2001). Imaging protein-protein interactions using fluorescence resonance energy transfer microscopy. *Methods*, *24*(3), 289–296. https://doi.org/10.1006/meth.2001.1189

Kikuchi, S., Ninomiya, T., Tatsumi, H., Sawada, N., & Kojima, T. (2010). Tricellulin is expressed in autotypic tight junctions of peripheral myelinating Schwann cells. *The Journal of Histochemistry and Cytochemistry : Official Journal of the Histochemistry Society*, *58*(12), 1067–73. https://doi.org/10.1369/jhc.2010.956326

Kiuchi-Saishin, Y., Gotoh, S., Furuse, M., Takasuga, A., Tano, Y., & Tsukita, S. (2002). Differential expression patterns of claudins, tight junction membrane proteins, in mouse nephron segments. *Journal of the American Society of Nephrology : JASN*, *13*(4), 875–886.

Kobrinsky, N. L., Packer, R. J., Boyett, J. M., Stanley, P., Shiminski-Maher, T., Allen, J. C., … Finlay, J. L. (1999). Etoposide With or Without Mannitol for the Treatment of Recurrent or Primarily Unresponsive Brain Tumors: A Children's Cancer Group Study, CCG-9881. *Journal of Neuro-Oncology*, *45*(1), 47–54. https://doi.org/10.1023/A:1006333811437

Kojima, T., Fuchimoto, J., Yamaguchi, H., Ito, T., Takasawa, A., Ninomiya, T., … Sawada, N. (2010). c-Jun N-terminal kinase is largely involved in the regulation of tricellular tight junctions via tricellulin in human pancreatic duct epithelial cells. *Journal of Cellular Physiology*, *225*(3), 720–733. https://doi.org/10.1002/jcp.22273

Kondoh, M., Takahashi, A., Fujii, M., Yagi, K., & Watanabe, Y. (2006). A novel strategy for a drug delivery system using a claudin modulator. *Biological & Pharmaceutical Bulletin*, *29*(9), 1783–9. https://doi.org/10.1248/bpb.29.1783

Krause, G., Winkler, L., Mueller, S. L., Haseloff, R. F., Piontek, J., & Blasig, I. E. (2008). Structure and function of claudins. *Biochimica et Biophysica Acta*, *1778*(3), 631–45. https://doi.org/10.1016/j.bbamem.2007.10.018

Kreuter, J., & Gelperina, S. (2008). Use of nanoparticles for cerebral cancer. *Tumori*, *94*(2), 271–277.

Krug, S., Amasheh, S., Richter, J., Milatz, S., & Günzel, D. (2009). Tricellulin forms a

barrier to macromolecules in tricellular tight junctions without affecting ion permeability. *Molecular Biology of the*. Retrieved from /citations?view_op=view_citation&continue=/scholar%3Fhl%3Den%26as_sdt%3D0,5%26scilib%3D1&citilm=1&citation_for_view=PD5Opp4AAAAJ:d1gkVwhDpl0C&hl=en&oi=p

Krug, S. M., Hayaishi, T., Iguchi, D., Watari, A., Takahashi, A., Fromm, M., … Kondoh, M. (2017). Angubindin-1, a novel paracellular absorption enhancer acting at the tricellular tight junction. *Journal of Controlled Release*, *260*(March), 1–11. https://doi.org/10.1016/j.jconrel.2017.05.024

Lee, H. J., & Zheng, J. J. (2010). PDZ domains and their binding partners: Structure, specificity, and modification. *Cell Communication and Signaling*, *8*, 1–18. https://doi.org/10.1186/1478-811X-8-8

Li, Y., Fanning, A. S., Anderson, J. M., & Lavie, A. (2005). Structure of the conserved cytoplasmic C-terminal domain of occludin: Identification of the ZO-1 binding surface. *Journal of Molecular Biology*, *352*(1), 151–164. https://doi.org/10.1016/j.jmb.2005.07.017

Lindmark, T., Schipper, N., Lazorová, L., de Boer, a G., & Artursson, P. (1998). Absorption enhancement in intestinal epithelial Caco-2 monolayers by sodium caprate: assessment of molecular weight dependence and demonstration of transport routes. *Journal of Drug Targeting*, *5*(3), 215–23. https://doi.org/10.3109/10611869808995876

Luissint, A.-C., Artus, C., Glacial, F., Ganeshamoorthy, K., & Couraud, P.-O. (2012). Tight junctions at the blood brain barrier: physiological architecture and disease-associated dysregulation. *Fluids and Barriers of the CNS*, *9*(1), 23. https://doi.org/10.1186/2045-8118-9-23

Marchiando, A. M., Graham, W. V., & Turner, J. R. (2010). Epithelial barriers in homeostasis and disease. *Annual Review of Pathology*, *5*, 119–144. https://doi.org/10.1146/annurev.pathol.4.110807.092135

Mariano, C., Palmela, I., Pereira, P., Fernandes, A., Falcão, A. S., Cardoso, F. L., … Brito, M. A. (2013). Tricellulin expression in brain endothelial and neural cells. *Cell and Tissue Research*, *351*(3), 397–407. https://doi.org/10.1007/s00441-012-1529-y

Markov, A. G., Veshnyakova, A., Fromm, M., Amasheh, M., & Amasheh, S. (2010). Segmental expression of claudin proteins correlates with tight junction barrier

properties in rat intestine. *Journal of Comparative Physiology B: Biochemical, Systemic, and Environmental Physiology*, *180*(4), 591–598. https://doi.org/10.1007/s00360-009-0440-7

Masuda, S., Oda, Y., Sasaki, H., Ikenouchi, J., Higashi, T., Akashi, M., … Furuse, M. (2011). LSR defines cell corners for tricellular tight junction formation in epithelial cells. *Journal of Cell Science*, *124*(Pt 4), 548–55. https://doi.org/10.1242/jcs.072058

Medina, R., Rahner, C., Mitic, L. L., Anderson, J. M., & Van Itallie, C. M. (2000). Occludin localization at the tight junction requires the second extracellular loop. *Journal of Membrane Biology*, *178*(3), 235–247. https://doi.org/10.1007/s002320010031

Mineta, K., Yamamoto, Y., Yamazaki, Y., Tanaka, H., Tada, Y., Saito, K., … Tsukita, S. (2011). Predicted expansion of the claudin multigene family. *FEBS Letters*, *585*(4), 606–612. https://doi.org/10.1016/j.febslet.2011.01.028

Morita, K., Furuse, M., Fujimoto, K., & Tsukita, S. (1999). Morita, K., Furuse, M., Fujimoto, K., & Tsukita, S. (1999). Claudin multigene family encoding four-transmembrane domain protein components of tight junction strands. Proceedings of the National Academy of Sciences of the United States of America, 96(2), 5. *Proceedings of the National Academy of Sciences of the United States of America*, *96*(2), 511–6. https://doi.org/10.1073/pnas.96.2.511

Mrsny, R. J., Brown, G. T., Gerner-Smidt, K., Buret, A. G., Meddings, J. B., Quan, C., … Nusrat, A. (2008). A key claudin extracellular loop domain is critical for epithelial barrier integrity. *The American Journal of Pathology*, *172*(4), 905–915. https://doi.org/10.2353/ajpath.2008.070698

Mullin, J. M., Agostino, N., Rendon-Huerta, E., & Thornton, J. J. (2005). Keynote review: Epithelial and endothelial barriers in human disease. *Drug Discovery Today*, *10*(6), 395–408. https://doi.org/10.1016/S1359-6446(05)03379-9

Narvekar, P., Diaz, M. B., Krones-Herzig, A., Hardeland, U., Strzoda, D., Stohr, S., … Herzig, S. (2009). Liver-specific loss of lipolysis-stimulated lipoprotein receptor triggers systemic hyperlipidemia in mice. *Diabetes*, *58*(5), 1040–1049. https://doi.org/10.2337/db08-1184

Nayak, G., Lee, S. I., Yousaf, R., Edelmann, S. E., Trincot, C., Van Itallie, C. M., … Riazuddin, S. (2013). Tricellulin deficiency affects tight junction architecture and cochlear hair cells. *Journal of Clinical Investigation*, *123*(9), 4036–4049.

https://doi.org/10.1172/JCI69031

Niraula, T. P., Bhattarai, A., & Chatterjee, S. K. (2014). Critical micelle concentration of sodium dodecyl sulphate in pure water and in methanol-water mixed solvent media in presence and absence of KCl by surface tension and viscosity methods, *11*(1), 103–112. https://doi.org/10.3126/bibechana.v11i0.10388

Nitta, T., Hata, M., Gotoh, S., Seo, Y., Sasaki, H., Hashimoto, N., … Tsukita, S. (2003). Size-selective loosening of the blood-brain barrier in claudin-5-deficient mice. *Journal of Cell Biology*, *161*(3), 653–660. https://doi.org/10.1083/jcb.200302070

Ohnishi, M., Ochiai, H., Matsuoka, K., Akagi, M., Nakayama, Y., Shima, A., … Inoue, A. (2017). Claudin domain containing 1 contributing to endothelial cell adhesion decreases in presence of cerebellar hemorrhage. *Journal of Neuroscience Research*, *95*(10), 2051–2058. https://doi.org/10.1002/jnr.24040

Olinger, E., Houillier, P., & Devuyst, O. (2018). Claudins: a tale of interactions in the thick ascending limb. *Kidney International*, *93*(3), 535–537. https://doi.org/10.1016/j.kint.2017.09.032

Oshima, T., Blaschuk, O., Gour, B., Symonds, M., Elrod, J. W., Sasaki, M., … Alexander, J. S. (2003). Tight junction peptide antagonists enhance neutrophil trans-endothelial chemotaxis. *Life Sciences*, *73*(13), 1729–1740. https://doi.org/10.1016/S0024-3205(03)00511-3

Pan, R., Yu, K., Weatherwax, T., Zheng, H., Liu, W., & Liu, K. J. (2017). Blood Occludin Level as a Potential Biomarker for Early Blood Brain Barrier Damage Following Ischemic Stroke. *Scientific Reports*, *7*(January), 1–9. https://doi.org/10.1038/srep40331

Pardridge, W. M., Triguero, D., & Farrell, C. R. (1990). Downregulation of blood-brain barrier glucose transporter in experimental diabetes. *Diabetes*, *39*(9), 1040–1044. https://doi.org/10.2337/diab.39.9.1040

Piehl, C., Piontek, J., Cording, J., Wolburg, H., & Blasig, I. E. (2010). Participation of the second extracellular loop of claudin-5 in paracellular tightening against ions, small and large molecules. *Cellular and Molecular Life Sciences*, *67*(12), 2131–2140. https://doi.org/10.1007/s00018-010-0332-8

Piontek, J., Winkler, L., Wolburg, H., Müller, S. L., Zuleger, N., Piehl, C., … Blasig, I. E. (2008a). Formation of tight junction: determinants of homophilic interaction between classic claudins. *The FASEB Journal : Official Publication of the Federation of*

American Societies for Experimental Biology, *22*(1), 146–158. https://doi.org/10.1096/fj.07-8319com

Piontek, J., Winkler, L., Wolburg, H., Müller, S. L., Zuleger, N., Piehl, C., … Blasig, I. E. (2008b). Formation of tight junction: determinants of homophilic interaction between classic claudins. *FASEB Journal : Official Publication of the Federation of American Societies for Experimental Biology*, *22*(1), 146–58. https://doi.org/10.1096/fj.07-8319com

Raleigh, D. R., Marchiando, A. M., Zhang, Y., Shen, L., Sasaki, H., Wang, Y., … Turner, J. R. (2010). Tight Junction-associated MARVEL Proteins MarvelD3, Tricellulin, and Occludin Have Distinct but Overlapping Functions. *Molecular Biology of the Cell*, *21*(7), 1200–1213. https://doi.org/10.1091/mbc.E09-08-0734

Reaves, D. K., Hoadley, K. A., Fagan-Solis, K. D., Jima, D. D., Bereman, M., Thorpe, L., … Fleming, J. M. (2017). Nuclear Localized LSR: A Novel Regulator of Breast Cancer Behavior and Tumorigenesis. *Molecular Cancer Research*, *15*(2), 165–178. https://doi.org/10.1158/1541-7786.MCR-16-0085-T

Riazuddin, S., Ahmed, Z. M., Fanning, A. S., Lagziel, A., Kitajiri, S., Ramzan, K., … Friedman, T. B. (2006). Tricellulin Is a Tight-Junction Protein Necessary for Hearing. *The American Journal of Human Genetics*, *79*(6), 1040–1051. https://doi.org/http://dx.doi.org/10.1086/510022

Rodriguez-Boulan, E., & Macara, I. G. (2014). Organization and execution of the epithelial polarity programme. *Nature Reviews Molecular Cell Biology*, *15*(4), 225–242. https://doi.org/10.1038/nrm3775

Saitou, M., Furuse, M., Sasaki, H., Schulzke, J. D., Fromm, M., Takano, H., … Tsukita, S. (2000). Complex phenotype of mice lacking occludin, a component of tight junction strands. *Molecular Biology of the Cell*, *11*(12), 4131–42. https://doi.org/10.1091/mbc.11.12.4131

Sánchez-Pulido, L., Martín-Belmonte, F., Valencia, A., & Alonso, M. A. (2002). MARVEL: A conserved domain involved in membrane apposition events. *Trends in Biochemical Sciences*, *27*(12), 599–601. https://doi.org/10.1016/S0968-0004(02)02229-6

Sauer, R. S., Krug, S. M., Hackel, D., Staat, C., Konasin, N., Yang, S., … Rittner, H. L. (2014). Safety, efficacy, and molecular mechanism of claudin-1-specific peptides to enhance blood-nerve-barrier permeability. *Journal of Controlled Release*, *185*(1), 88–

98. https://doi.org/10.1016/j.jconrel.2014.04.029

Schlüter, H., Moll, I., Wolburg, H., & Franke, W. W. (2007). The different structures containing tight junction proteins in epidermal and other stratified epithelial cells, including squamous cell metaplasia. *European Journal of Cell Biology*, *86*(11–12), 645–655. https://doi.org/10.1016/j.ejcb.2007.01.001

Schneeberger, E. E., & Lynch, R. D. (2004). The tight junction: a multifunctional complex. *American Journal of Physiology. Cell Physiology*, *286*(6), C1213–C1228. https://doi.org/10.1152/ajpcell.00558.2003

Schuetz, A., Radusheva, V., Krug, S. M., & Heinemann, U. (2017). Crystal structure of the tricellulin c-terminal coiled-coil domain reveals a unique mode of dimerization. *Annals of the New York Academy of Sciences*, *1405*(1), 147–159. https://doi.org/10.1111/nyas.13408

Schulzke, J. D., Gitter, A. H., Mankertz, J., Spiegel, S., Seidler, U., Amasheh, S., … Fromm, M. (2005). Epithelial transport and barrier function in occludin-deficient mice. *Biochimica et Biophysica Acta - Biomembranes*, *1669*(1), 34–42. https://doi.org/10.1016/j.bbamem.2005.01.008

Sekar, R. B., & Periasamy, A. (2003). Fluorescence resonance energy transfer (FRET) microscopy imaging of live cell protein localizations. *Journal of Cell Biology*, *160*(5), 629–633. https://doi.org/10.1083/jcb.200210140

Shen, L., Weber, C. R., & Turner, J. R. (2008). The tight junction protein complex undergoes rapid and continuous molecular remodeling at steady state. *Journal of Cell Biology*, *181*(4), 683–695. https://doi.org/10.1083/jcb.200711165

Shen, Y., Maupetit, J., Derreumaux, P., & Tufféry, P. (2014). Improved PEP-FOLD Approach for Peptide and Miniprotein Structure Prediction. *Journal of Chemical Theory and Computation*, *10*(10), 4745–4758. https://doi.org/10.1021/ct500592m

Shimada, H., Satohisa, S., Kohno, T., Takahashi, S., Hatakeyama, T., Konno, T., … Kojima, T. (2016). The roles of tricellular tight junction protein lipolysis-stimulated lipoprotein receptor in malignancy of human endometrial cancer cells. *Oncotarget*, *7*(19). https://doi.org/10.18632/oncotarget.8408

Sohet, F., Lin, C., Munji, R. N., Lee, S. Y., Ruderisch, N., Soung, A., … Daneman, R. (2015). LSR/angulin-1 is a tricellular tight junction protein involved in blood-brain barrier formation. *Journal of Cell Biology*, *208*(6), 703–711. https://doi.org/10.1083/jcb.201410131

Staat, C., Coisne, C., Dabrowski, S., Stamatovic, S. M., Andjelkovic, A. V., Wolburg, H., … Blasig, I. E. (2015). Mode of action of claudin peptidomimetics in the transient opening of cellular tight junction barriers. *Biomaterials*, *54*, 9–20. https://doi.org/10.1016/j.biomaterials.2015.03.007

Staat, C. (2015) *Claudin-Peptide zur Modulation der tight junction-Dichtheit* (Doctoral dissertation). Retrieved from https://refubium.fu-berlin.de/handle/fub188/5840

Staehelin, L. A., Mukherjee, T. M., & Williams, A. W. (1969). Freeze-etch appearance of the tight junctions in the epithelium of small and large intestine of mice. *Protoplasma*, *67*(2–3), 165–184. https://doi.org/10.1007/BF01248737

Staehelin L.A. (1973). Further observations on the fine structure of freeze-cleaved tight junctions. *Journal of Cell Science*, *13*, 763–786. https://doi.org/10.1007/BF00339283

Steed, E., Elbediwy, A., Vacca, B., Dupasquier, S., Hemkemeyer, S. A., Suddason, T., … Matter, K. (2014). MarvelD3 couples tight junctions to the MEKK1-JNK pathway to regulate cell behavior and survival. *Journal of Cell Biology*, *204*(5), 821–838. https://doi.org/10.1083/jcb.201304115

Steed, E., Rodrigues, N. T. L., Balda, M. S., & Matter, K. (2009). Identification of MarvelD3 as a tight junction-associated transmembrane protein of the occludin family. *BMC Cell Biology*, *10*(95), 1–14. https://doi.org/10.1186/1471-2121-10-95

Stevenson, B. R., Siliciano, J. D., Mooseker, M. S., & Goodenough, D. A. (1986). Identification of Z0-1: a high molecular weight polypeptide associated with tight junction (zonula occludens) in a. *J. Cell Biol*, *103*(September), 755–766. https://doi.org/10.1083/jcb.103.3.755

SUMIO OHTSUKI, SAORI SATO, HIROFUMI YAMAGUCHI, M. K., & TOMOKO ASASHIMA, A. T. T. (2007). Exogenous Expression of Claudin-5 Induces Barrier Properties in Cultured Rat Brain Capillary Endothelial Cells. *Journal of Cellular Physiology*, *210*, 81–86. https://doi.org/10.1002/JCP

Sumitomo, T., Nakata, M., Higashino, M., Yamaguchi, M., & Kawabata, S. (2016). Group A Streptococcus exploits human plasminogen for bacterial translocation across epithelial barrier via tricellular tight junctions. *Scientific Reports*, *7*(January), 1–8. https://doi.org/10.1038/srep20069

Suzuki, H., Nishizawa, T., Tani, K., Yamazaki, Y., Tamura, a, Ishitani, R., … Fujiyoshi, Y. (2014). Crystal structure of a claudin provides insight into the architecture of tight junctions. *Science (New York, N.Y.)*, *344*(6181), 304–307.

https://doi.org/10.1126/science.1248571

Takasawa, A., Murata, M., Takasawa, K., Ono, Y., Osanai, M., Tanaka, S., … Sawada, N. (2016). Nuclear localization of tricellulin promotes the oncogenic property of pancreatic cancer. *Scientific Reports*, *6*, 1–12. https://doi.org/10.1038/srep33582

Tatsuya Katsuno, †, Kazuaki Umeda, §?, Takeshi Matsui, ¶, Masaki Hata, #, Atsushi Tamura,* Masahiko Itoh, @, Takeuchi, K., … *Laboratory. (2008). Deficiency of Zonula Occludens-1 Causes Embryonic Lethal Phenotype Associated with Defected Yolk Sac Angiogenesis and Apoptosis of Embryonic Cells. *Molecular Biology of the Cell*, *19*(1), 2465–2475. https://doi.org/10.1091/mbc.E07

Tavelin, S., Hashimoto, K., Malkinson, J., Lazorova, L., Toth, I., & Artursson, P. (2003). A new principle for tight junction modulation based on occludin peptides. *Molecular Pharmacology*, *64*(6), 1530–40. https://doi.org/10.1124/mol.64.6.1530

Thévenet, P., Shen, Y., Maupetit, J., Guyon, F., Derreumaux, P., & Tufféry, P. (2012). PEP-FOLD: An updated de novo structure prediction server for both linear and disulfide bonded cyclic peptides. *Nucleic Acids Research*, *40*(W1), 288–293. https://doi.org/10.1093/nar/gks419

Tiwary, S., Morales, J. E., Kwiatkowski, S. C., Lang, F. F., Rao, G., & McCarty, J. H. (2018). Metastatic brain tumors disrupt the blood-brain barrier and alter lipid metabolism by inhibiting expression of the endothelial cell fatty acid transporter Mfsd2a. *Scientific Reports*, *8*(1), 1–13. https://doi.org/10.1038/s41598-018-26636-6

Tsukita, S., & Furuse, M. (1998). Overcoming barriers in the study of tight junction functions: from occludin to claudin. *Genes to Cells : Devoted to Molecular & Cellular Mechanisms*, *3*(9), 569–573.

Tsukita, S., Furuse, M., & Itoh, M. (2001). Multifunctional strands in tight junctions. *Nature Reviews. Molecular Cell Biology*, *2*(4), 285–293. https://doi.org/10.1038/35067088

Umeda, K., Matsui, T., Nakayama, M., Furuse, K., Sasaki, H., Furuse, M., & Tsukita, S. (2004). Establishment and Characterization of Cultured Epithelial Cells Lacking Expression of ZO-1. *Journal of Biological Chemistry*, *279*(43), 44785–44794. https://doi.org/10.1074/jbc.M406563200

Van Itallie, C. M., Rogan, S., Yu, A., Vidal, L. S., Holmes, J., & Anderson, J. M. (2006). Two splice variants of claudin-10 in the kidney create paracellular pores with different ion selectivities. *American Journal of Physiology. Renal Physiology*, *291*(6),

F1288–F1299. https://doi.org/10.1152/ajprenal.00138.2006

Van Itallie, C., Rahner, C., & Anderson, J. M. (2001). Regulated expression of claudin-4 decreases paracellular conductance through a selective decrease in sodium permeability. *Journal of Clinical Investigation*, *107*(10), 1319–1327. https://doi.org/10.1172/JCI12464

Veshnyakova, A., Piontek, J., Protze, J., Waziri, N., Heise, I., & Krause, G. (2012). Mechanism of Clostridium perfringens enterotoxin interaction with claudin-3/-4 protein suggests structural modifications of the toxin to target specific claudins. *Journal of Biological Chemistry*, *287*(3), 1698–1708. https://doi.org/10.1074/jbc.M111.312165

Wade, J. B., & Karnovsky, M. J. (1974). The structure of the zonula occludens: A single fibril model based on freeze-fracture. *Journal of Cell Biology*, *60*(1), 168–180. https://doi.org/10.1083/jcb.60.1.168

Werle, M., & Bernkop-Schnürch, A. (2006). Strategies to improve plasma half life time of peptide and protein drugs. *Amino Acids*, *30*(4), 351–367. https://doi.org/10.1007/s00726-005-0289-3

Werle, M., & Föger, F. (2018). Peroral peptide delivery: Peptidase inhibition as a key concept for commercial drug products. *Bioorganic & Medicinal Chemistry*, *26*(10), 2906–2913. https://doi.org/10.1016/J.BMC.2017.08.028

Westphal, J., Dörfel, M., Krug, S., & Cording, J. (2010). Tricellulin forms homomeric and heteromeric tight junctional complexes. *Cellular and Molecular Life*. Retrieved from /citations?view_op=view_citation&continue=/scholar%3Fhl%3Den%26as_sdt%3D0,5%26scilib%3D1&citilm=1&citation_for_view=PD5Opp4AAAAJ:u-x6o8ySG0sC&hl=en&oi=p

Weyermann, J., Lochmann, D., & Zimmer, A. (2005). A practical note on the use of cytotoxicity assays. *International Journal of Pharmaceutics*, *288*(2), 369–376. https://doi.org/10.1016/j.ijpharm.2004.09.018

Winkler, L., Gehring, C., Wenzel, A., Müller, S. L., Piehl, C., Krause, G., … Piontek, J. (2009). Molecular determinants of the interaction between clostridium perfringens enterotoxin fragments and claudin-3. *Journal of Biological Chemistry*, *284*(28), 18863–18872. https://doi.org/10.1074/jbc.M109.008623

Wittchen, E. S., Haskins, J., & Stevenson, B. R. (1999). Protein Interactions at the Tight Junction, *274*(49), 35179–35185.

Wong, C.-H., Mruk, D. D., Lee, W. M., & Cheng, C. Y. (2007). Targeted and reversible disruption of the blood-testis barrier by an FSH mutant-occludin peptide conjugate. *FASEB Journal : Official Publication of the Federation of American Societies for Experimental Biology*, *21*(2), 438–48. https://doi.org/10.1096/fj.05-4144com

Wong, V., & Gumbiner, B. M. (1997). Synthetic peptide corresponding to the extracellular domain of occludin perturbs the tight junction permeability barrier. *Journal of Cell Biology*, *136*(2), 399–409. https://doi.org/10.1083/jcb.136.2.399

Yaffe, Y., Shepshelovitch, J., Nevo-yassaf, I., Yeheskel, A., & Shmerling, H. (2012). The MARVEL transmembrane motif of occludin mediates oligomerization and targeting to the basolateral surface in epithelia. https://doi.org/10.1242/jcs.100289

Yamane, T., Kaneko, A., & Mohri, M. (2004). The technique of ophthalmic arterial infusion therapy for patients with intraocular retinoblastoma. *International Journal of Clinical Oncology*, *9*(2), 69–73. https://doi.org/10.1007/s10147-004-0392-6

Yang, J. T., Wu, C. S. C., & Martinez, H. M. (1986). Calculation of Protein Conformation from Circular Dichroism. *Methods in Enzymology*, *130*(C), 208–269. https://doi.org/10.1016/0076-6879(86)30013-2

Yen, F. T., Masson, M., Clossais-Besnard, N., André, P., Grosset, J. M., Bougueleret, L., … Bihain, B. E. (1999). Molecular cloning of a lipolysis-stimulated remnant receptor expressed in the liver. *Journal of Biological Chemistry*, *274*(19), 13390–13398. https://doi.org/10.1074/jbc.274.19.13390

Zahraoui, A., Louvard, D., & Galli, T. (2000). Tight junction, a platform for trafficking and signaling protein complexes [In Process Citation]. *J Cell Biol*, *151*(5), F31-6. Retrieved from http://www.ncbi.nlm.nih.gov/cgi-bin/Entrez/referer?http://www.jcb.org/cgi/content/full/151/5/F31

Zhong, L., & Johnson, W. C. (1992). Environment affects amino acid preference for secondary structure. *Proceedings of the National Academy of Sciences*, *89*(10), 4462–4465. https://doi.org/10.1073/pnas.89.10.4462

Zihni, C., Mills, C., Matter, K., & Balda, M. S. (2016). Tight junctions: From simple barriers to multifunctional molecular gates. *Nature Reviews Molecular Cell Biology*, *17*(9), 564–580. https://doi.org/10.1038/nrm.2016.80

Zwanziger, D., Hackel, D., Staat, C., Böcker, A., Brack, A., Beyermann, M., … Blasig, I. E. (2012). A peptidomimetic tight junction modulator to improve regional analgesia. *Molecular Pharmaceutics*, *9*(6), 1785–1794. https://doi.org/10.1021/mp3000937

Zwanziger, D., Staat, C., Andjelkovic, A. V., & Blasig, I. E. (2012). Claudin-derived peptides are internalized via specific endocytosis pathways. *Annals of the New York Academy of Sciences*, *1257*(1), 29–37. https://doi.org/10.1111/j.1749-6632.2012.06567.x

SUPPLEMENTARY MATERIAL

Table S1 Messenger RNA (mRNA) expression of tricellulin (Tric) in different wild type (WT) mouse organs

	Genotype	Whole brain	Brain cortex	Spleen	Testis	Eye	Heart	Lung
Tric	**WT**	(7.8±1.3) $\times10^{-1}$	(7.3±0.9) $\times10^{-1}$	(7.7±1) $\times10^{-1}$	(18±3.5) $\times10^{-1}$	8.8±1.9	3.8±1.1	5.1±1.1
	Genotype	**Liver**	**Kidney cortex**	**Kidney medulla**	**Jejunum**	**Duodenum**	**Ileum**	**Colon**
Tric	**WT**	(1.6±0.3) $\times10^{1}$	(1.6±0.3) $\times10^{1}$	(2.5±0.6) $\times10^{1}$	5.4±1.2	3.8±0.5	4.3±0.7	7±0.5

Table contains numerical values from Fig. 4.1. mRNA expression of Tricellulin (Tric) in C57BL/6 mouse normalized to β-actin (Actb) ($\Delta Ct = Ct_{junction\ protein} - Ct_{actin}$); Ct, Cycle threshold; mean ± SEM, n = 8.

Table S2 Messenger RNA (mRNA) expression of designated proteins in human colon carcinoma epithelial cells after peptide-free medium, 150 μM scrambled trictide and 150 μM trictide administrations.

	Untreated	150 μM trictide	150 μM scrambled trictide
Tric	(12±0.7) $\times10^{-3}$	(5.3±1.2) $\times10^{-3}$	(10.7±0.7) $\times10^{-3}$
Occl	(1.8±0.3) $\times10^{-2}$	(1.3±0.2) $\times10^{-2}$	(1.6±0.1) $\times10^{-2}$
MD3	(7.3±0.7) $\times10^{-4}$	(2.7±0.6) $\times10^{-4}$	(3.8±0.5) $\times10^{-4}$
LSR	(1.6±0.2) $\times10^{-2}$	(1±0.05) $\times10^{-2}$	(1.7±0.09) $\times10^{-2}$
Cldn1	(4.4±0.1) $\times10^{-3}$	(2.6±0.5) $\times10^{-3}$	(6.8±0.5) $\times10^{-3}$
Cldn5	(3±0.6) $\times10^{-6}$	(1.8±0.4) $\times10^{-6}$	(3.9±0.4) $\times10^{-6}$
ZO-1	(7.4±1) $\times10^{-3}$	(8±0.5) $\times10^{-3}$	(4.8±0.3) $\times10^{-3}$

Table contains absolute values (ΔCt) of Fig. 4.10. mRNA expressions normalized to β-actin (Actb) ($\Delta Ct = Ct_{junction\ protein} - Ct_{actin}$); Ct, Cycle threshold; Tric, tricellulin; Occl, occludin; MD3, marvelD3; LSR, anti-lipolysis stimulated lipoprotein receptor; Cldn1, claudin-1; Cldn5, claudin-5; ZO-1, zonula occludens protein 1; mean ± SEM, n = 10.

Table S3 Messenger RNA (mRNA) expression of designated proteins in mouse brain endothelial cells after peptide-free medium, 100 µM scrambled trictide, 75 µM and 100 µM trictide administrations.

	Untreated	75 µM trictide	100 µM trictide	100 µM scrambled trictide
Cldn1	(8±1.6) $\times10^{-6}$	(2.9±0.7) $\times10^{-6}$	(3.8±2) $\times10^{-6}$	(7.7±1.4) $\times10^{-7}$
Cldn5	(11.6±1) $\times10^{-2}$	(8.6±0.8) $\times10^{-2}$	(3.3±0.2) $\times10^{-2}$	(8±0.4) $\times10^{-2}$
Tric	(4.6±1.1) $\times10^{-6}$	(3.2±0.7) $\times10^{-6}$	(19.6±2) $\times10^{-6}$	(19±1.6) $\times10^{-6}$
LSR	(9.1±1) $\times10^{-5}$	(2.4±0.4) $\times10^{-5}$	(0.5±0.04) $\times10^{-5}$	(2.8±0.2) $\times10^{-5}$
Cldn25	(1.5±0.2) $\times10^{-3}$	(1.4±0.2) $\times10^{-3}$	(2.1±0.08) $\times10^{-3}$	(1±0.03) $\times10^{-3}$
ZO-1	(2.1±0.08) $\times10^{-2}$	(1.3±0.08) $\times10^{-2}$	(2.4±0.2) $\times10^{-2}$	(1.3±0.07) $\times10^{-2}$
Occl	(5.5±0.7) $\times10^{-3}$	(2.8±0.3) $\times10^{-3}$	(1.1±0.06) $\times10^{-3}$	(1.6±0.08) $\times10^{-3}$

Table contains absolute values (ΔCt) of Fig. 4.13 and Fig. S 1. mRNA expressions normalized to β-actin (Actb) ($\Delta Ct = Ct_{junction\ protein} - Ct_{actin}$); Ct, Cycle threshold; Tric, tricellulin; Occl, occludin; LSR, anti-lipolysis stimulated lipoprotein receptor; Cldn1, claudin-1; Cldn5, claudin-5; Cldn25, claudin-25; ZO-1, *zonula occludens* protein 1; mean ± SEM, n ≥8.

Table S 4 Messenger RNA (mRNA) expression of designated proteins in wild type (WT) mouse brain and kidney upon phosphate-buffered saline (PBS) and 4 h and 24 h after 800 µM of trictide (3.6 µmol/kg) administrations.

	Administration	Brain	Kidney
Tric	**PBS**	(1.3±0.3) $\times10^{-4}$	(3.2±0.1) $\times10^{-3}$
	Trictide (4 h)	(1.5±0.3) $\times10^{-4}$	(2.1±0.2) $\times10^{-3}$
	Trictide (24 h)	(1.4±0.2) $\times10^{-4}$	(1±0.3) $\times10^{-3}$
LSR	**PBS**	(6.8±0.7) $\times10^{-4}$	(4.7±0.3) $\times10^{-3}$
	Trictide (4 h)	(5±0.5) $\times10^{-4}$	(5.4±0.3) $\times10^{-3}$
	Trictide (24 h)	(4.7±0.3) $\times10^{-4}$	(4±0.4) $\times10^{-3}$
Occl	**PBS**	(39±1.5) $\times10^{-4}$	(6.8±0.2) $\times10^{-3}$
	Trictide (4 h)	(8.8±1.1) $\times10^{-4}$	(8±0.2) $\times10^{-3}$

	Trictide (24 h)	(7.9±0.5) $\times10^{-4}$	(6.2±0.1) $\times10^{-3}$
MD3	**PBS**		(1.9±0.1) $\times10^{-4}$
	Trictide (4 h)		(1.8±0.2) $\times10^{-4}$
	Trictide (24 h)		(0.7±0.2) $\times10^{-4}$
Cldn5	**PBS**	(3.9±0.1) $\times10^{-3}$	
	Trictide (4 h)	(3.2±0.05) $\times10^{-3}$	
	Trictide (24 h)	(5.6±0.8) $\times10^{-3}$	
ZO-1	**PBS**	(7.9±1.1) $\times10^{-3}$	(7.8±0.2) $\times10^{-3}$
	Trictide (4 h)	(7±0.9) $\times10^{-3}$	(10.3±0.9) $\times10^{-3}$
	Trictide (24 h)	(6.2±0.3) $\times10^{-3}$	(7.5±1) $\times10^{-3}$
Cldn1	**PBS**		(4.4±0.9) $\times10^{-3}$
	Trictide (4 h)		(4.9±0.2) $\times10^{-3}$
	Trictide (24 h)		(4.1±0.4) $\times10^{-3}$
Cldn12	**PBS**	(3.4±0.3) $\times10^{-3}$	
	Trictide (4 h)	(3.4±0.09) $\times10^{-3}$	
	Trictide (24 h)	(3.4±0.04) $\times10^{-3}$	
Cldn25	**PBS**	(6.7±0.2) $\times10^{-3}$	(4.2±0.2) $\times10^{-3}$
	Trictide (4 h)	(6.4±0.2) $\times10^{-3}$	(4.1±0.4) $\times10^{-3}$
	Trictide (24 h)	(6±0.3) $\times10^{-3}$	(2.5±0.6) $\times10^{-3}$

Table contains absolute values (ΔCt) of Fig. 4.22. mRNA expressions normalized to β-actin (Actb) (ΔCt = $Ct_{junction\ protein}$ - Ct_{actin}); Ct, Cycle threshold; Tric, tricellulin; Occl, occludin; MD3, marvelD3; LSR, anti-lipolysis stimulated lipoprotein receptor; Cldn1, claudin-1; Cldn5, claudin-5; Cldn12, claudin-12; Cldn25, claudin-25; ZO-1, *zonula occludens* protein 1; mean ± SEM, n ≥4.

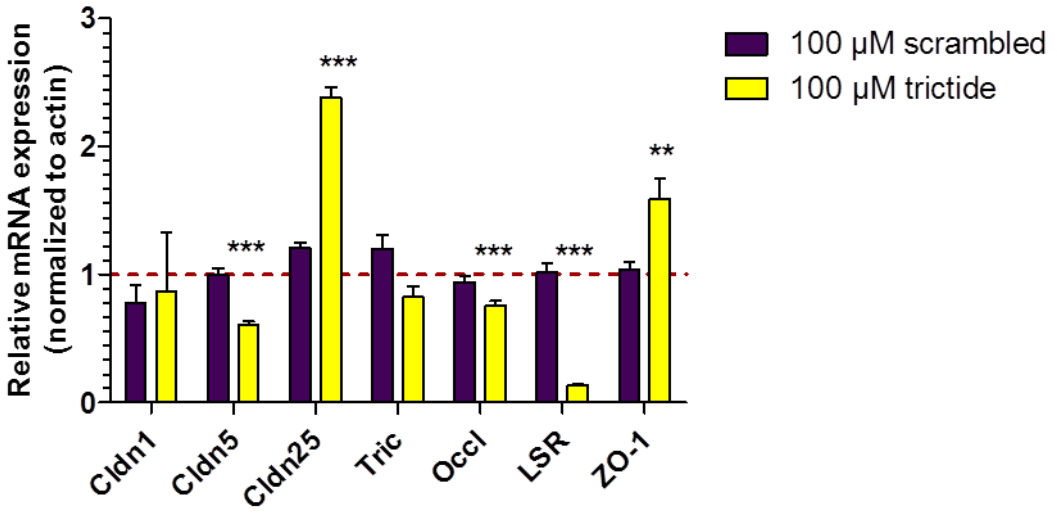

Fig. S5 Trictide down-regulates mRNA expression of claudin-5, LSR, occludin and up-regulates Cldn25 and ZO-1 in mouse brain endothelial cells. (A) Effect on messenger RNA (mRNA) of designated proteins; upon trictide and scrambled trictide treatment compared to untreated control ($2^{\Delta\Delta Ct}$) (red dotted line). mRNA normalized to β-actin (Actb) ($\Delta Ct = Ct_{junction\ protein} - Ct_{actin}$); Ct, Cycle threshold; total incubation time, 16 h; two-way ANOVA test was applied prior to Bonferroni's comparison post hoc test; Mean ± SEM; n =10; ** $P \leq 0.01$, *** $P \leq 0.001$ versus untreated control. Cldn1, claudin-1; Cldn5, claudin-5; Cldn25, claudin-25; Tric, tricellulin; Occl, occluding; LSR, anti-lipolysis stimulated lipoprotein receptor; ZO-1, *zonula occludens* protein 1.

Basak Arslan

Education

Since 2015	**Ph.D. in Biology,** Freie University Berlin, Faculty of Biology, Chemistry and Pharmacy, Berlin
2011 – 2012	**M.Sc. in Molecular Biotechnology**, University of Birmingham (UoB), School of Biosciences Edgbaston, Birmingham
2006 – 2011	**B.Sc. in Biological Sciences and Bioengineering,** Sabanci University (SU), Faculty of Engineering& Natural Sciences (FENS) İstanbul
	Minor: Chemistry
	Fluor Daniel Corporation Scholarship: Awarded for outstanding accomplishment (2008).

Publication: Arslan, B.*, Cording, J.*, Staat, C., Dithmer, S., Krug, S. M., Krüger, A., Berndt, P., Günther, R., Winkler, L., Blasig, I. E. and Haseloff, R. F. (2017). Trictide, a tricellulin-derived peptide to overcome cellular barriers. *Annals of the New York Academy of Sciences*, *1405*(1), 89–101. https://doi.org/10.1111/nyas.13392

***** These authors contributed equally to this work.

Presentations:

B. Arslan. Trictide, a tricellulin-derived peptide to overcome cellular barriers. 19th Bad Herrenalber transporter and barrier meeting. 2017. Bad Herrenalb, Germany.

J. Cording, **B. Arslan**, A. Krüger, R. Günther, C. Staat and I.E. Blasig. TricSI - Development of a Tricellulin Peptidomimetic to Modify Tissue Barriers. Tight junctions and their proteins international conference. 2016. Berlin, Germany. (*Selected for short talk in addition to poster presentation*)

B. Arslan, J. Cording, A. Krüger, R. Günther, C. Staat and I.E. Blasig. TricSI - Development of a Tricellulin Peptidomimetic to Modify Tissue Barriers. German Society for Experimental and Clinical Pharmacology and Toxicology (DGPT) meeting. 2016. Berlin, Germany.

Declaration of Authorship

I hereby certify that this submitted thesis has been composed by me and is based on my own work, unless stated otherwise. No other person's work has been used without acknowledgement in this thesis. All references and verbatim extracts have been quoted, and all sources of information, including graphs and data sets, have been specifically acknowledged.

Berlin, 9 October 2018

Başak Arslan